AN ABSTRACT OF THE THESIS OF

Jacob K. Kollen for the degree of Master of Science in Water Resources Engineering and Soil Science presented on March 14th, 2016

Title: Experiences in Implementing the White Method: Estimating Evapotranspiration Using Fluctuations of Water Table Elevation

Abstract Approved:

John S. Selker Maria I. Dragila

Evapotranspiration (ET) is the process by which water is transferred from land to the atmosphere. ET is the second most important component of a hydrologic budget and remains difficult to estimate. The primary objective of this project was to determine the limitations of estimating ET from water table elevation fluctuations analyzed using the White Method (White, 1932). Secondary objectives include: determining if specific yield is a function of water table depth, investigating the effect of hysteresis on water table fluctuation shape, estimating groundwater recharge rate, and using vegetation data to gain clues regarding spatiotemporal water availability.

They are 5 major results from this investigation. Nachabe's modified soil moisture balance (Nachabe et al. 2005) outperformed the classical White Method (White, 1932) in ability to estimate a daily rate of evapotranspiration. Specific yield is not a constant and changes with water table depth below ground surface level. Hysteresis can explain the break in slope in water table rise observed during the night of many records of water table fluctuations. The White Method is more suitable to estimate groundwater upwelling rather than evapotranspiration. Finally, vegetation sampling can provide clues to intra-seasonal and inter-seasonal water availability across a site.

Experiences in Implementing the White Method:

Estimating Evapotranspiration Using Fluctuations of Water Table Elevation

by
Jacob K. Kollen

A THESIS

submitted to

Oregon State University

In partial fulfillment of
the requirements for the
degree of

Master of Science

Presented March 14, 2016
Commencement June 2016

Master of Science thesis of Jacob K. Kollen presented on March 14, 2016

APPROVED:

Co-Major Professor, representing Water Resources Engineering

Co-Major Professor, representing Soil Science

Director of the Water Resources Graduate Program

Head of the Department of Crop and Soil Science

Dean of the Graduate School

I understand that my thesis will become part of the permanent collection of Oregon State University libraries. My signature below authorizes release of my thesis to any reader upon request.

Jacob K. Kollen, Author

ACKNOWLEDGEMENTS

I have had to privilege of working in the Selker Lab Group at Oregon State University where I have experienced constant motivation, support, and encouragement through the process of scientific inquiry.

Special thanks to:

Lia Shrewsbury for emotional and physical support through graduate school

John Selker for premier advising and constant motivation through the scientific process

Maria Dragila for inspiration of curiosity into soil water movement

Rebecca Hochreutener for logistical support and excellence in field method execution

Clement Roques for the bottomless support with writing MATLAB code

The Higgins Lab for expert contributions to atmospheric sensing and ET quantification

Nicolas Gosselin for high quality field work in groundwater, soils and instrumentation

Manon Gevaudan for high quality field work in vegetation sampling and data processing

John Haseltine for high quality lab work and data processing

The Confederated Tribes of the Warm Springs for access to land to perform field work

TABLE OF CONTENTS

LIST OF FIGURES

LIST OF FIGURES (Continued)

LIST OF FIGURES (Continued)

LIST OF FIGURES (Continued)

LIST OF FIGURES (Continued)

Figure Page

LIST OF TABLES

Chapter 1: Introduction

Context

The practice of quantifying the amount of water flowing through a watershed is known as hydrologic budgeting. Hydrologic budgeting is typically used to make predictions about the amount of water that will be available for irrigation, municipal supply and habitat maintenance. The need for hydrologic budgeting becomes greater as long term weather patterns change. The primary components of a hydrologic budget are the inputs to the system (e.g. precipitation), the outputs from the system (e.g. evapotranspiration, discharge) and the changes in storage (e.g. volumetric moisture content) (Fig.1). In semi-arid watersheds evapotranspiration from riparian zones represent ~35% of the annual evapotranspirative loss from the watershed while riparian zones occupy ~5% of the catchment area (Scott et al., 2008).

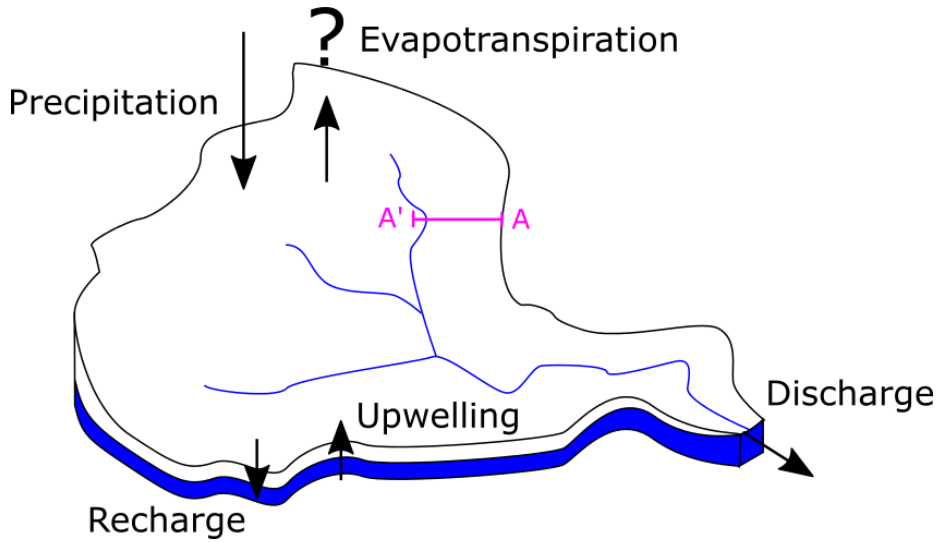

Figure 1. The practice of hydrologic budgeting.

Landscape Position

Shallow aquifers typically occur at low points in the landscape where the elevation of the groundwater position in the hillslopes maintains a shallow depth between the soil surface and water surface within the area of interest (Fig. 2). The position of the area of interest is along a cross section of a hill slope perpendicular to the rivers primary flow path. In semi-arid watersheds an area of interest could be riparian zones, wetlands, or pastures that remain green into the dry season without irrigation. To measure the water table elevation in the area of interest I used groundwater observation wells.

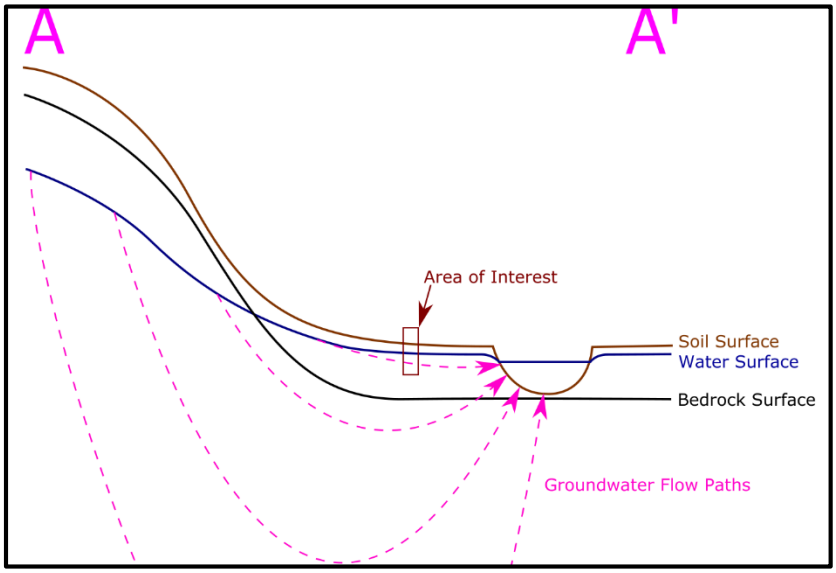

Figure 2. A generalized hillslope model.

The 1-D System in Question

A groundwater observation well extends downwards and the vertical component of the groundwater flow vector can be observed. Since the system is inherently 1-D because the lateral extent of the shallow sloped meadows are large relative to the change in vertical depth to water table across the site, as well as the vertical components of water transfer are large in relation to the horizontal components water transfer (Fig. 3). The adoption of a 1-D model (Fig. 4) is useful because the primary field instrument can only sense along the vertical dimension.

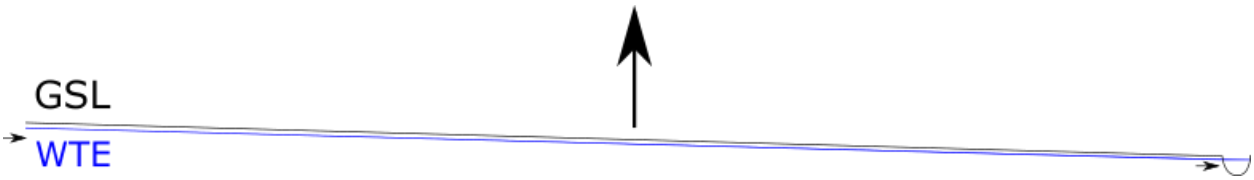

Figure 3. The shallow sloped meadow system is 1-D. The black line is the ground surface level (GSL). The blue line is the water table elevation (WTE). The vertical arrow is evapotranspiration. The horizontal arrow on the left is groundwater inflow. The horizontal arrow on the right is groundwater discharge to the stream.

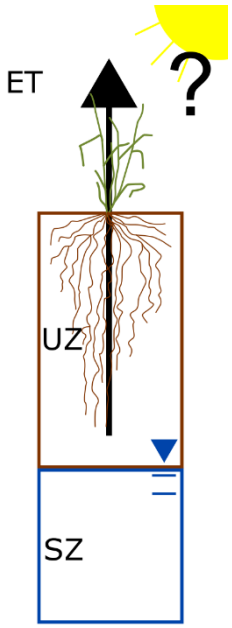

Figure 4. The one dimensional shallow aquifer model. The evapotranspirative flux (ET) is governed by the behavior of the saturated zone (SZ), unsaturated zone (UZ), atmosphere, and vegetation.

Evapotranspiration (ET) is the process by which water is transferred from liquid water below the ground surface to water vapor above the ground surface. The two components of evapotranspiration are evaporation as direct transfer and transpiration through vegetation as an indirect transfer. Since I have selected a one dimension model the ET rate [$L^3 * T^{-1}$] becomes an ET flux [$L^1 * T^{-1}$] communicated as lengths of water per day. The one dimensional shallow aquifer model is single vertical component of a three dimensional landscape.

Water Table Fluctuations

If we were able to observe the water table position in an observation well within an area of interest (Fig. 2) an interesting pattern would arise (Fig. 5). During the night groundwater supply into the area pushes the water table higher, referred to as apparent groundwater upwelling. During the day apparent groundwater upwelling occurs, however evapotranspiration occurs potentially with larger magnitude driving the water table lower. The process of ET coupled with apparent groundwater upwelling creates a wave of the water table elevation through time referred to as a daily diurnal water table fluctuation.

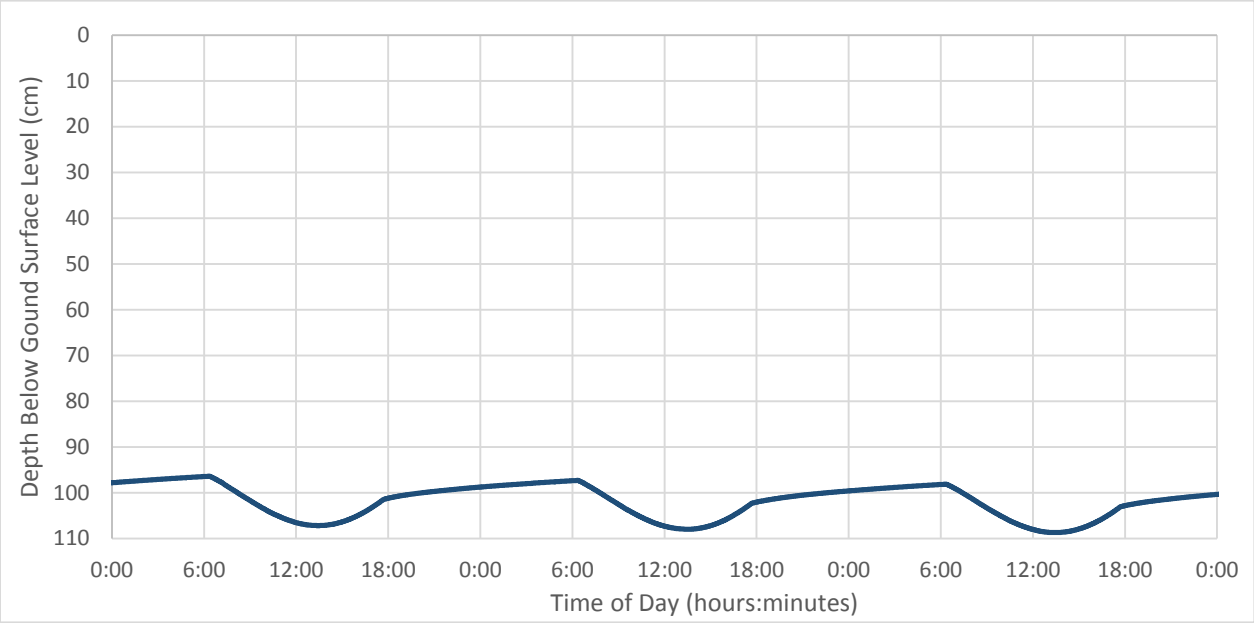

Figure 5. Daily diurnal water table fluctuations. This is a record modeled using HYDRUS 1-D (Simunek et al., 1998).

The Dry Season Transition

At the start of the dry season the water table positions tend to drop as an exponential decay (Said et al., 2005). The transition from a shallow to deep water table on the monthly timescale coupled with the diurnal water table fluctuations produces a decaying wavy signal with a decreasing amplitude through time (Fig. 6).

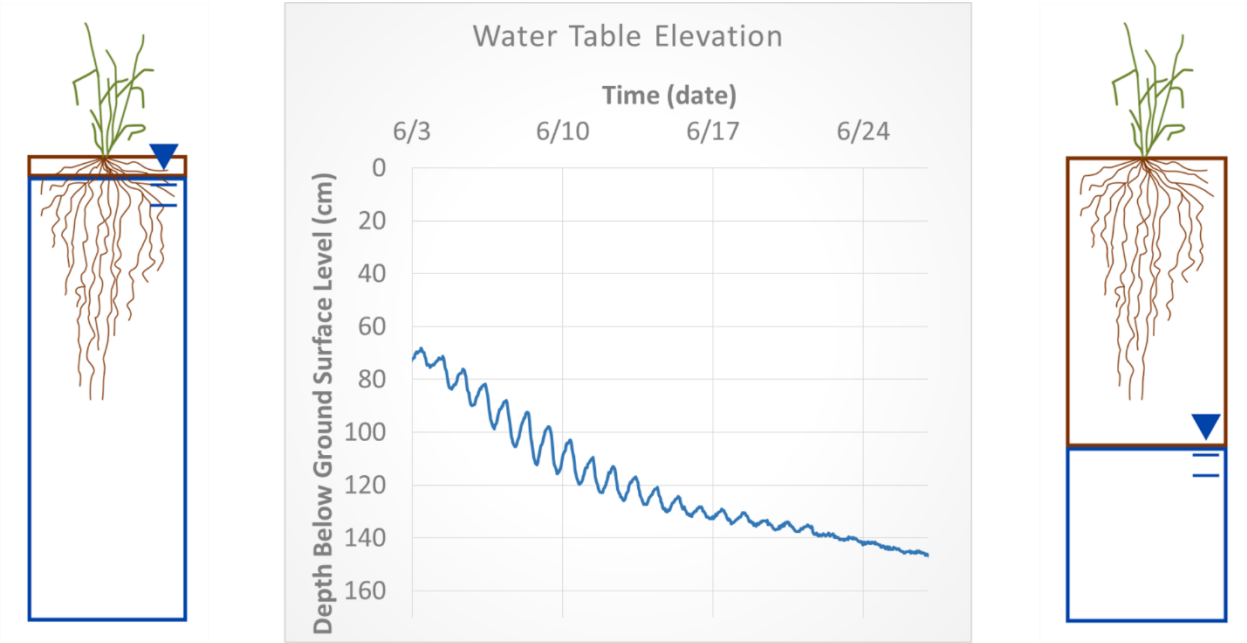

Figure 6. The dry season transition. This record was obtained at Granite Boulder Pasture at OB28 during June of 2015.

The White Method

The primary objective of this project was to determine the limitations of estimating evapotranspiration using daily diurnal water table fluctuations analyzed with the White Method (White, 1932) (Eq. 1) (Fig. 7).

$$ET = S_y\,(r \pm s) \qquad \text{Eq. 1}$$

Where:

ET = Daily evapotranspiration rate [L_{water}/T]

Sy = Specific yield [L_{water}/$L_{aquifer}$]

r = Apparent Groundwater Upwelling Rate [$L_{aquifer}$/T]

s = Change of Water Table in 24 Hour Period [$L_{aquifer}$/T]

[$L_{aquifer}$] = Depth of aquifer

[L_{water}] = Depth of water

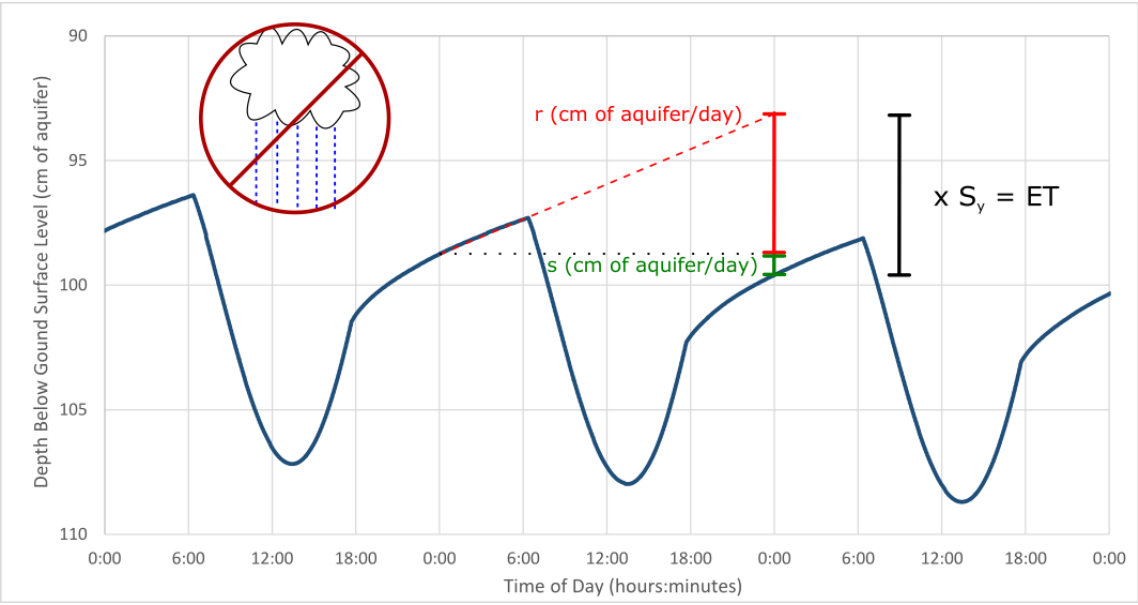

Figure 7. White's approach to water table fluctuation analysis.

Walter White made key observations and assumptions while analyzing a record of daily diurnal water table level fluctuations (Fig. 5). White's first assumption was that in a precipitation free period, the origination of water to be transpired is that of a groundwater source. Another assumption was that the apparent groundwater upwelling rate **r** (depth of aquifer/day) can be obtained by finding the height difference between the observed water table height and the projected water table height using a fitted regression line to the previous night's data set, a time period where the only major process affecting the water table position is the apparent groundwater upwelling. Another key assumption was that the change in storage **s** (depth of aquifer/day) is the net change in water table position in a 24h period. The last key assumption was that the sum of both the **r** and **s** are scaled by the specific yield $\mathbf{S_y}$ (depth of water/depth of aquifer) resulting in a daily estimate of evapotranspiration **ET** (depth of water/day).

White Method Advantages

In the context of evapotranspiration methods the White Method is cost effective. The White Method requires a shallow observation well, an automated pressure logger, and installation which costs roughly $500. The classical method of Penman-Monteith requires a conventional weather station and installation which costs roughly $2,000. The scientific standard method of Eddy Covariance requires a 3-D ultrasonic anemometer, an open path gas analyzer, and installation which costs roughly $20,000. The White Method costs either 2.5% to 25% of the competing evapotranspiration methods. Another major advantage of the White Method is that it does not require the assumption that evapotranspiration is homogeneous

within a station's fetch, an assumption required by both the Penman-Monteith and Eddy Covariance Methods. Since the White Method doesn't require the assumption that ET is homogeneous in the spatial extent, it can be applied to sites where ET is expected to be heterogeneous in the spatial extent. The White Method is limited in its application, however the advantages of cost effectiveness and applicability to heterogeneous sites provides the incentive to determine its limitations.

Specific Yield

To the hydrologic budgeter, the amount of water moving into and out of a system is a more valuable metric than apparent changes in water table elevation. For a given change in water table elevation **ΔWT** (depth of aquifer), there is a smaller amount of water yielded $\mathbf{W_y}$ (depth of water). Mathematically, a coefficient specific yield $\mathbf{S_y}$ (depth of water/depth of aquifer) can be used to set an equivalence between $\mathbf{W_y}$ and **ΔWT** (Fig. 8) (Eq. 2).

$$W_y = S_y * \Delta WT \qquad \text{Eq.2}$$

Where:

S_y = specific yield (depth of water/depth of aquifer)

W_y = water yield (depth of water)

ΔWT = change in water table elevation (depth of aquifer)

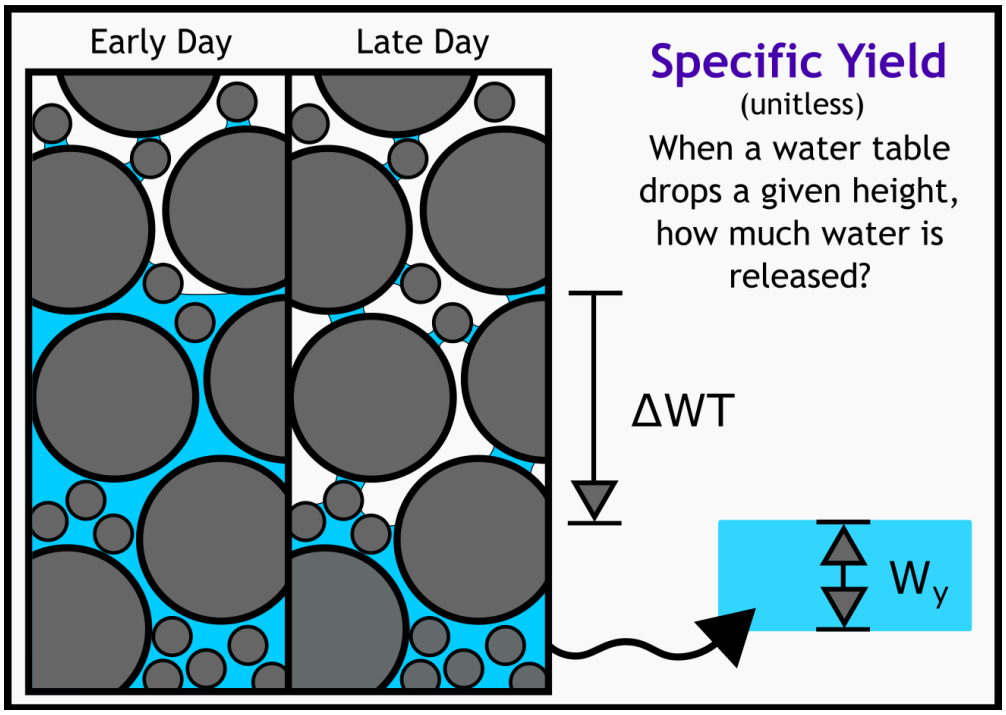

Figure 8. Specific yield for an unconfined aquifer.

S_y is always going to be less than 1 because the solids of the aquifer take up space that is not displaced by water. There three physical processes that need to be taken into account for determining a case specific **S_y**: pore drainage, the decompression of water, and the compression of the aquifer. However in an unconfined aquifer the amount of water yielded from the pore draining process is typically two orders of magnitude greater than the other two processes (Dawson and Istok, 1991). Thus, in the unconfined aquifer case, **S_y** is merely a fractional quantity describing the pore drainage process.

In the case of a shallow aquifer, where evapotranspiration is a significant process, the maximum pressures exerted by plants to drain pores can be upwards of -15,000 cm of water during the day at the upper portions of the 1-D system (Veihmeyer and Hendrickson, 1928). The pressure exerted to fill the pores during the night is a positive pressure change communicate at the bottom of the 1-D system equal to the change in water table elevation.

After making the assumption that during the dry season in a semi-arid watershed evaporation from soil is negligible, evapotranspiration becomes transpiration. Transpiration is mediated by a plant which strives to meet the evaporation potential but is limited by either anoxic conditions or their inability to exert pressures to drain pores, this behavior is often modeled using the Feddes Function (Feddes et al., 1978) (Fig. 9).

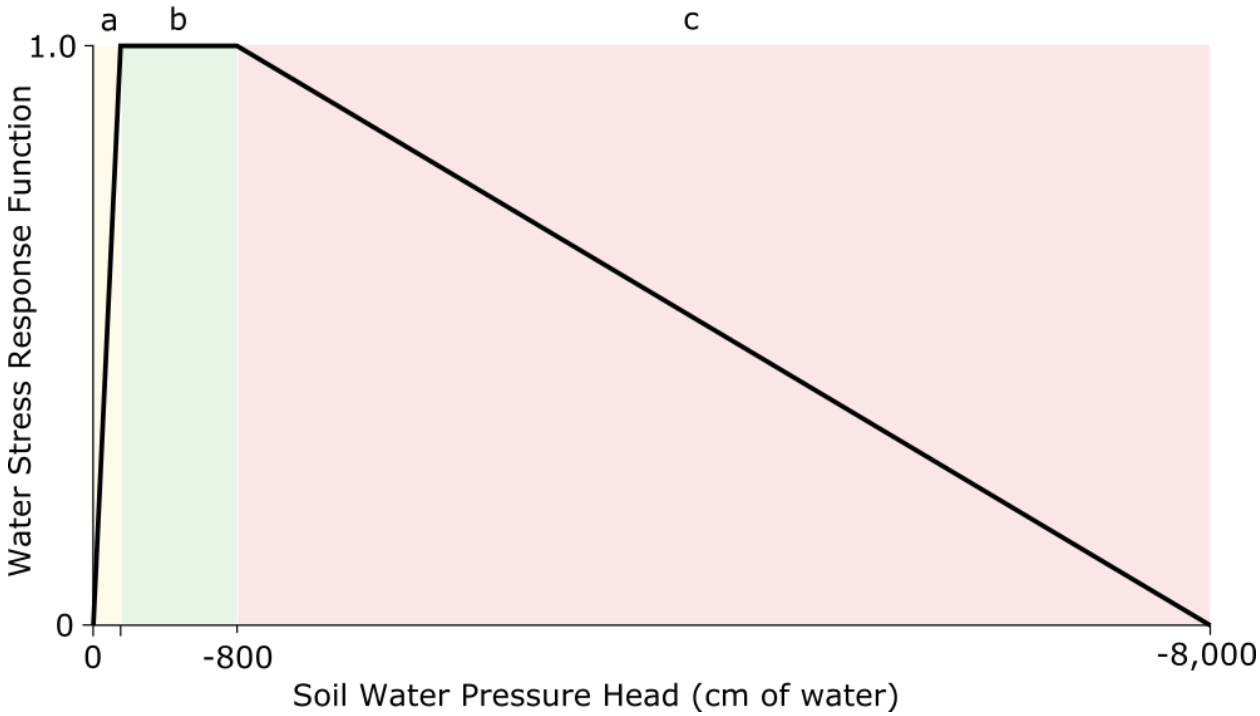

Figure 9. The Feddes Function. Zone **a** is where plants regulate their transpiration rate due to anoxic conditions. Zone **b** is the where the plant are optimally transpiring water. Zone **c** is where plants regulate their transpiration due their inability to exert pressures to drain pores. Feddes Function values are Wesseling's value for pasture (Wesseling, 1991).

Apparent Groundwater Upwelling

The secondary objective of this experiment was to demonstrate the quantification of the apparent groundwater upwelling using the White Method (Fig. 8). Since our field instrumentation can only measure along the vertical axis, I have adopted a 1-D model (Fig. 4) and have defined the apparent groundwater upwelling as the positive vertical component of the regional groundwater vector. The question remains what is the apparent groundwater upwelling rate (Fig. 10)? They are two ways to conceptualize apparent groundwater upwelling rate (Fig. 11).

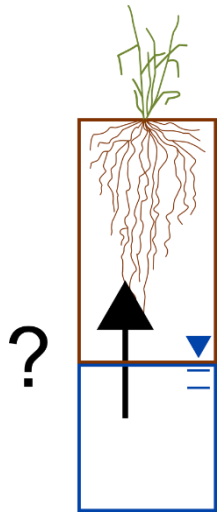

Figure 10. How big groundwater upwelling [$L_{water} * T^{-1}$]?

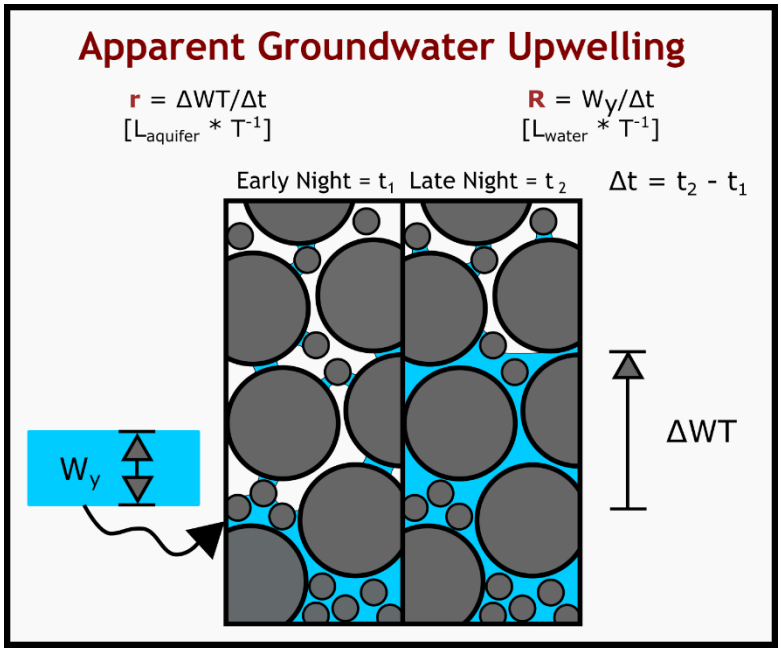

Figure 11. Apparent groundwater upwelling rates as **r** [$L_{aquifer} * T^{-1}$] and **R** [$L_{water} * T^{-1}$].

While **r** is easily observable from a record of water table position, **R** has more utility to a hydrologic budgeter. A potential application of the White Method is to estimate **R**. In White's equation (Eq. 1) **r** is scaled by specific yield $\mathbf{S_y}$ resulting in a term with units of (depth of water/time) which are the units of **R**. By simply rearranging White's equation produces the following expression (Eq. 3):

$$R = S_y * r = ET - S_y * s \qquad \text{Eq. 3}$$

Spatial Extent of Evapotranspiration

A tertiary objective of this experiment was to investigate the accuracy of the assumption of spatial uniformity in evapotranspiration (Fig. 12). A common assumption made by methods that analyze weather station data for estimation of evapotranspiration is that evapotranspiration is spatially homogeneous in the fetch of the station. In riparian zones, heterogeneity in vegetation, soils and water table position are common and we felt required greater attention.

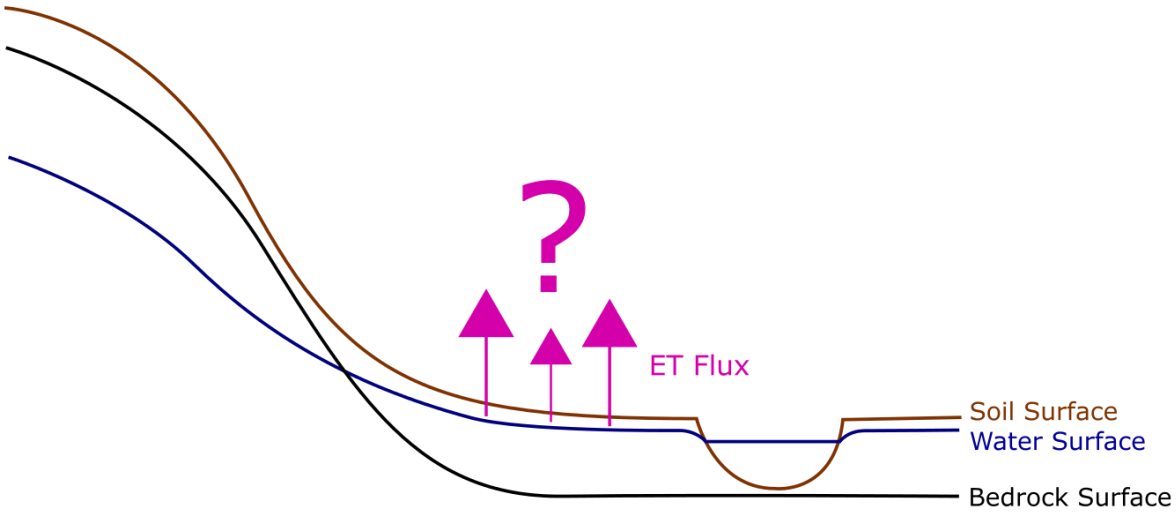

Figure 12. Spatial extent of evapotranspiration.

State of the Art

Walter White proposed the White Method in 1932 (White, 1932). With the advent of automated submersible pressure transducers there has been a revitalization in the investigation of the White Method. The White Method has been observed to be a valuable potential contributor to the suit of evapotranspiration methods (Loheide, 2008). A large limitation in the White Method is the uncertainty in the estimate of specific yield (Loheide et

al., 2005). In White's own words 'The specific yield, however, is exceedingly difficult to determine.' In groundwater literature, where the term has a different interpretation, the specific yield is often referred to as an aquifer material property that does not change with vegetation type or available soil moisture (Lautz, 2007). Some have suggested that specific yield should not be a constant, but rather, specific yield should be function of depth of the water table below the ground surface level (Duke, 1972; Loheide et al., 2005; Said et al., 2005). A great effort within this investigation was to use field methods to measure specific yields, as well as to conceptualize the process of specific yield in the shallow unconfined aquifer case.

There are several analytical methods to analyze diurnal water table fluctuations. Some changed the time range of data to fit the apparent groundwater upwelling rate (Fahle and Dietrich, 2014). Soylu took a sinusoidal approach by applying a Fourier-based improvement to the White Method (Soylu et al., 2012). Wang states that a record of daily diurnal groundwater fluctuations can be treated as a stochastic periodic time series, in which a statistical approach can be applied (Wang and Pozdniakov, 2014). My criticism in solely developing the data-driven methods is that the insight and connection to a physical understanding of the system is lost. For example, what is producing the break in slope apparent in Soylu's data at roughly 10pm (Fig. 13)? Nachabe took a step back from the White Method to develop an approach based on a record of total soil moisture (Nachabe et al., 2005). Nachabe's approach removes the need for the specific yield term by measuring the volumetric moisture content by depth. It is in my option, that before fine tuning the analytical methods it is important to deal with the specific yield and the uncertainty it imposes.

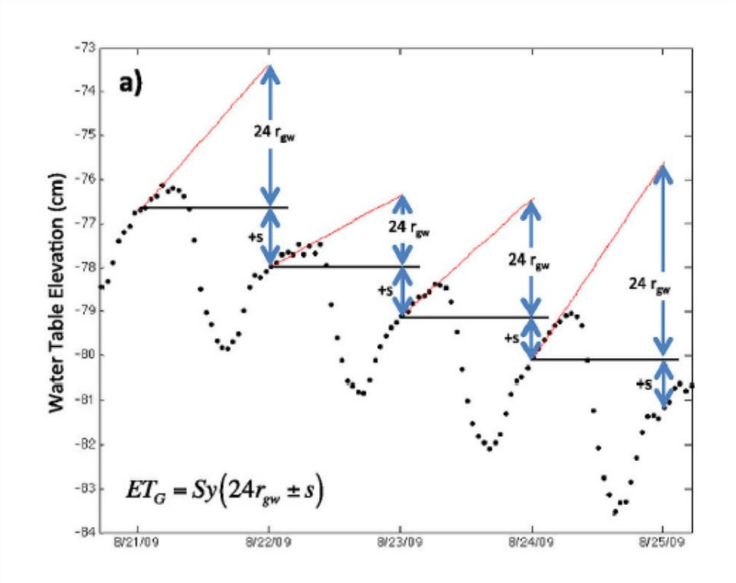

Figure 13. Break in slope. This is figure 1 in Soylu et al., 2012.

To understand the shallow aquifer system, it is important to conceptualize the effects of evapotranspiration upon the water content, pressure and flux, by depth. Evaporation from porous media can be compartmentalized into stage one evaporation, where evaporation is only limited by vapor exchange, and stage two evaporation where evaporation is controlled by vapor diffusion (Lehman et al., 2008). Stage one evaporation is relatively large compared to stage two evaporation (Lehman et al., 2008). The maximum depth below ground surface level (BGSL) where the transition between stage one evaporation and stage two evaporation is known as the evaporation extinction depth (Lehman et al., 2008). The evaporation extinction depth is controlled by the pore size distribution of the porous media (Lehman et al., 2008). Lehman et al. measured the evaporation extinction depth for a fine sand to be 9cm BGSL, and would expect it to be shallower as the pore size distribution becomes finer (Lehman et al., 2008). Transpiration is the evaporation potential communicated through the vegetation. Complete understanding of how transpiration works and which roots are doing the work

remain an open question (Hunt and Massori, 2016). Transpiration is a function of the ecophysiology of the plant species within the system (Baird and Maddock, 2005) and is often modeled using the Feddes Function (Feddes at al., 1978). Transpiration is also a function of the root distribution by depth (Hao et al., 2013). The effects of evapotranspiration upon the shallow aquifer can be compartmentalized into two depths: the evaporation affected zone and the transpiration affected zone. This compartmentalization by process affected zones help understanding how specific yield changes with depth BGSL and helps in setting initial conditions for numerical models.

Chapter 2: Materials and Methods

Introduction

To answer the research question 'Can diurnal water table fluctuations in shallow level meadows be used to accurately estimate daily evapotranspiration rate?' the experimental design employed sensors at the field sites, observations at the field sites, laboratory analysis of field samples, numerical modeling, and data analysis of sensor readings. The objectives of the sensing technologies were to

- Sense the water table elevation to an accuracy of ± 1 mm at an hourly resolution;
- Sense the volumetric moisture content to an accuracy of ± 3% [$L^3 * L^{-3}$] at an hourly resolution;
- Sense the negative water pressure to an accuracy of ± 25 cm water at a hourly resolution;
- Sense the standard weather variables to ± 5% at an 10 minute resolution;
- Sense the eddy station variables to ± 2% at a 0.1 second resolution.

The objectives of the observations at the field site where to

- Observe the lithology and root distribution using soil pits and auguring holes;
- Observe the vegetation distribution across the sites;
- Perform pump tests to determine aquifer characteristics.

The objectives of the laboratory analysis of field samples were to

- Characterize the soil hydraulic properties of saturated hydraulic conductivity, the moisture retention curve, particle size distribution, porosity, and bulk density;
- Identify vegetation samples to species.

The objectives of the numerical modeling were to

- Estimate a specific yield using the soil hydraulic characterization;
- Test three model setups for the applicability of the white method;
- Determine if hysteresis affects the break in slope observed during the night;
- Determine if the accuracy of the White Method using a constant and variable specific yield;
- Determine the relationship between specific yield and depth of the water table BGSL.

Field Experimental Design

On the Middle Fork John Day River (MFJD) existing infrastructure was a contributing factor in the determination of field site placement. An existing array of groundwater observation wells had been installed in select wetlands adjacent to the MFJD. The records from these observation wells were inspected for daily diurnal fluctuations, and the two field sites were situated where the clearest daily diurnal fluctuations were observed. Other critical pieces of existing infrastructure were two weather stations located in the riparian zone of the MFJD. One located up drainage and one down drainage. The final experimental design utilized this existing infrastructure as well as installation of many new sensors and access tubes.

The three most important pieces of instrumentation which were installed included a weather station with a fetch that encompassed the site; an array of groundwater observation wells with a small spatial extent; and an instrumented pit instrumented to monitor volumetric moisture content and negative soil water pressure by depth (Fig. 14). Auxiliary instrumentation installed included a series of tensiometers which measured water pressure at specified depths (7.5, 15, 27.5 and 40 cm BGSL), and an array of diviner access tubes that measured volumetric moisture content by depth. In addition to infrastructure, field sampling was employed which included collection of groundwater, soils, and vegetation data. Pump test were conducted to determine aquifer characteristics. Soils description were performed to determine the lithology of the sites. Vegetation sampling was employed to investigate the role of plant heterogeneity on the pattern of ET.

Field Methods

Figure 14. Instrumented pit and an observation well.

Instrumented Pits

A one meter deep soil pit were instrumented to gather water pressure and moisture content with depth. Two data loggers (CR200, Campbell Scientific) were connected to four soil water pressure sensors (MPS-1, Decagon Devices), and eight volumetric moisture content sensors (5TE, Decagon Devices) (Table 1).

Table 1. Soil pit instrument placement.

Granite Boulder Pasture				Ruby Pasture			
Soil Pressure		Moisture Content		Soil Pressure		Moisture Content	
Depth (cm BGSL)	Sensor (title)	Depth (cm BGSL)	Sensor (title)	Depth (cm BGSL)	Sensor (title)	Depth (cm BGSL)	Sensor (title)
10	MPS-1	15	5TE	7.5	MPS-1	10	5TE
15	MPS-1	40	5TE	15	MPS-1	20	5TE
25	MPS-1	50	5TE	27.5	MPS-1	30	5TE
40	MPS-1	60	5TE	40	MPS-1	40	ECTM
		65	5TE			50	ECTM
		70	5TE			60	ECTM
		80	5TE			70	5TE
		90	5TE			78	ECTM

Soil Pit Description

Along the pit face horizon designations were made based on color, texture, structure, and root distribution. Field variable, such as soil texture, rock fragments, root distribution, color, organic matter, initial moisture content and the presence of redoximorphic features were gathered by horizon. Field methods were informed by the Natural Resource Conservation Service's Field Book for Describing and Sampling Soils (NRCS, 2012).

Auguring Hole Description

AMS 2 ¼ inch standard mud or sand auger with an open bail were used to extract soil, by depth, for field description. Limitations in gathering variables such as root distribution, depth to bedrock and large rock fragments occurred due to the sampling method.

Volumetric Moisture Content Profiles

A capacitance probe (Diviner 2000, Sentek) was used to gather volumetric soil moisture content of the soil profile. The probe slid inside a 1.6 m long access tube that was in direct contact with the soil. Emitting a high frequency (100 MHz) every ten centimeters below a datum plate, the capacitance probe measures the dielectric of the soil around the access tube, from which the volumetric moisture content by depth could be estimated. (Diviner 2000 User's Manual).

Tensiometers

Tensiometers (Irrometer) were used to obtain a direct measure of soil water pressure above the water table. Tensiometers were installed at depths below ground surface level to with the objective to sense soil water pressure at approximately 10, 20 and 30 cm above the water table during the intensive data collection period (Table 2).

Table 2. Tensiometer placement.

Tensiometer Depth	
Granite Boulder Pasture (depth BGSL)	Ruby Pasture (depth BGSL)
30	28
43	48
48	60
53	70
82	

Core Sampling

A core sampler (0200 Soil Core Sampler, Soilmoisture Equipment Co.) was used to gather 3 cm tall by 5.4 cm diameter cores by horizon. The core sampler was driven horizontally into the profile from the pit wall at the center of each identified horizon. Near the center of the pump test location an 8 cm diameter auger was used to clear soil material to the top of a horizon identified by a nearby soil auger field description. The soil core tool was placed vertically and driven downward yielding two cores per horizon.

Pump Test

A well array was installed using a handheld vibratory driver (Multi-Pro, Rhino) in the center of each site (Fig. 15). The wells were further developed using an air compressor and wand that pushed air through the well screen from inside the well. Automated pressure loggers (Hobo Water Level Loggers, Onset) were placed in each well to allow for the observation of water table depth. An additional automated logger transducer was placed above ground to record the barometric pressure. A pumping rate was selected by evaluating a stepped drawdown test (Freeman et al., 2004). Before the pump test was performed the initial water level was measured manually (101 P2 Water Level Meter, Solinst). A constant discharge rate was imposed for roughly 2 h on the pumping well (L/S Peristaltic Pump with Precision Variable-Speed Drive by Masterflex: Model # 7017-20, Tubing size unknown). Manual measurements and automated measurements of the depth of the water table were observed for the pumping well and observation wells. The recovery of the water table was only observed with pressure transducers. Further pump test analysis is provided in appendix a.V.

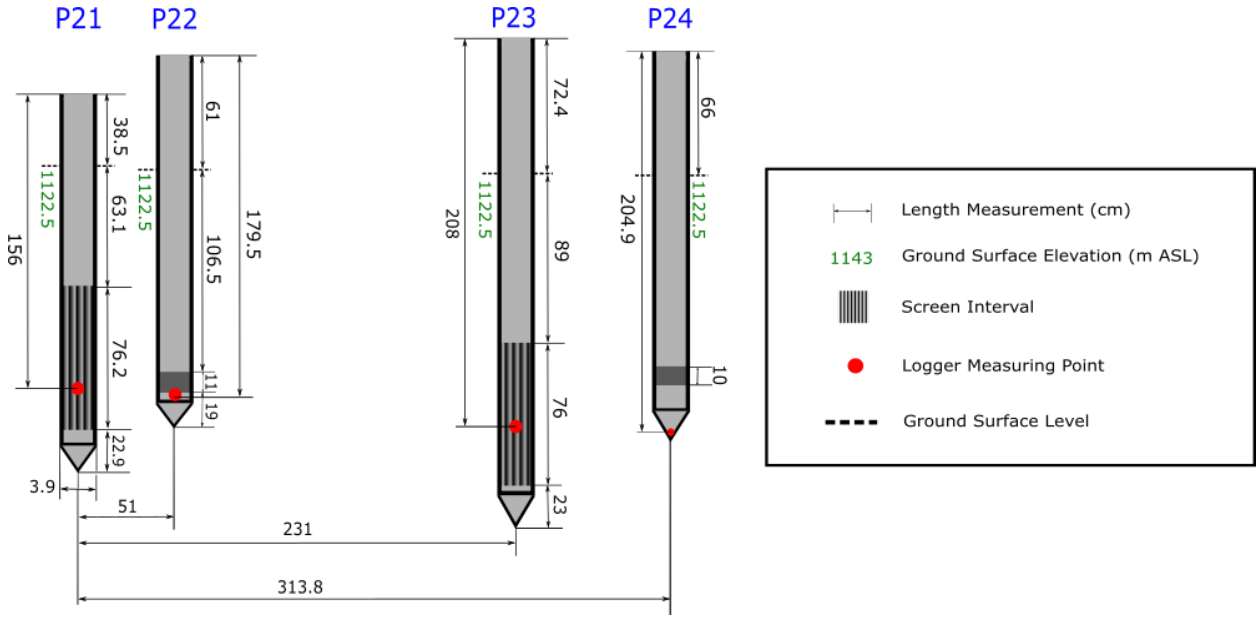

Figure 15. Well geometry of the pump test at Ruby Pasture.

Large Array of Observation Wells

Throughout the duration of the experiment the large well arrays were used to observe the water table level at a large spatial extent (300 meters) using automated pressure loggers (Hobo Water Level Loggers, Onset) and confirmed using manual measurements (101 P2 Water Level Meter, Solinst). Water table elevation data is provided (electronic appendix foldername: Water Table Elevation by Well).

Vegetation Sampling Design

Trends in vegetation were observed at Granite Boulder Pasture. The trends in vegetation appeared to be distributed in linear zones from Northeast to Southwest. To capture the diversity of in vegetation zones three parallel transects were placed from Southeast to

Northwest. Ten sampling points were randomly placed by drawing a number from hat representing the distance to the next point along transect. At each sampling point a sampling square (84cm by 84cm) was placed where the following data was collected using visual inspection:

- Species identification
- Percent cover of each species
- Minimum height, maximum height, and mean height of each species
- Percent bare ground
- Percent standing dead

The trends in vegetation at Ruby Pasture were not in linear features. To capture the diversity in vegetation a zigzag transect was placed across the site. Ten random sampling points were placed along each leg of the zigzag. The same sampling procedure was employed.

Lab Methods

Moisture Retention Curve

A pressure extraction (15 Bar Ceramic Plate Extractor, Soilmoisture Equipment) was used to apply a pressures of 0 bars, 1/10th bar, 1/3rd bar, 1 bar, and 3 bars to initially saturated 5.4 cm diameter by 3 cm tall undisturbed soil cores. The masses of the cores were weighed at each pressure interval to determine the amount of water released. A curve was fit to the plot of volumetric moisture content vs log negative pressure for each soil (Fig. 16). The fitted curves provided the van Genucten's α (inverse of the air entry pressure) and n (a measure of the pore size distribution) parameters which were used in HYDRUS 1-D modeling procedures. Data is provided in electronic appendix filename: Water Retention Analysis.

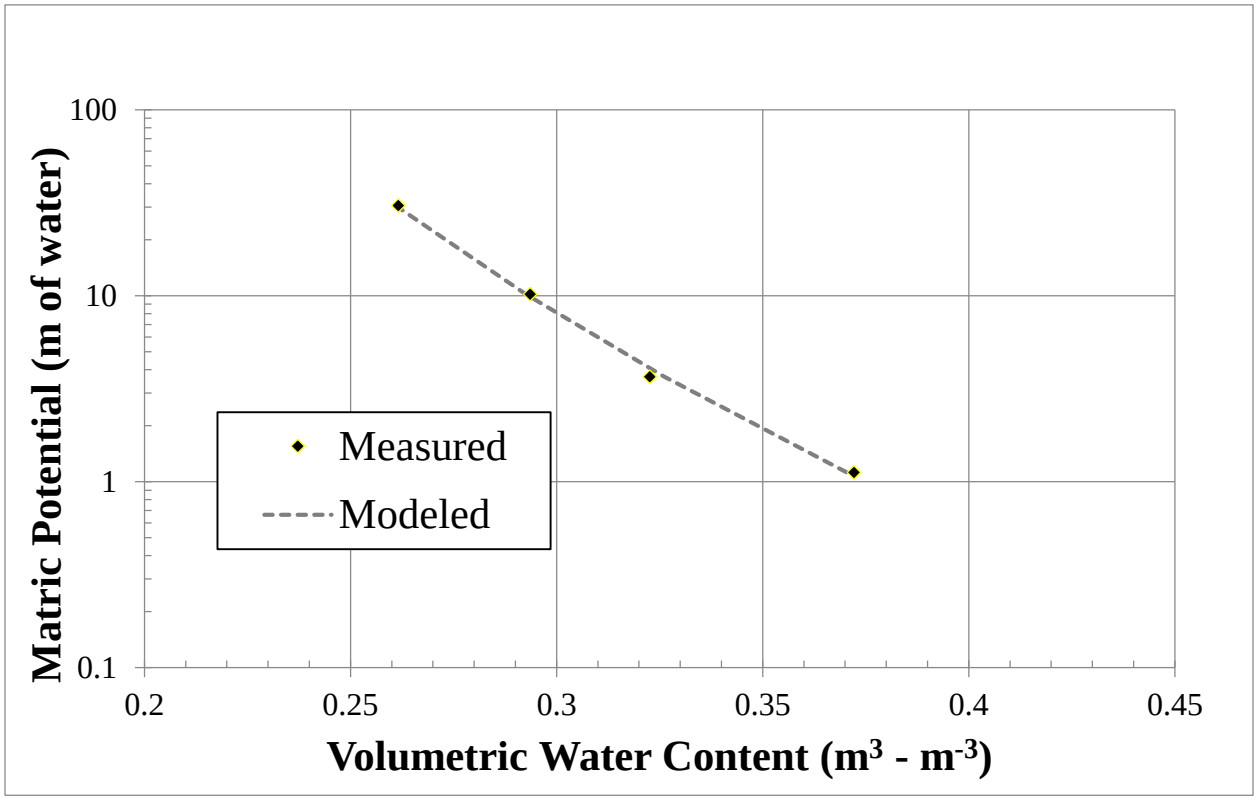

Figure 16. Moisture retention curve for a core collected at Ruby Pasture Pit in Horizon 2.

Particle Size Distribution

Oven dried soil samples were weighed and physically broken down using a mortar and pestle. The samples were suspended in a sodium hexametaphosphate solution (25mL of a 50g/L solution) and sonicated for 5 min and then poured into an empty 1 L graduated cylinder. The soil sample was placed into the 1 L graduated cylinder and topped off with distilled water. The graduated cylinder was shaken to suspend the soil particles and placed on the countertop. A soil hydrometer (ASTM Standard-D422) was used to measure the density of the solution over time as particles settled out of suspension. The solution density over time is related to soil particle size by Stoke's Law. As the hydrometer method accurately characterized silt and clay sized fraction a sieving procedure was employed to characterize the sand size fraction. The soil particles on the bottom of the graduated cylinder after settling were oven dried and applied to a sieve stack (#10 - #20 - #30 - #50 - #80 - #100, USDA Standard Sieves). The sieve stack was mechanically agitated for 20 min. The mass of soil accumulated in each sieve measured as was the total dried soil material placed in the sieve stack. Through this procedure particle size distribution, texture class, porosity, bulk density and saturated volumetric moisture content was determined.

Saturated Hydraulic Conductivity

An apparatus (generic Mariotte bottle and Tempe Cell, Soilmoisture Equipment) was used to apply a constant head of pressure on an undisturbed soil core. To achieve saturation the soil core was flushed with 10 pore volumes of carbon dioxide and then flushed with 10 pore volumes of de-aired simulated rainwater solution (1g of thymol and excess of $CaSO_4$ were added to 5 L of deionized water followed by a vacuum pump applied to the solution for 24 h).

The pressure head before and after and the discharge rate through the apparatus was measured and related to effective hydraulic conductivity using Darcy's Law. Saturated hydraulic conductivity was then calculated by correcting for the friction loss due to the apparatus itself.

Modeling and Analysis Methods

HYRDUS 1-D Modeling

The software package HYDRUS 1-D (Simunek et al., 1998) was used to investigate many questions. The objectives and questions include:

- Determining specific yield from soil hydraulic characterization. Model parameters are provided (appendix a.VII, electronic appendix filenames: Specific Yield at Granite Boulder Pasture_Full Soil Hydraulic Characterization.h1d, Specific Yield at Ruby Pasture_Full Soil Hydraulic Characterization.h1d);
- Determining specific yield from texture class. Model parameters are provided (electronic appendix filenames: Specific Yield from Field Texture_ Granite Boulder Pasture,h1d, Specific Yield from Field Texture_Ruby Pasture.h1d);
- Does hysteresis have an effect on the break in slope of diurnal water table fluctuation during the night? Model parameters are provided (electronic appendix filenames: With Hysteresis Enabled_Loam.h1d, With Hysteresis Enabled_SiCL.h1d, With Out Hysteresis Enabled_SiCL.h1d, Large Difference in Alpha_SiCL.h1d, Small Difference in Alpha_SiCL.h1d);

- Which performs better, a variable or constant specific yield? Model parameters are provided (appendix a.VI, electronic appendix filename: Variable vs Constant Specific Yield.h1d);
- Which performs better, a record to water table elevation or a record of total soil moisture? Model parameters are provided (appendix a.VII, electronic appendix filenames: Triangular Root Distribution.h1d, Inverted Triangular Root Distribution.h1d, Rectangular Root Distribution.h1d, Disconnected Water Table.h1d);
- How does the specific yield change with water table depth BGSL? Model parameters are provided (appendix a.VIII, electronic appendix filename: Length BGSL vs Specific Yield_No Wave_1 Soil.h1d, Length BGSL vs Specific Yield_No Wave_2 Soils.h1d, Length BGSL vs Specific Yield_Yes Wave_2 Soils.h1d);
- Determining evapotranspiration using Penman-Monteith. Model parameters are provided (electronic appendix filename: Evapotranspiration Using Penmam Monteith_Ruby Pasture.h1d).

Nachabe's Modified Soil Water Budget

A time series of observed soil moisture content was generated by using volumetric moisture content probes by depth where each sensor represented a given soil thickness. At Ruby Pasture the volumetric moisture content sensors at 10, 20, and 30 cm BGSL produced reasonable readings. Each sensor was corrected for effects of temperature according to Decagons standard calibration procedure (Decagon, 2007). The temperature corrected readings from each probe were weighted by the soil thickness that it represented. The sum of the

weighted volumetric soil moisture probe readings were taken to compute a total soil moisture time series. Applying Nachabe's modified White expression (Eq. 5)

$$Q = \frac{(TSM_{0400h} - TSM_{midnight})}{4} \quad \text{Eq. 4}$$

$$ET = TSM_i - TSM_{i+1} + 24 * Q \quad \text{Eq. 5}$$

Where:

TSM = total soil moisture (length of water)

i = time step (days)

ET = evapotranspiration (length of water/day)

Nachabe's **Q** (depth of water/hour) is similar to White's **r** (depth of aquifer/hour) in that it is computed by fitting a line to the record of total soil moisture between midnight and 4am. By working with a record of total soil moisture instead of water table elevation the need for the specific yield value is eliminated.

Pump Test Analysis

Two conceptual groundwater models were selected. The Theis (1935) Model for a transient, confined aquifer was selected due to its relative simplicity. The Neuman (1972) Model for a transient, unconfined, and anisotropic aquifer was selected because our field data suggests an unconfined aquifer and the Neuman Model solves directly for specific yield. The details of the data analysis can be observed in appendix a.V

Fitting Evaporation for Specific Yield

From a record of water table elevation through time at the small observation well array the White parameters **s** (net change in a 24 hour period) and **r** (the slope between midnight and 4am) were determined for a given day using a Matlab script (electronic appendix filename: Evapotranspiration from Water Table Elevation_Field Data_White Method.m) . The terms $\mathbf{s}_{(white)}$ and $r_{(white)}$ as well as the daily estimate of $ET_{(penman\text{-}montieth)}$ were taken into excel. The White Method was applied to the $s_{(white)}$ $r_{(white)}$ and an assumed constant specific yield term producing a daily estimate of $ET_{(white)}$. The sum of squared error between $ET_{(penman\text{-}montieth)}$ and $ET_{(white)}$ was minimized while changing the specific yield term to find the value of specific yield that produced the best fit between the two ET estimates using excels GRG nonlinear solver (electronic appendix filename: Specific Yield from Fitting ET White to ET Penman Montieth.xlsx).

Vegetation Mapping

To investigate the spatial extent in inter-season water availability a vegetation hydrologic index was developed. Each species observed at the field site a hydrologic classification was referenced based on the ecophysiology of the species response to water (delta-intkey.com). The hydrologic index employed assigned a number according to the hydrologic classification, where 1 for xerophyte, 2 for xeromesophyte, 3 for mesophyte, 4 for mesohydrophyte, and 5 for hydrophyte. For each species at each sampling point the hydrologic index number was weighted by the percent cover of the respective species resulting in hydrologic index that could average between 1 and 5. These points were put in an ordinary

Kriging Model (Geostatistical Wizard in ArcMap 10.1) to produce a continuous surface of the vegetation hydrologic index (electronic appendix filenames: Vegetation Points_GBP.shp, Vegetation Points_RP.shp).

To investigate the spatial extent of intra-seasonal water availability the observed values of percent standing dead were put in an ordinary Kriging Model (Geostatistical Wizard in ArcMap 10.1) to produce a continuous surface of the percent standing dead.

Eddy Covariance

An integrated CO_2/H_20 open-path gas analyzer and 3D sonic anemometer (Irgason, Campbell Scientific) was deployed at a height of 2m and 140m downwind the experiment towards at Granite Boulder Pasture. The Irgason measures absolute carbon dioxide, water vapor densities, 3D wind speed, sonic air temperature, air temperature, and barometric pressure at a frequency of 10 observations per second. Matlab code authored by Higgins, C., which solves for the sum of the moisture flux, which was used to estimate the evapotranspiration at the field scale.

Penman Monteith at Ruby Pasture

A weather station (Vantage Pro2, Davis Instruments) was deployed at a height of 1.75 m at the center of Ruby Pasture. The Vantage Pro2 measured barometric pressure, dew point, temperature, relative humidity, rain fall, solar radiation, wind speed, and wind direction. A software package (Penman-Monteith Package in HYDRUS 1-D Simunek et al., 1998) was used to take the record of variables collected at the weather station to an estimate of

evapotranspiration. The variable of bulk surface resistance we determined from the mean vegetation height and mean percent ground cover at Ruby Pasture.

The Vantage Pro2 at Ruby Pasture was only successfully deployed for a small fraction of the length of the experiment. To produce a complete record at Ruby Pasture weather station variables were extrapolated from a nearby station. Ruby Pasture was bounded upstream by the Forrest Weather Station, which was deployed 11km upstream in the riparian zone of the main channel, and bounded by the Dunstan Weather Station, which was deployed 8km downstream in the riparian zone of the main channel. The Ruby, Forrest and Dunstan records were compared when simultaneous data was collected. The following expression was developed

$$Error = |a * Forrest_{short} + b * Dunstan_{short} + Ruby_{observed}|$$

Using solver, the sum of square errors between the data sets were minimized by changing coefficients a and b. The long time series of data at ruby was then modeled by

$$Ruby_{modeled} = a * Forrest_{long} + b * Dunstan_{long}$$

The modeled data (electronic appendix filename: EkoModeledData.xlsx) was then processed for the Penman-Montieth inputs, and the Penman Montieth Package in HYDRUS 1-D (Simunek et al., 1998) was used to estimate evapotranspiration (electronic appendix filename: Evapotranspiration Using Penmam Monteith_Ruby Pasture.h1d).

Summary of Materials and Methods

Due to limitations in equipment, time, and unfortunate circumstances some of our data collection effort was compromised. Most notably were

- That by the time we installed the instruments at Granite Boulder Pasture the transition from a shallow water table to a deep water table and the diurnal water table fluctuations had already occurred;
- The failure of 5 volumetric moisture content sensors (40, 50, 60, 70, and 78 cm BGSL) at the Ruby Pasture Pit;
- That the daily change in volumetric moisture content at Granite Boulder Pasture was not detected likely due to the application of water when filling in the clay dominated pit;
- The first 10d of Eddy Covariance data was deleted when rebooting the Irgason after a power supply failure;
- The weather station was only logging data at Ruby Pasture for 3 consecutive days;
- The error associate with the measurement of water table elevation after correcting for the barometric pressure was ± 3mm greater that the targeted ± 1mm

Although we faced limitations in the field and shortcomings in our datasets we proceeded through the data analysis with an awareness of the data gaps.

Chapter 3: Site Description

Situation of the Sites

The field sites were 2km apart in the semi-arid Middle Fork John Day Watershed (Fig. 17, 18, 19 and 20).

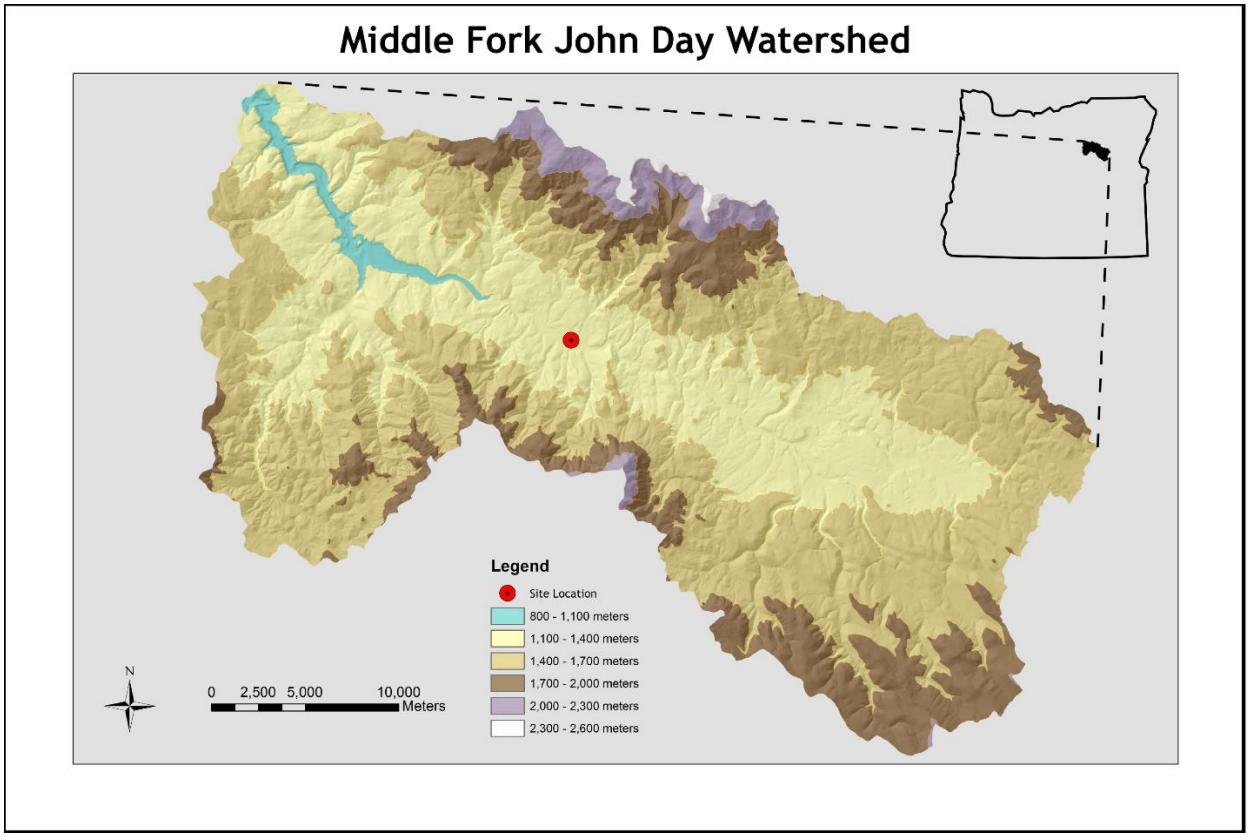

Figure 17. The situation of the Middle Fork John Day (MFJD) Watershed.

The MFJD Watershed is an Eastern Oregon semi-arid watershed experiences a xeric moisture regime and a mesic temperature regime. The headwaters of this watershed demonstrate relatively shallow hillslopes compared to the central and down drainage sections.

The site location is positioned between the two high points of the watershed, Vinegar Hill to the northeast and Dimple Hill to the southeast.

Figure 18. The situation of the field sites.

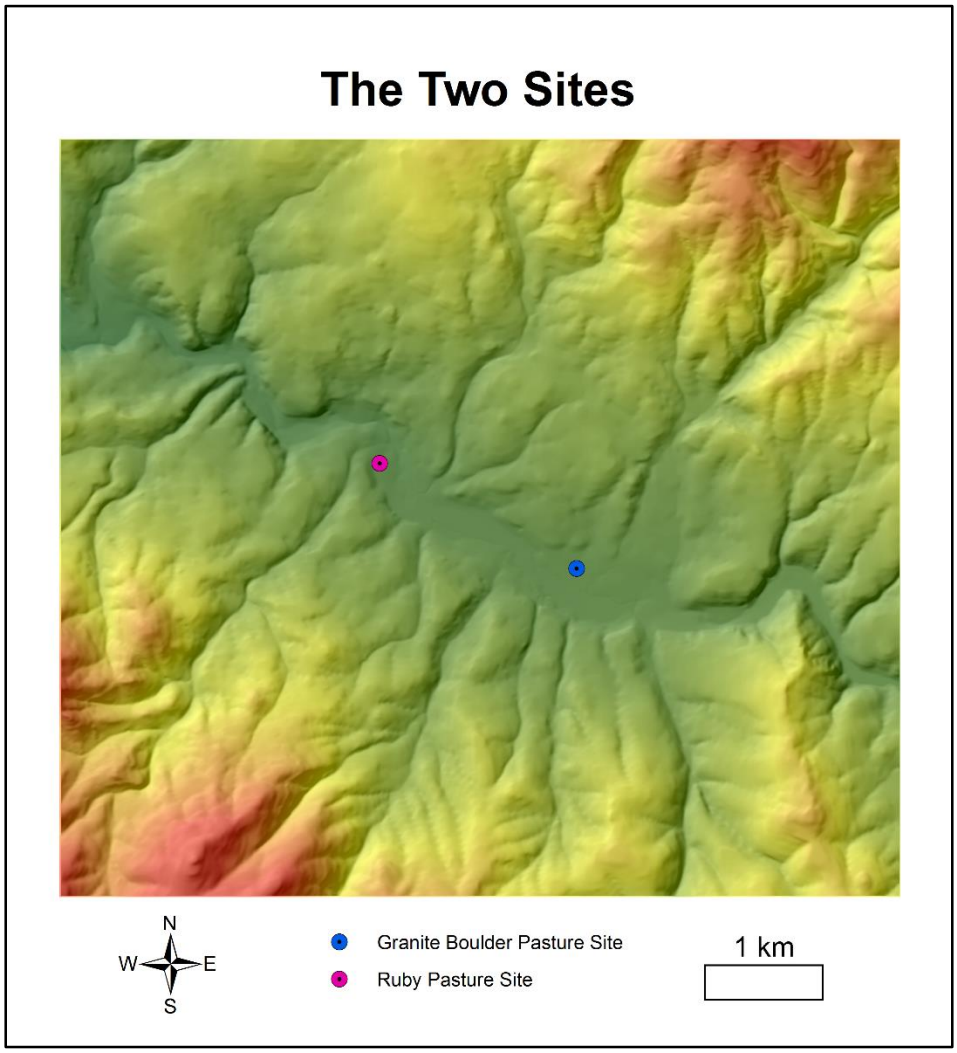

Granite Boulder Pasture is located on the alluvial fan of Granite Boulder Creek (Fig. 18). Ruby Pasture is located on the MFJDR flood deposits, just on the up drainage side of an alluvial fan which forces the MFJDR into a constrained channel.

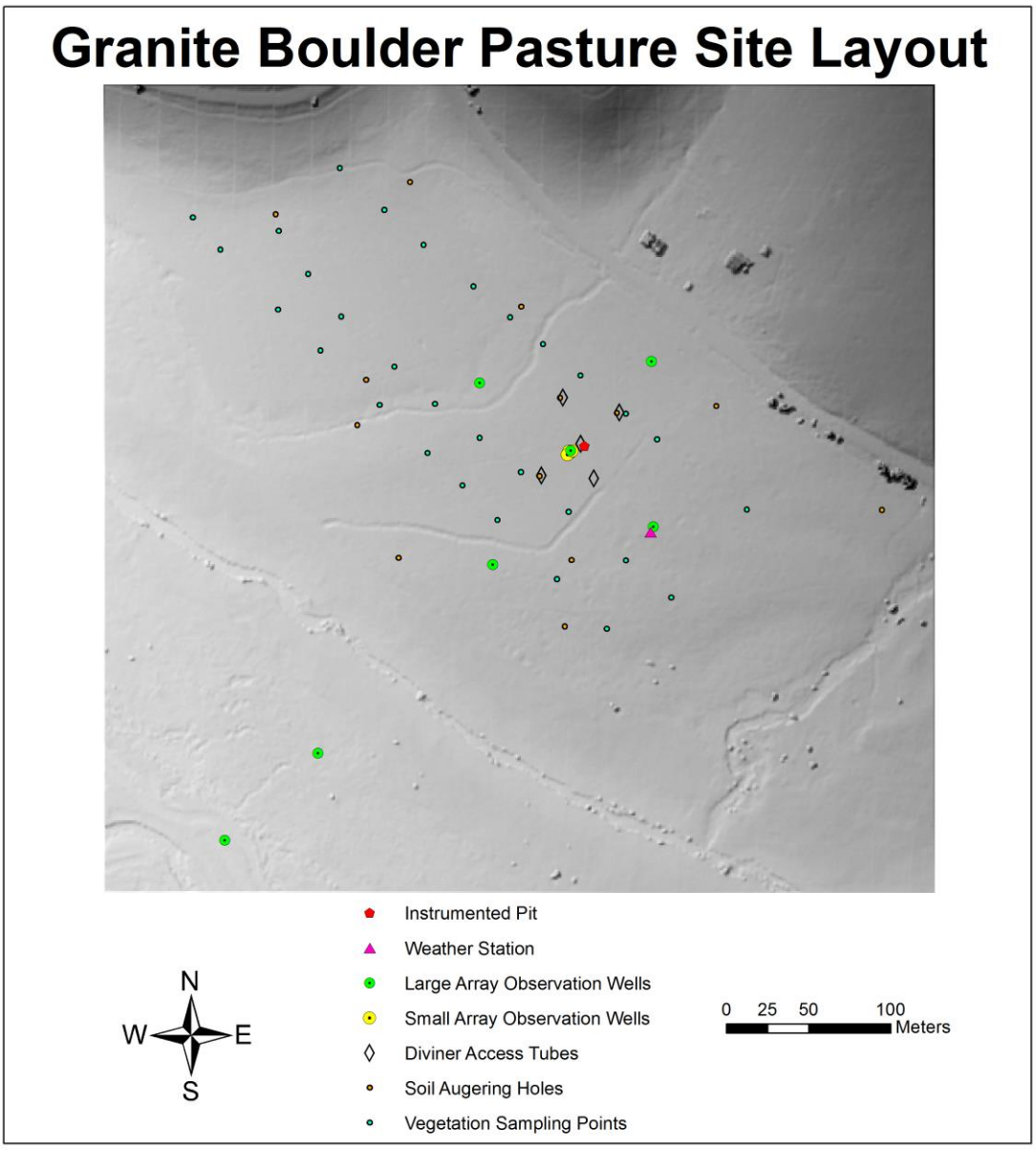

Figure 19. The experiment layout at Granite Boulder Pasture.

The central cluster of instruments is located in proximity to key surface features (Fig. 19). The current channel of Granite Boulder Creek lies to the Southeast, which drains to the MFJDR located along the Southwest corner of this map. The zone affected by dredge mining runs parallel to the MFJDR, boarding the site of the Southwest. The historic Duwit homestead remains to the Northwest, with an associated access road and flood irrigation ditch boarding

the site to the Northeast. Two seemingly artificial drainages run through the site from Northwest to Southeast. This site has experienced frequent natural and anthropogenic disturbances.

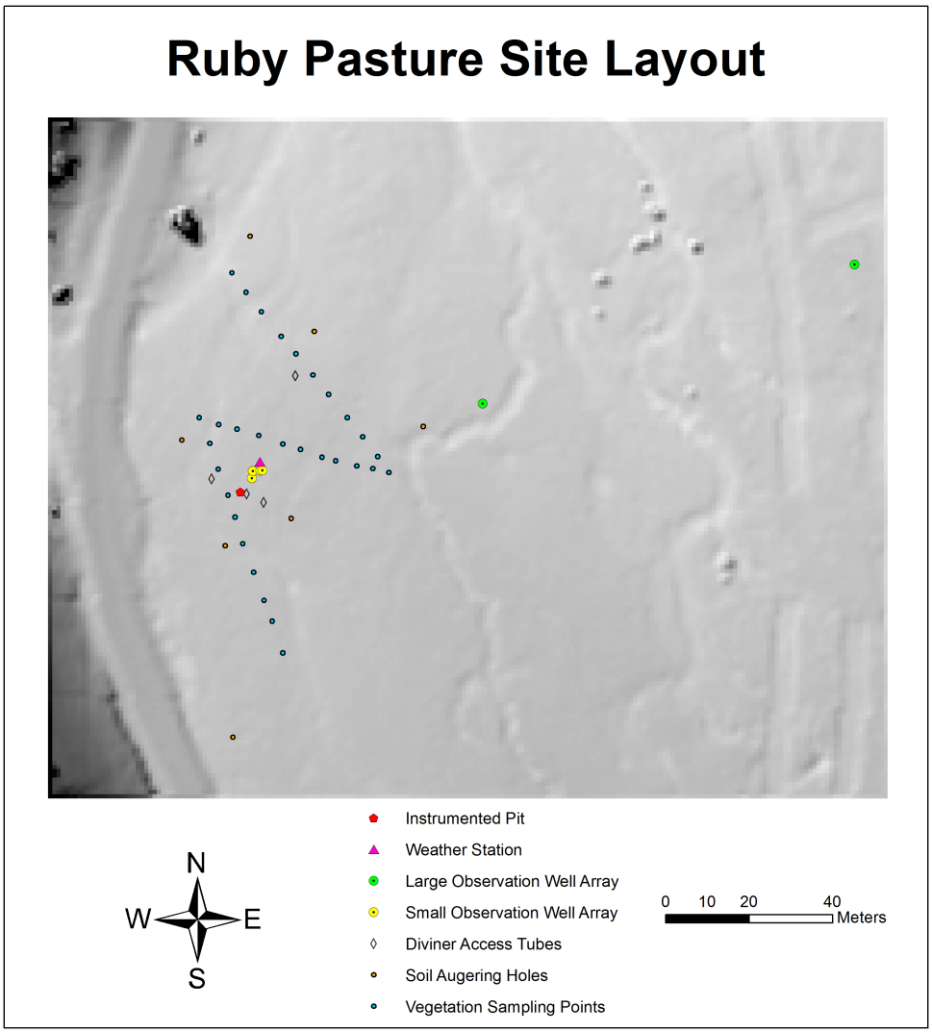

Figure 20. The experimental layout at Ruby Pasture.

A paved roadway boarders the site to the West along the transition from floodplain alluvial desposits to the hillslopes (Fig. 20). The main channel is located to the northeast of this map. Notice the braided historic surface channels through the alluvial flood deposits. The

vegetation sampling points at this site were aligned on zig zag transect which is different than the three parallel transects performed at Granite Boulder Pasture.

Soil Description

Auger holes were used to identify the spatial distribution of aquifer materials at Granite Boulder Pasture (Fig. 21).

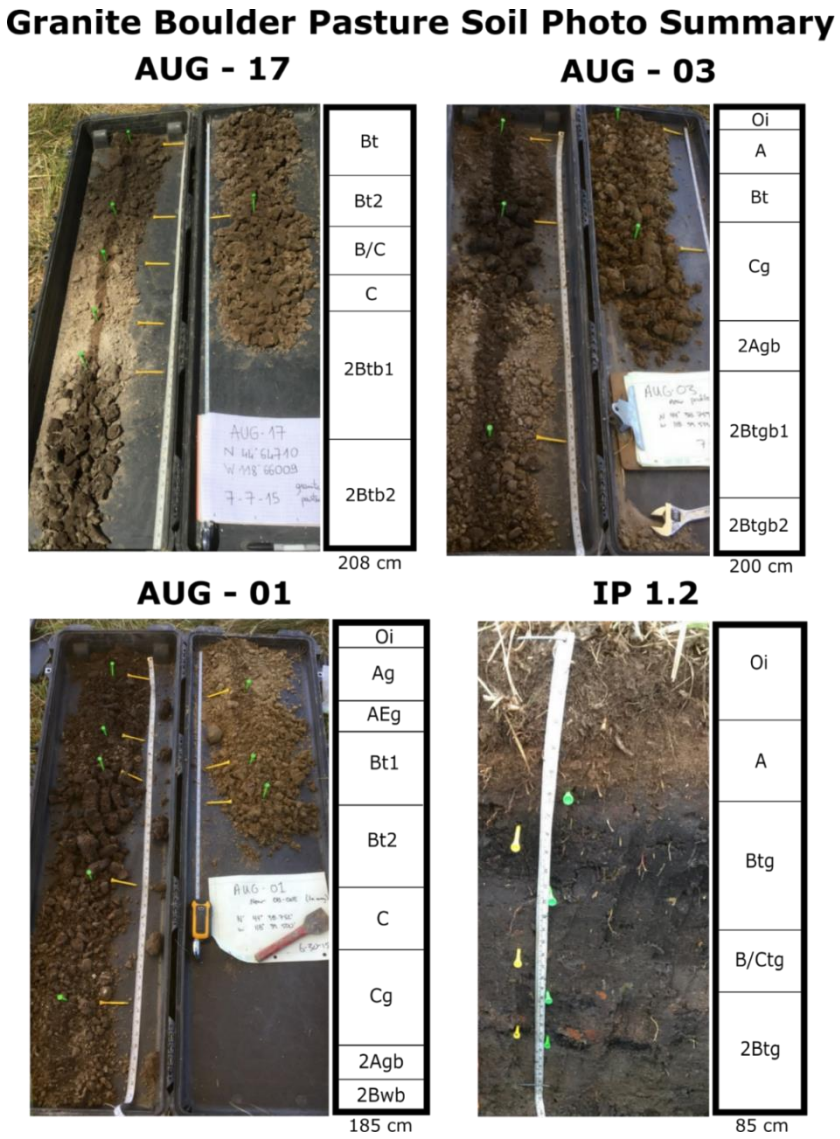

Figure 21. Four soils found at Granite Boulder Pasture.

The main soil type at Granite Boulder Pasture is a sandwich soil where a well-developed soil was buried by reworked volcanic ash and subsequently followed by soil development. A medium textured A horizon was positioned over a fine textured Bt horizon, over a medium textured C horizon, over a fine textured 2At or 2Bt horizon.

The parent material deposition can be explained by a volcanic ash deposits across the watershed, subsequent reworking by Granite Boulder Creek and re-deposition when the creek visited the furthest extent of its alluvial fan. The redeposited material provided an unweathered ground surface level. As weathering processes occurred over time the soils become more clay enriched. This sequence of events occurred more than once generating many buried soils.

The observation of an extensive Oi horizon is inconsistent with expectations of soil underlying a pasture because the organic matter additions of pasture is either at depth via their roots or easily decomposable material of their above ground biomass. However, a potential explanation is that it is of anthropogenic origin due to the proximity of the pasture to the barn of the Duwit homestead. Animal waste generated at the barn, located on the uphill side of the site, was probably spread in the most convenient location. Another explanation for the long residence time of this organic matter is that the decomposition rate was hampered by soil saturation.

Gleyed horizons were regularly found in the lower elevations of the site providing evidence for a seasonally shallow groundwater table on the centennial time scale (electronic appendix filenames: Field Soil Descriptions_GBP.xlsx).

Auger holes were used to identify the spatial distribution of aquifer materials at Ruby Pasture (Fig. 22).

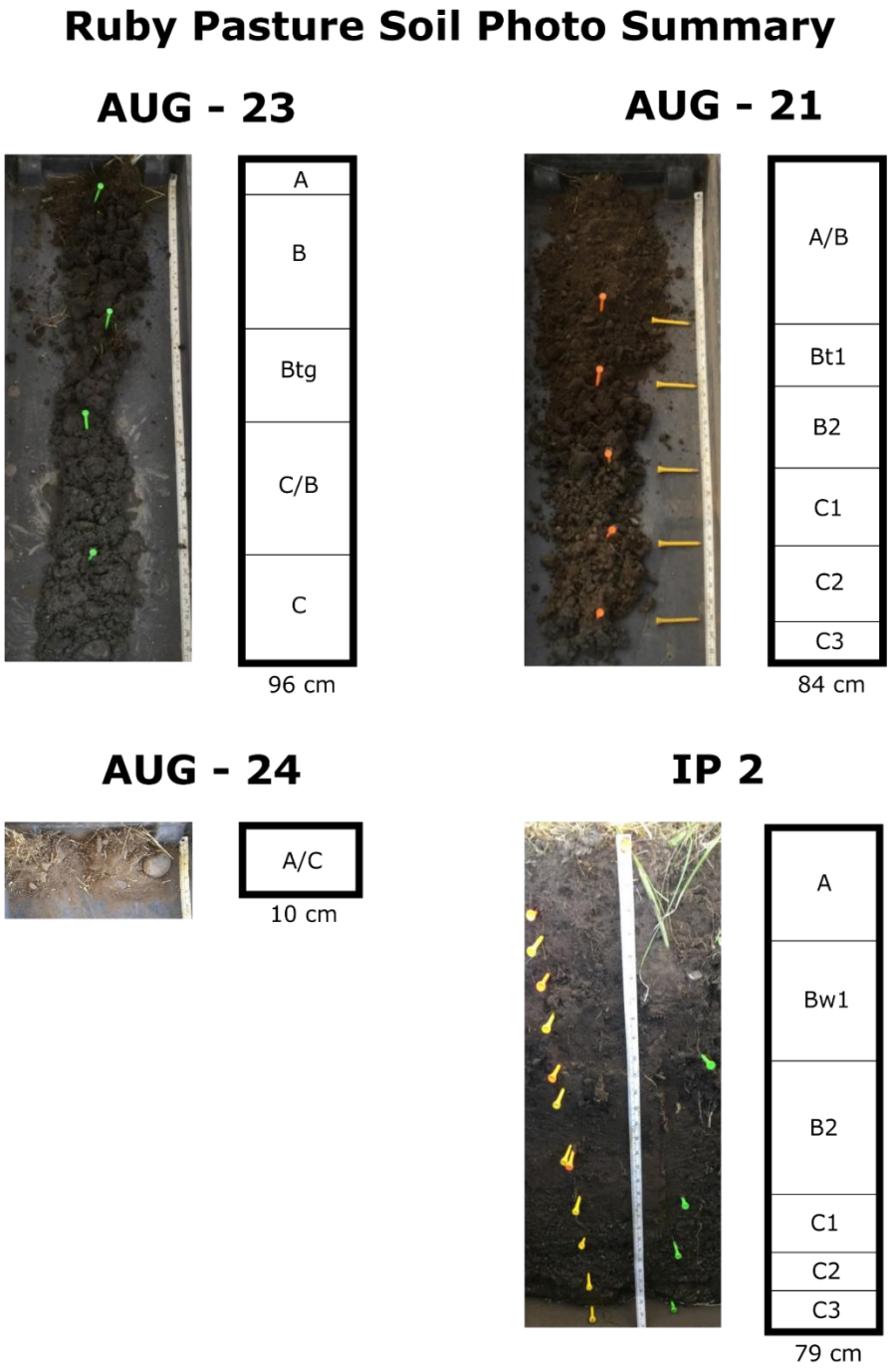

Figure 22. Four soil profiles at Ruby Pasture.

Ruby Pasture is in the flood plain deposits of the Middle Fork John Day River. Ruby Pasture is on the up drainage side of an alluvial fan which creates a channel constriction for the Middle Fork John Day River. The channel constriction forces high energy water flow to reduce its energy to get through the constriction. The transition from a high energy flow to a low energy flow reduces the capacity of the fluid to suspend particles and thus deposits particle with sizes proportionate to that of the flow energy change. The resulting main soil type at Ruby Pasture is an expression of Stoke's Law, in which, a gradient in particle size from finer to coarser with depth from ground surface is observed. At Ruby Pasture there tends to be a medium textured A horizon over a slightly clay enriched medium textured B horizon over a fine sandy C1 horizon over a sandy C2 horizon over a cobbly and sandy C3 horizon.

Spatial soil heterogeneity at Ruby Pasture is large. This heterogeneity was likely caused by uneven initial distribution of material from a series flood events, which may have reworked with removal of material in subsequent events.

Due to the limitations in the augur sampling method, material below cobbles encountered with the soil augur were not collected. In areas of the site where standing dead vegetation were observed on June 22nd, a very shallow (1-5cm) layer of volcanic ash positioned over cobbles was found (AUG-24, Fig. 19). Old shallow surface drainage patterns bordered the site and the soils at those locations tended to be a sand layer positioned over cobbles. The vegetation at the shallow surface drainages demonstrated a more hydrophilic ecophysiology than the other vegetation at the site. Any slight mounds tended to demonstrate an 80 cm deep soil with a medium textured A horizon over a slightly clay accumulated medium textured B

horizon over a fine sandy C1 horizon over a sandy C2 horizon over a cobbly and sandy C3 horizon (electronic appendix filenames: Field Soil Descriptions_RP.xlsx)

Vegetation Description

The vegetation at Granite Boulder Pasture (Fig. 23) was different than the vegetation at Ruby Pasture (Fig.24) in their species composition (Table 3 and 5), and Shannon's Diversity (Table 4 and 6). Similarities existed in their mean vegetated height and mean surface fraction. Both sites were most likely seeded to pasture during the settlement of the area by the Duwit family approximately 80 years ago. Both pastures are lightly used for grazing (~2 to 4 weeks per year). Granite Boulder Pasture was grazed from June 1st to June 14th 2015.

Figure 23. Granite Boulder Pasture. Image taken on July 22nd 2015.

Table 3. Predominate cover types at Granite Boulder Pasture.

Predominant Cover Types (title)	Average Percent Cover (%)	Occurrence (%)
Alopecurus	20	87
Poa	10	80
Juncus	3	70
Carex	2	70
Standing Dead	63	100
Bare Ground	2	100

Table 4. Vegetated cover properties at Granite Boulder Pasture.

Mean Vegetation Height	26.1	(cm)
Mean Surface Fraction	35	(%)
Mean Shannon's Diversity	0.57	(-)

Figure 24. Ruby Pasture. Image taken on July 22nd 2015.

Table 5. Predominate cover types at Ruby Pasture.

Predominant Cover Type	Average Percent Cover (%)	Occurrence (%)
Carex	8	93
Trifolium hybridum	4	50
Phleum pratense	3	67
Poa	3	87
Juncus	2	80
Standing Dead	60	100
Bare Ground	11	73

Table 6. Vegetated cover properties at Ruby.

Mean Vegetation Height	30	(cm)
Mean Surface Fraction	29	(%)
Mean Shannon's Diversity	1.66	(-)

Summary of the Site Description

The field sites are both quite heterogeneous in soil and vegetation distribution making these sites preferable for testing the limitations of the White Method. Granite Boulder Pasture is located on the far edge of Granite Boulder Creek's alluvial fan (Fig. 19) producing a sandwich soil (Fig. 21) and a moderately diverse vegetation (Table 3) that exhibits a mesophytic ecophysiology. Ruby Pasture is located on the up drainage side of a channel constriction (Fig. 18) producing a Stoke's soil with subsequent redistribution of material (Fig.22) and a highly diverse vegetation (Table 5) that exhibits a mesohydrophytic ecophysiology.

Chapter 4: Estimating Evapotranspiration

Introduction

In this chapter we present the results of the field efforts to estimate evapotranspiration. The field results inspired the question 'Would a water table elevation record or a total soil moisture record be more effective in estimating evapotranspiration?' This question was answered using numerical modeling results presented in this chapter.

Field Data

Four methods of estimating evapotranspiration were employed to interpret the data obtained from the field sites during July of 2015 (Fig. 25). The Eddy Covariance Method is the most accurate method (Ding et al., 2010) employed in the field. For our purposes the Eddy Corvariance results are considered to be the true value of daily evapotranspiration. The Penman Monteith Method is a classical model using weather station variables but requires an estimate surface resistance which is difficult to accurately estimate (Allen et al., 2006) The White Method and Nachabe Method are two below ground methods that were explored using a record of water table elevation and total soil moisture respectively.

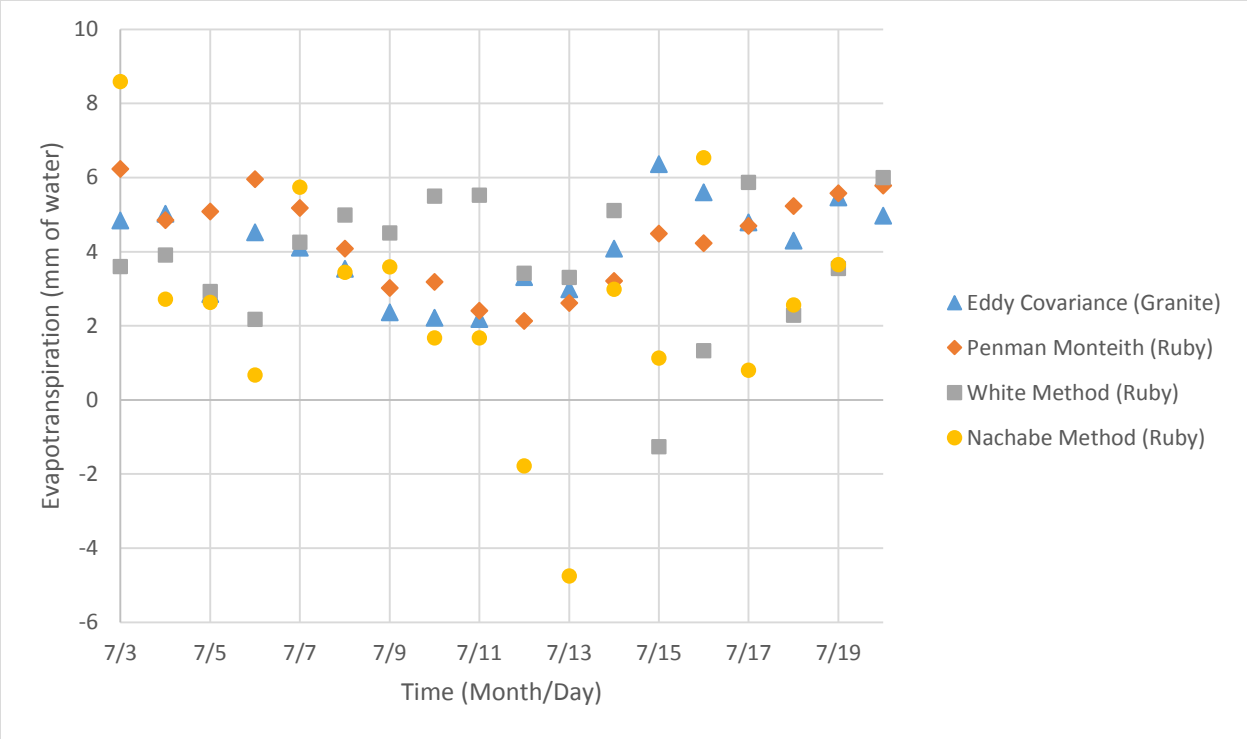

Figure 25. Estimating evapotranspiration from field data.

What can explain the seemingly accurate estimates of evapotranspiration from the Nachabe Method during the time period of 7/7 to 7/11? The evapotranspiration rate declined during, and the soil water pressure at 15cm BGSL decreased from -2000cm to -4000cm. The decline in evapotranspiration rate and decrease in soil water pressure suggests that the vegetation was transitioning into a stress period, thus limiting the transpiration. During the plant stress period of 7/7 to 7/11 the Nachabe Method tracks the evapotranspiration rate determined from the local weather stations fairly well ($R^2 = 0.77$) (Fig. 28). Note that the record of total soil moisture was done mostly by one volumetric moisture content sensor placed at 30cm BGSL.

The precipitation event on 7/12 and 7/13 confounded both the White and the Nachabe Methods. The precipitation event was patchy across the watershed and rain gauges at the field

sites were not logging data during the event. The Nachabe Method responded quickly to the precipitation event by producing negative estimates of evapotranspiration on the days of precipitation, which suggests that the Nachabe method might be measuring the daily net water flux across the ground surface level rather than evapotranspiration alone. The White Method responded slowly to the precipitation event, producing a negative estimate of evapotranspiration two days after the days of precipitation. This suggests that the White Method might be able to pick up a precipitation pulse delayed by the friction loss of the watershed. One of White's assumptions is that the method only works during a precipitation free period. Thus the precipitation period was not taken into the direct comparison of daily evapotranspiration rates (Fig. 26, 27 and 28).

Penman Monteith, White, and Nachabe methods were performed at the Ruby Pasture site. Eddy Covariance was performed two kilometers up drainage at the Granite Boulder Pasture site. The Eddy Covariance results were compared to the Penman Monteith results to determine coefficient of determination between the two sites and two methods (($R^2 = 0.40$) (Fig. 23). The White Method results were compared to Penman Monteith results during the time period when the assumption of no precipitation was not violated ($R^2 = 0.23$) (Fig. 27). Lastly I compared the Nachabe Method to Penman Monteith to determine the coefficient of determination between the two methods at the same site (Fig. 28).

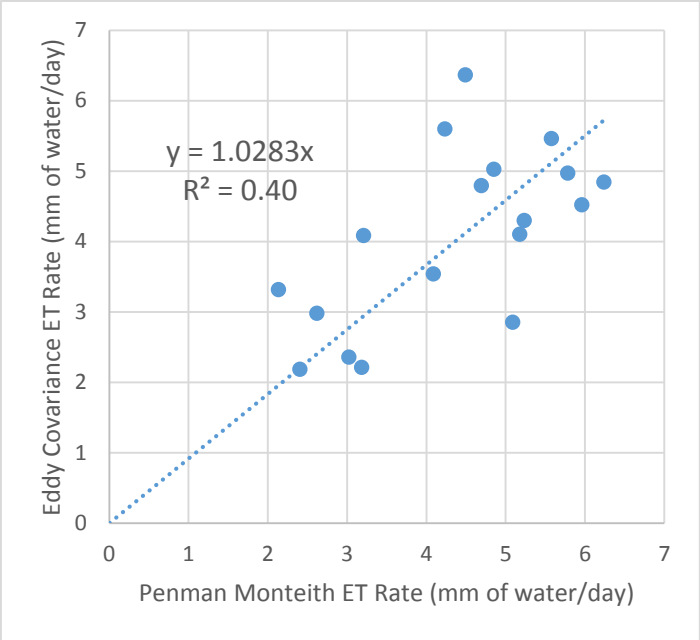

Figure 26. Comparing the results of the Eddy Covariance against Penman Monteith. By comparing these two above ground methods across two sites we can see that the ET range should be between 2 to 6.5 mm/day.

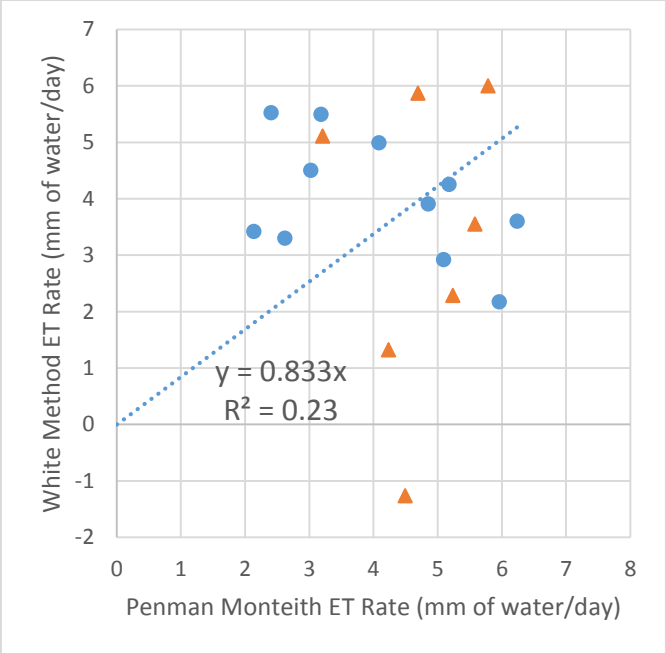

Figure 27. Comparing the results of the White Method against Penman Monteith. The orange triangles were not included in the correlation because of the violation of the precipitation free period required for the White Method.

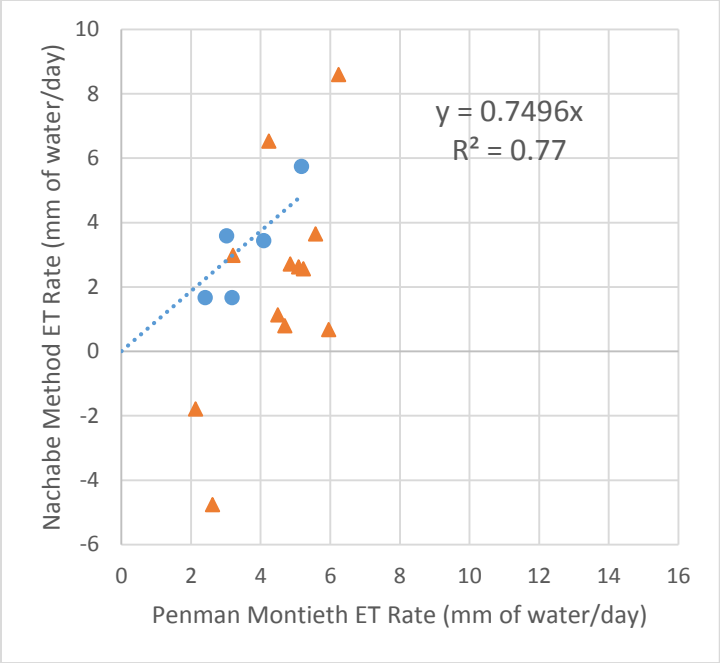

Figure 28. Comparing the results of the Nachabe Method against Penman Monteith. The orange triangles were included in the correlation due to the limitations in sensing a total soil moisture record caused by sensor failure.

Table 6. R^2 summary table for field results.

R^2 Summary Table for Field Results			
Full Time Series			
Dependent	Independent	Same Site (Y/N)	R^2
Penman Monteith	Eddy Covariance	N	0.4
White Method	Penman Monteith	Y	0.04
Nachabe Method	Penman Monteith	Y	0.3
White Method	Eddy Covariance	N	0.26
Nachabe Method	Eddy Covariance	N	0.1
Selected Time Series			
Dependent	Independent	Time Range	R^2
White Method	Penman Monteith	7/3 to 7/13	0.23
Nachabe Method	Penman Monteith	7/7 to 7/11	0.77
White Method	Eddy Covariance	7/3 to 7/13	0.26
Nachabe Method	Eddy Covariance	7/7 to 7/11	0.75

Field Data Conclusion

By comparing the R^2 values between the four methods during both (Table 6), I come to the conclusion that the White Method is not informative regarding evapotranspiration estimation ($R^2 = 0.23$) (Fig. 27). The two weather stations separated by only 2km slightly agreed ($R^2 = 0.4$) (Fig. 26). After excluding the data when the functional volumetric moisture content sensor was not representative of the total soil moisture of the profile the Nachabe Method correlated with the local weather station ($R^2 = 0.77$) (Fig. 28). By looking at the field data alone it appears that the Nachabe Method ($R^2 = 0.77$) outperformed the White Method ($R^2 = 0.23$) when compared to the local weather station.

The Spark for Numerical Modeling

Given the all of the environmental limitations, equipment failure, and data scarcity the uncanny accuracy of a single volumetric moisture content sensor placed at 30cm BGSL used to compute a total soil moisture record (Fig. 29) than used to estimate evapotranspiration inspired a new line of thought. If sensor cost and sensor error were not considered, a record of total soil moisture would probably be more accurate and applicable to longer time frame than a record of water table elevation.

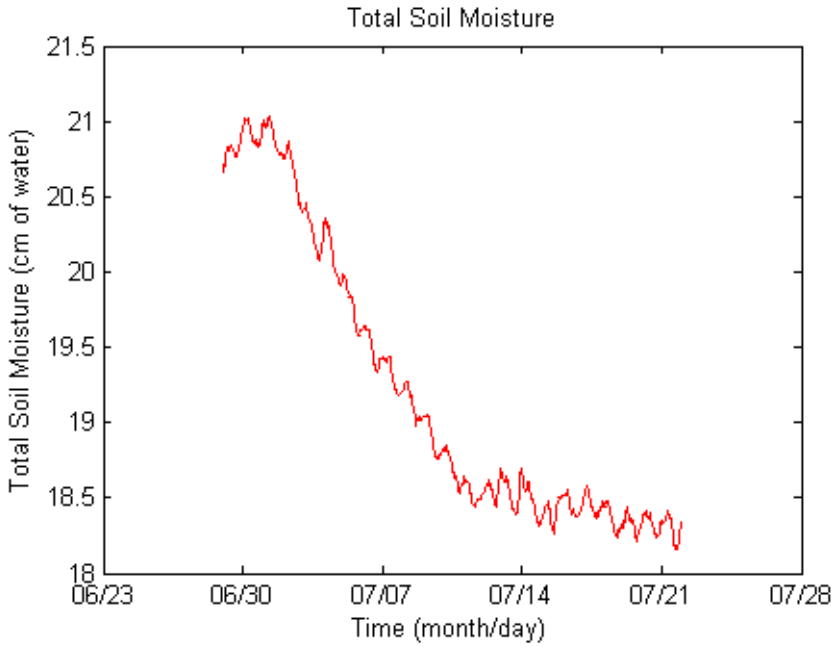

Figure 29. Total soil moisture record at Ruby Pasture.

Numerical Modeling Setup

I dove into this new line of thought and explored two questions. First, does the White Method or the Nachabe Method perform better in their ability to accurately estimate evapotranspiration? Second, under which environmental circumstances does the White Method and the Nachabe method estimate evapotranspiration more accurately? The beauty in numerical modeling is that there is no error associated with sensing a signal, only the error is the lack of the operator's conceptual understanding of the system introduced by the selection of boundary and initial conditions. The specific yield constant was selected as a reasonable value for readily available specific yield for a silty clay loam (S_y = 0.07) (Loheide et al., 2005).

In HYDRUS 1-D two cases were modeled

1. Initially Saturated Profile with a Triangular Root Distribution (electronic appendix filename: Triangular Root Distribution.h1d)
2. Initially Saturate Profile with an Inverted Triangular Root Distribution (electronic appendix filename: Inverted Triangular Root Distribution.h1d)

To help interpret the numerical modeling results the output of numerical modeling runs were explored and plotted using a Matlab script (electronic appendix filename: ET output vs White results and Nachabe results.m). Four plots are provided for each model run (Fig. 30). Figure 30 includes 4 subplots, each of which are informative in coming to a qualitative conclusion regarding the applicability of the White and Nachabe Methods. These subplots can also be used to identify different system behaviors and hopefully provide insight into which conditions the White and Nachabe Methods work.

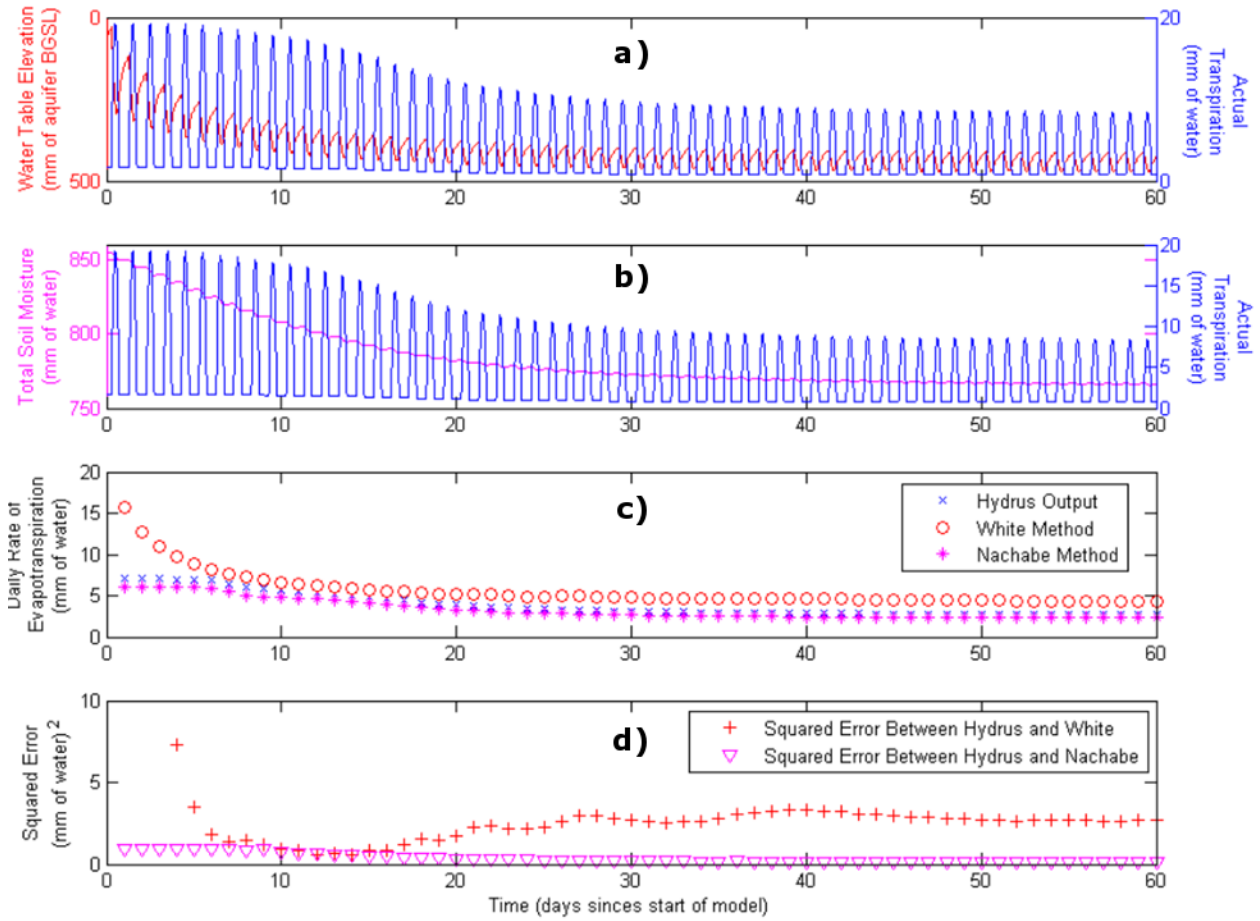

Figure 30. Model results evaluated for the applicability of the White and Nachabe Methods. The specific yield was set to 0.07 [$L_{water} * L_{aquifer}^{-1}$]. **a)** is a dual y axis plot where the known transpiration rate and the water table elevation are plotted versus time. **b)** is a dual y axis plot where total soil moisture content and transpiration rate are plotted versus time. **c)** is a single y axis plot where the daily estimates of evapotranspiration are plotted versus time for three methods: the known HYDRUS Output, the White Method estimate, and the Nachabe Method estimate. **d)** is a single y axis plot where the squared error between the estimated values and the known values are plotted versus time.

By looking at the error alone (Fig. 30.d) the effectiveness and limitations of the White Method can easily be misinterpreted. Theyre are three distinct behaviors within the time series. First, days 1 to 6 where the water table amplitude is affected by the air entry pressure of the material producing a large amplitude (Fig. 30.a) for a small about of water exiting the system. The White Method performed poorly during the air entry affected time period (RMSE = 0.313 cm of water) Second, days 7 to 18 where the actual transpiration rate is declining and there is little change in the water table elevation slope during the night and change in a 24 hour period (Fig. 30.a), the decline in transpiration rate indicates that the plants are beginning to limit their transpiration rate due to plant stress. During the onset of plant stress period, a portion of the water being transpired is from the change in volumetric moisture content, a variable that the White Method cannot detect, however due to our selection of the specific yield this period demonstrates a favorable sample standard deviation (RMSE = 0.115 cm of water) (Table 7). Third, days 19 to 60 where the transpiration rate and the water table shape has stabilized (Fig. 30.a) indicating that the plant has depleted all of the plant accessible volumetric moisture content and the water being transpired is the daily rate of groundwater upwelling. The White Method should perform well during the period of groundwater transpiration, however since we over estimated specific yield the estimates of evapotranspiration are over estimated (Fig. 30.d) (RMSE = 0.176 cm of water). We could optimize the specific yield for the groundwater transpiration time period by minimizing the RMSE from days 19 to 60 by changing specific yield. By doing so the specific yield becomes 0.043 [$L_{water}/L_{aquifer}$] and the root mean squared errors for

the air entry pressure dominated period, the onset of plant stress period, and the groundwater transpiration period are 0.436, 0.183, and 0.004 cm of water respectively (Table 8) (Plot not shown).

The beauty in numerical modeling is the ability to test different configurations of environmental variables. One of the outstanding unknowns in ecohydrology is the effectiveness of roots ability to access water with depth (Hunt and Massori, 2016). To explore this unknown, I selected an inverted triangular root distribution (Fig. 31) re-ran the model and analyzed the modeled results after optimizing the specific yield for the least error during the groundwater transpiration period (Fig. 32).

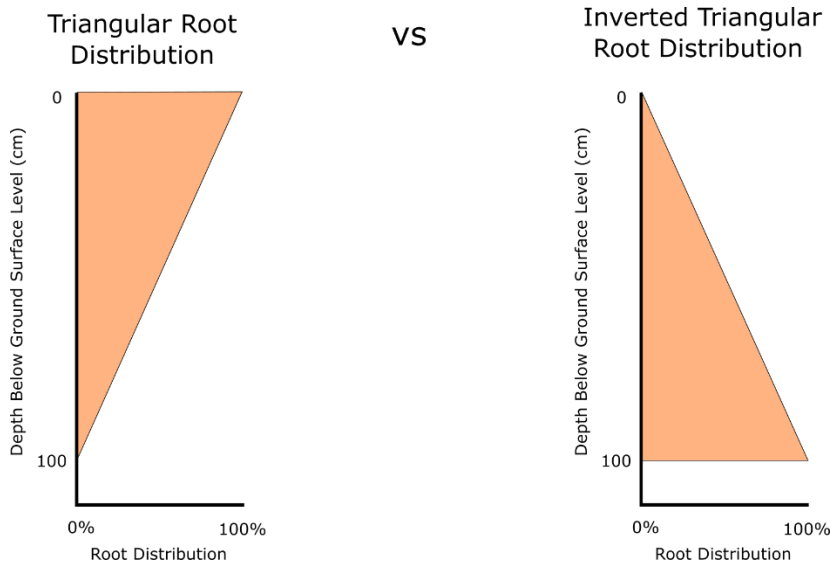

Figure 31. Triangular root distribution versus a rectangular root distribution.

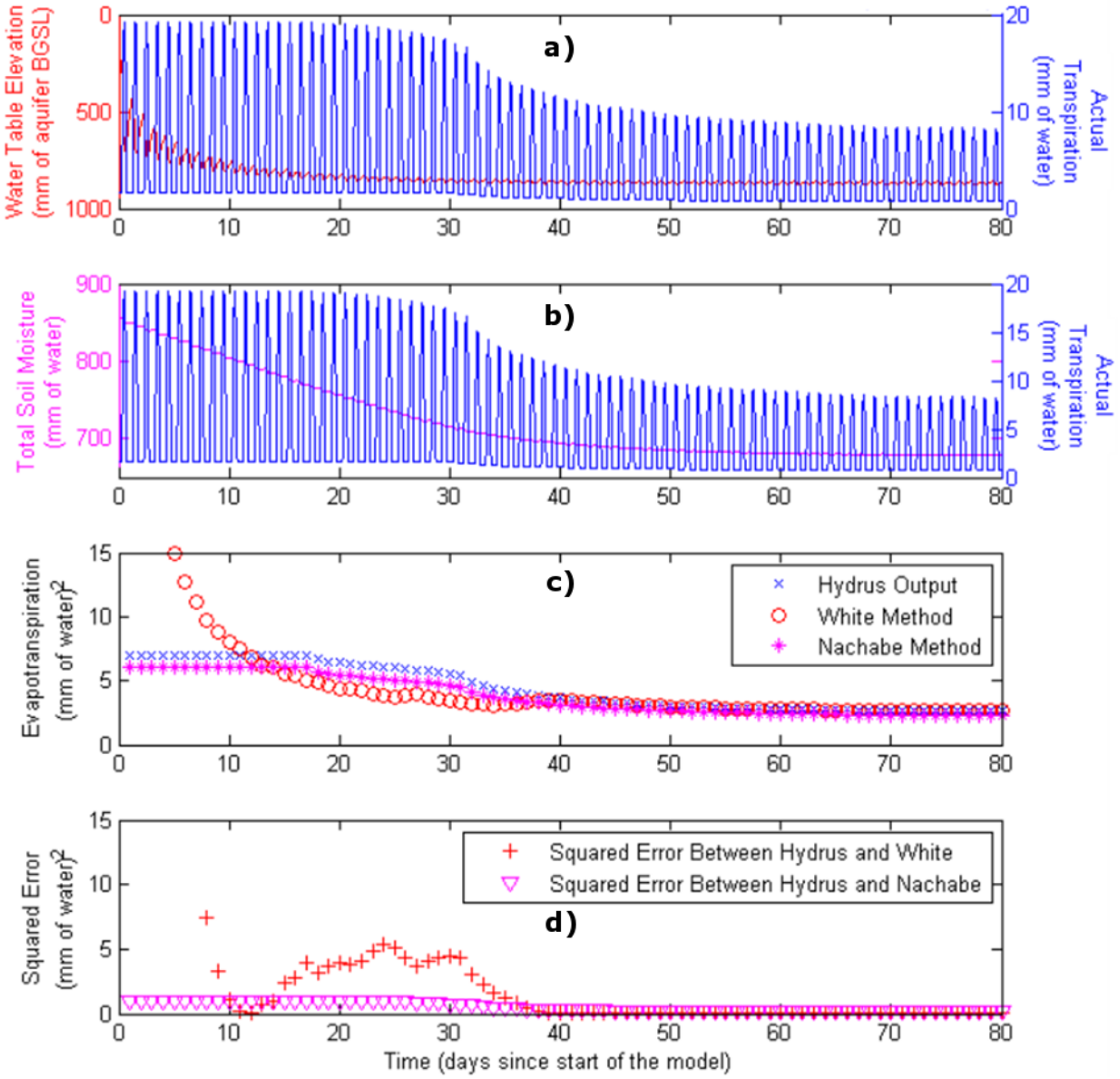

Figure 32. Model results of the inverted triangular root distribution. Specific yield was set to an optimized 0.09 [$L_{water}/L_{aquifer}$] by reducing the RMSE from days 61 through 80.

There are several noticeable difference between the results from the triangular root (Fig. 30) and the inverted triangular root (Fig. 32) models (Table 7).

Table 7. Summary of the differences between the triangular and inverted triangular roots.

	Triangular Root	Inverted Triangular Root	Units
Period of no plant stress	1 to 6	1 to 25	days
Period of plant stress	7 to 18	26 to 40	days
Period of groundwater transpiration	19 to 60	61 to 80	days
Period of slight VMC access	N/A	41 to 61	days
Specific yield	0.07	0.09	[L/L]
Specific yield optimized	n	y	(y/n)
White's accurate period	plant stress	groundwater transpiration	text

By paying attention to the maximum value of the actual transpiration rate (Fig. 32.a) I identified four noticeable behaviors; a period of no plant stress, a period of plant stress, a period of slight volumetric moisture content access, and a period of direct groundwater transpiration. An optimized specific yield value was selected. The most accurate the period when the White Method was the direct groundwater transpiration period (RMSE = 0.029).

Table 8. Summary of error by model run and time period.

Root Mean Squared Error Summary Table			
Model (title)	Time Period (day to day)	RMSE White (cm of water)	RMSE Nachabe (cm of water)
Triangular Root Distribution Non-Optimized Specific Yield (Sy = 0.07)	1 to 6	0.313	0.093
	7 to 18	0.105	0.065
	19 to 60	0.176	0.037
Triangular Root Distribution Optimized Specific Yield (Sy = 0.043)	1 to 6	0.436	0.093
	7 to 18	0.183	0.065
	19 to 60	0.004	0.037
Inverted Triangular Root Distribution Optimized Specific Yield (Sy = 0.09)	1 to 25	9.7	0.958
	26 to 40	1.525	0.77
	41 to 60	0.125	0.469
	61 to 80	0.029	0.391

Discussion

The limitation in solely using a record of water table elevation to estimate evapotranspiration is that the change in volumetric moisture content inferred. The numerical simulations suggest that the White Method performs well during the groundwater transpiration period (Table 8) meaning that the White Method performs well when change in total soil moisture in a 24 hours period is zero (Fig. 33).

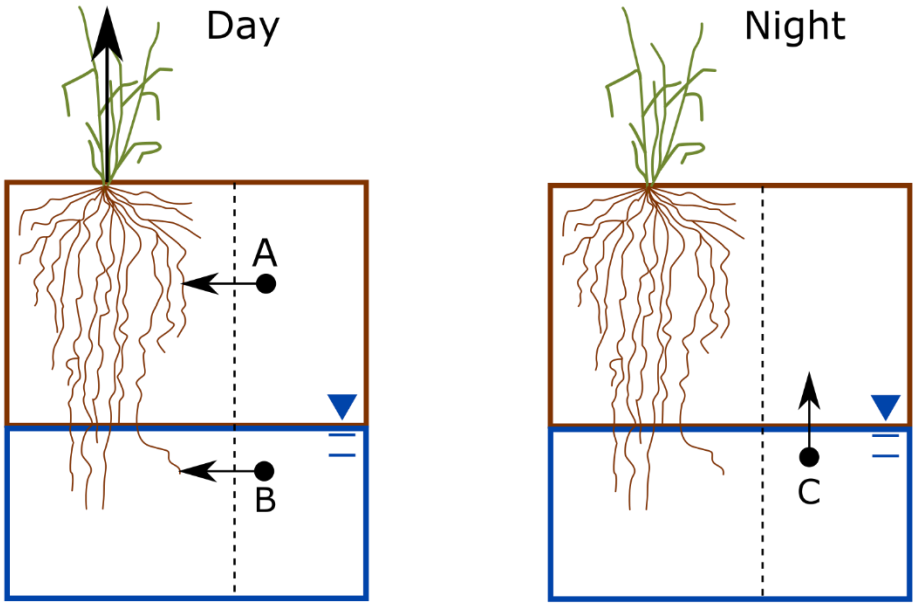

Figure 33. Water source and White Method applicability. The 'A' arrow represents amount of water supplied by draining pores thus changing the volumetric moisture content. The 'B' arrow represents the amount of water transpired from the water table. The 'C' arrow represents the amount of water filling the pores from groundwater upwelling.

Theoretically the White Method works when magnitude of the vector B >> A or when C = A. The change in volumetric moisture content 'A' is not directly observed using the White Method. 'A' is large during the no plant stress period. The magnitude of A transitions from

large to the magnitude of C through the plant stress period. The magnitude of A is that of C during direct groundwater transpiration period.

The Nachabe Method tracked the evapotranspiration rate in the numerical simulations (Fig. 30 and 32) (Table 8). The Nachabe Method performed well in the field during a time when the limited sensor array was sensing a volumetric moisture content that was representative of the total soil moisture (Fig. 29). The Nachabe Method utilizes total soil moisture a significantly more difficult record to accurately sense than a record of water table elevation.

Conclusion

The White Method limitations are clear. The White Method does not work

- After a precipitation event;
- When the air entry pressure produces a large water table amplitude;
- When the specific yield is inaccurately estimated;
- When the change in volumetric moisture content during the day is larger than the change in volumetric moisture content during the night.

Given these limitations the White Method does have a period when it can work (Fig 34).

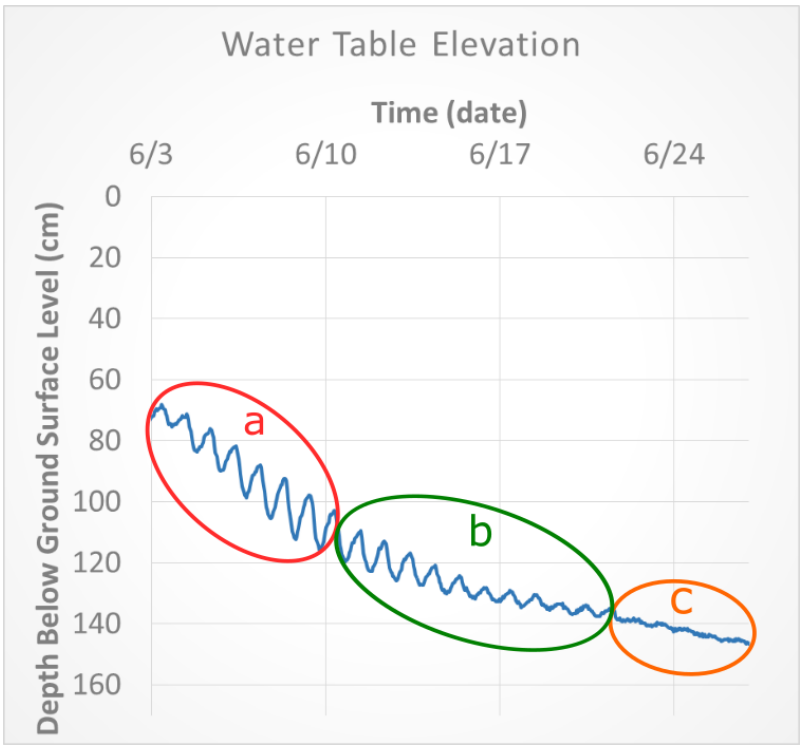

Figure 34. When the White Method is applicable to field data.

During a period when the change in volumetric moisture content during the day is suspected to be greater than the change in volumetric moisture content during the night the White Method should not be expected to produce accurate results (Fig. 34.a). When the water being transpired is near the upwelling rate the White Method should be expected to work (Fig. 34.b). In the late time period (Fig. 34.c) the groundwater upwelling appeared to cease which could be caused to the lowering of the water table by the nearby surface drainage, during this period the White Method shouldn't be applied.

By directly sensing record of total soil moisture the evapotranspiration rate can be computed directly without need for the specific yield term. In the numerical simulations an accurate total soil moisture record is computed and the Nachabe Method performs well across all time period and model parameters (Table 8). Physical reality is not as forgiving as the

numerical environment. Accurately sensing volumetric moisture content by depth to produce a total soil moisture record with an accuracy of ± 1mm is difficult due to system discretization and that the dielectric of water changes with temperature thus where and when volumetric moisture content sensed so should temperature.

An expression of a variable specific yield could be a solution that would expand the applicability of the White Method to longer periods of time as well as depth of the water table below ground surface level (appendix a.I). Such an expression would infer the change in volumetric moisture content for a given water table change. This expression would need to account for material transitions was the water table dropped past horizon boundaries to able to be applicable in the field.

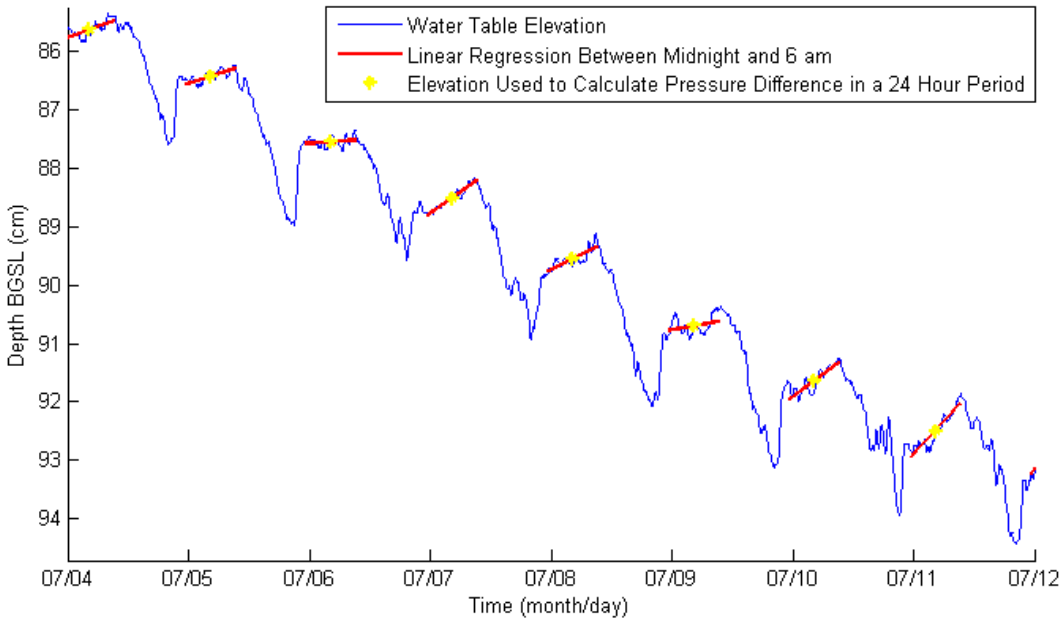

Figure 35. Visualizing the White Method data analysis at Ruby Pasture.

Bibliography

Acharya, S., Jawitz, J. W., & Mylavarapu, R. S. (2012). Analytical expressions for drainable and fillable porosity of phreatic aquifers under vertical fluxes from evapotranspiration and recharge. *Water Resources Research*, *48*(11), n/a–n/a. http://doi.org/10.1029/2012WR012043

Allen, R. G., Pruitt, W. O., Wright, J. L., Howell, T. A., Ventura, F., Snyder, R., … Elliott, R. (2006). A recommendation on standardized surface resistance for hourly calculation of reference ET o by the FAO56 Penman-Monteith method. *Agricultural Water Management*, *81*, 1–22. http://doi.org/10.1016/j.agwat.2005.03.007

Assouline, S., & Or, D. (2014). The concept of field capacity revisited: Defining intrinsic static and dynamic criteria for soil internal drainage dynamics. *Water Resources Research*, (50), 4787–4802. http://doi.org/10.1002/2014WR015475.Received

Baird, K. J., & Iii, T. M. (2005). Simulating riparian evapotranspiration : a new methodology and application for groundwater models. *Hydrology*, *312*, 176–190. http://doi.org/10.1016/j.jhydrol.2005.02.014

Bossong, C., Karlinger, M., Troutman, B., & Vecchia, A. (1999). Overview and technical and practical aspects for use of geostatistics in hazardous-, toxic-, and radioactive- waste-site investigations. *USGS Publication*, *Water-Reso*.

Brinson, M. (1993). A Hydrogeomorphic Classification for Wetlands.

Cobos, D., Campbell, C., & Devices, D. (2007). Correcting temperature sensitivity of ECH2O soil moisture sensors.

Ding, R., Kang, S., Li, F., Zhang, Y., Tong, L., & Sun, Q. (2010). Evaluating eddy covariance method by large-scale weighing lysimeter in a maize field of northwest China. *Agricultural Water Management*, *98*(1), 87–95. http://doi.org/10.1016/j.agwat.2010.08.001

Duke, H. R. (1972). Capillary properties of soils-influence upon specific yield. *Trans ASAE*, 688 – 699.

Fahle, M., & Dietrich, O. (2014). Estimation of evapotranspiration using diurnal groundwater level fluctuations : Comparison of different approaches with groundwater lysimeter data. *Water Resources Research*, *50*, 273–286. http://doi.org/10.1002/2013WR014472

Feddes, R. A., Kowalik, P. J., Zaradny, H. (1978). *Simulation of Field Water Use and Crop Yield*. John Wiley and Sons, New York, NY.

Freeze, R., A., & Cherry, John, A. (1979). *Groundwater*. Pretence Hall.

Gribovszki, Z. (2014). Diurnal Method for Evapotranspiration Estimation from Soil Moisture Profile. *Acta Silv. Ling. Hung.*, *10*(1), 67–75. http://doi.org/10.2478/aslh-2014-0005

Grygoruk, M., Batelaan, O., Mirosław-Świątek, D., Szatyłowicz, J., & Okruszko, T. (2014). Evapotranspiration of bush encroachments on a temperate mire meadow – A nonlinear function of landscape composition and groundwater flow. *Ecological Engineering*, *73*, 598–609. http://doi.org/10.1016/j.ecoleng.2014.09.041

Halford, K. J., Weight, W. D., & Schreiber, R. P. (2006). Interpretation of Transmissivity Estimates from Single-Well Pumping Aquifer Tests Interpretation of Transmissivity Estimates from Single-Well Pumping Aquifer Tests. *Groundwater*, *44*(3), 467–471. http://doi.org/10.1111/j.1745-6584.2005.00151.x

Hao, X. M., Li, W. H., & Guo, B. (2013). Simulation of the effect of root distribution on hydraulic redistribution in a desert riparian forest. *The Ecological Society of Japan*, *28*, 653–662. http://doi.org/10.1007/s11284-013-1058-5

Heath, R. C. (2004). Basic Ground-Water Hydrology. *USGS Publication*.

Johnson, A. (1967). Specific Yield Compilation of Specific Yields for Various Materials. *USGS Publication*, *Water Supp*(1662-D).

Lautz, L. K. (2007). Estimating groundwater evapotranspiration rates using diurnal water-table fluctuations in a semi-arid riparian zone. *Hydrogeology Journal*, *16*(3), 483–497. http://doi.org/10.1007/s10040-007-0239-0

Lawrence A. Freeman Michael C. Carpenter, D. O. R., & Joseph P. Rousseau, Randy Unger, and J. S. M. (2004). Use Of Submersible Pressure Transducers In Water-Resources Investigations Use of Submersible Pressure Transducers in Water-Resources Investigations. *USGS Publication*.

Lehmann, P., Assouline, S., & Or, D. (2008). Characteristic lengths affecting evaporative drying of porous media. *Physical Review*, *E77*(056309), 1–16. http://doi.org/10.1103/PhysRevE.77.056309

Loescher, H., Ayres, E., Duffy, P., Luo, H., & Brunke, M. (2014). Spatial Variation in Soil Properties among North American Ecosystems and Guidelines for Sampling Designs. *PLoS ONE*, *9*(1). http://doi.org/10.1371/journal.pone.0083216

Loheide, S. P. (2008). A method for estimating subdaily evapotranspiration of shallow groundwater using diurnal water table fluctuations. *Ecohydrology*, *66*(1), 59–66. http://doi.org/10.1002/eco

Loheide, S. P., Butler, J. J., & Gorelick, S. M. (2005). Estimation of groundwater consumption by phreatophytes using diurnal water table fluctuations: A saturated-unsaturated flow assessment. *Water Resources Research*, *41*(7), n/a–n/a. http://doi.org/10.1029/2005WR003942

Middleton, & Wilcock. (1994). Dimension Analysis and the Theory of Models.

Nachabe, M. H. (2002). Analytical expressions for transient specific yield and shallow water table drainage. *Water Resources Research*, *38*(10), 1–7. http://doi.org/10.1029/2001WR001071

Nachabe, M., Shah, N., Ross, M., & Vomacka, J. (2005). Evapotranspiration of Two Vegetation Covers in a Shallow Water Table Environment. *Soil Science Society of America*, *69*, 492–499.

Natural Resources Conservation Service. (2012). Field Book for Describing and Sampling Soils Version 3.0.

Noël, P. (2011). Second year internship at IMFT in collaboration with Oregon State University Study of groundwater in meadows alongside the Middle Fork, 1–39.

Ping Wang and Sergey P. Pozdniakov. (2014). A statistical approach to estimating evapotranspiration from diurnal groundwater level fluctuations Ping. *Water Resources Research*, (1), 2276–2292. http://doi.org/10.1002/2013WR014251.Received

Prickett, T. (1965). Type-Curve Solution to Aquifer Tests under Water-Table Conditions. National Water Well Association.

Ramsahoye, L. E., & Lang, S. M. (1961). A Simple Method for Determining Specific Yield from Pumping Tests. *USGS*.

Renard, P., Glenz, D., & Mejias, M. (2009). Understanding diagnostic plots for well-test interpretation. *Hydrogeology Journal*, *17*(3), 589–600.

Said, A., Nachabe, M., Ross, M., & Vomacka, J. (2005). Methodology for Estimating Specific Yield in Shallow Water Environment Using Continuous Soil Moisture Data. *Irrigation and Drainage Engineering*, *131*(December), 533–538.

Scott, R. L., Cable, W. L., Huxman, T. E., & Nagler, P. L. (2008). Multiyear riparian evapotranspiration and groundwater use for a semiarid watershed, *72*, 1232–1246. http://doi.org/10.1016/j.jaridenv.2008.01.001

Shah, N., Nachabe, M., & Ross, M. (2007). Extinction Depth and Evapotranspiration from Ground Water under Selected Land Covers. *Groundwater*, *45*(3), 329–338. http://doi.org/10.1111/j.1745-6584.2007.00302.x

Simunek, J., Kodesova, R., Grib, M., & Genuchten, M. (1999). Estimating hysteresis in the soil water retention function from cone permeameter experiments. *Water Resources Research*, *35*(5), 1329–1345.

Simunek, J., Senja, M., & Van Genuchten, M. T. (1998). HYDRUS 1-D Simulating the One-Dimensional Movement of Water, Heat, and Multiple Solutes in Variably-Saturated Media, Version 2.

Soylu, M. E., Lenters, J. D., Istanbulluoglu, E., & Loheide, S. P. (2012). On evapotranspiration and shallow groundwater fluctuations: A Fourier-based improvement to the White method. *Water Resources Research*, *48*(6), W06506. http://doi.org/10.1029/2011WR010964

Tiner, R. (1991). The Concept of a Hydrophyte for Wetland Indentification. *BioScience*, *41*(4), 236–247.

Van Genuchten, M. T. (1980). A Closed-form Equation for Predicting the Hydraulic Conductivity of Unsaturated Soils. *Soil Science Society of America*, *44*(5).

Veihmeyer, F., & Hendrickson, A. (1928). Soil Moisture at Permanent Wilting of Plants. *Plant Physiology*, *3*(3), 355–357.

White, W. (1932). A Method of Estimating Ground-water Supplies Based on Discharge by Plants and Evaporation from Soil. *USGS Publication*, *Contributi*.

Appendix

Table of Contents

Electronic Appendix

Field data, lab data and numerical models can be found in the electronic appendix accompanying this document.

Appendix a.I: Specific Yield for a Shallow Aquifer

The Target

The specific yield parameter in the White Equation (Eq. 1) introduces error into the final estimate of evapotranspiration (White, 1932; Loheide, 2005). The specific yield is often considered to be a constant value for an aquifer (Lautz, 2007) and most field methods designed the measure specific yield report a constant value (Loheide, 2005). The objective of this appendix is to develop a conceptual understanding of the process that gives rise to the value of specific yield for an unconfined aquifer. To reach the objective I share with you my experiences implementing field method of estimating specific yield and then I adapt the concept of specific yield for an unconfined aquifer to the concept of specific yield for a shallow aquifer. By shallow aquifer, I mean that the water from the water table can move vertically into the atmosphere through evapotranspiration.

General Form of the Equation

The general form of the equation for specific yield can most simply be a restatement of equation 2 (Eq. 2) (Fig. 6).

$$S_y = \frac{W_y}{\Delta WT} \quad \text{Eq. 6}$$

Where:

S_y = specific yield (depth of water/depth of aquifer)

W_y = water yield (depth of water)

ΔWT = change in water table elevation (depth of aquifer)

Specific Yield for an Unconfined Aquifer

Specific yield was initially a term coined in groundwater hydrology literature (Heath, 2004). From the groundwater hydrologist perspective they are three physical processes that need to be taken into account for determining a case specific storage coefficient: pore drainage, the decompression of water, and the compression of the aquifer. However in an unconfined aquifer the amount of water yielded from the pore draining process is typically two orders of magnitude greater than the other two processes (Dawson and Istok, 1991). In the unconfined aquifer case, the storage coefficient is specific yield, a fractional quantity describing the pore drainage process.

Field Efforts to Measure Specific Yield

At the Ruby Pasture field site, specific yield was estimated from other variables that were directly measured (Table 9). The first method was the standard groundwater hydrology approach of performing a pump test (appendix a.VI). The second method was to fully characterize the hydraulic properties of the soil by depth by analyzing soil cores (appendix a.VII). The third method was to estimate the soils hydraulic properties from texture class alone. The impetus of the third method was to explore if a less laborious method would yield the same result as the second method. The fourth method was to use solver to estimate specific yield by minimizing the sum of squared errors between the weather station evapotranspiration rate and the White Method evapotranspiration rate by changing specific yield.

Table 9. Summary of Specific Yield.

Method (title)	Specific Yield (cm of water/cm of aquifer)
Pump Test	0.01
Full Soil Hydraulic Characterization	0.22
Hydraulic Characterization from Texture Class	0.34
Fitting $ET_{(penman)}$ to $ET_{(white)}$	0.21

Out of the four field methods the method of fitting evapotranspiration for specific yield stood out as the easiest to apply and accurate due it convergence upon the same answer as the full soil hydraulic characterization method.

The results derived from pump test analysis were up to an order of magnitude smaller than reasonable values for alluvial unconfined aquifers. Field data collection required an experienced crew to install an array of wells and operate expensive instrumentation. A large

number of assumptions were required to be made to analyze the raw data. The pump test method required the most resources and produced inaccurate results when analyzed for specific yield (Appendix a.VI).

The Full Soil Hydraulic Characterization method took into account many physical processes such at root water uptake, soil water hysteresis, and gravity drainage. Data collection required a full soil pit description, field soil core collection, laboratory equipment, laboratory procedures and data analysis to fully characterize the soil hydraulics found in the field. The soil hydraulic characterization data (appendix a.VIII) was inputted into HYRUDS 1-D as the material distribution. A record of water table elevation nearby the pit was simulated using HYDRUS 1-D and the output was analyzed for specific yield. The specific yield from the Full Soil Hydraulic Characterization method (Sy = 0.22) converged with the result from the Fitting $ET_{(penman)}$ to $ET_{(white)}$ method (Sy = 0.21).

The method of Hydraulic Characterization from Texture Class is similar to the method of Full Soil Hydraulic Characterization except that the soil hydraulic parameters were estimated using texture class alone. I tested this method to see if saving the labor costs of fully characterizing the soils hydraulic parameters compromised the resulting estimate of specific yield. The result was reasonable (Sy = 0.34), however it is over 150% of the results from the Full Soil Hydraulic Characterization and Fitting $ET_{(penman)}$ to $ET_{(white)}$ methods (Sy = 0.22: Sy 0.21).

The method of Fitting $ET_{(penman)}$ to $ET_{(white)}$ requires a record of water table observation, a weather station data, an analysis for evapotranspiration, and excels GRG nonlinear solver. A critical assumption is that the evapotranspiration estimate derived from the water table

elevation is representative to the evapotranspiration occurring across the entire fetch of the weather station. The method of Fitting $ET_{(penman)}$ to $ET_{(white)}$ is statistically based and produced a reasonable estimate of specific yield (Sy = 0.21) using easily collectable field data. The key benefit of the Fitting $ET_{(penman)}$ to $ET_{(white)}$ is that the data analysis can be performed in under a day.

Out of the methods applied to determine specific yield the method of Fitting $ET_{(penman)}$ to $ET_{(white)}$ was the easiest to perform and produced reasonable results. The method of Full Soil Hydraulic Characterization seemed reasonable but required a lot of labor. The method of Hydraulic Characterization from Texture Class seemed to overestimate specific yield. The Pump Test dramatically underestimated specific yield.

Developing the Shallow Aquifer Case

We can conceptualize the specific yield for an unconfined aquifer (Fig. 6), and we can even estimate a constant specific yield from field parameters (Table 7). However, in shallow aquifers groundwater is lost to the atmosphere through evapotranspiration. The pressure distribution through the soil imposed by evapotranspiration affects the specific yield value. It is my argument that as the water table drops throughout the dry season (Fig. 36) the specific yield should increase because the amount of aquifer drainable porosity for a small change in pressure becomes larger. This is a hypothesis in which numerical modeling could provide some insight, but first let's spend some time developing our conceptual understanding of a shallow aquifer.

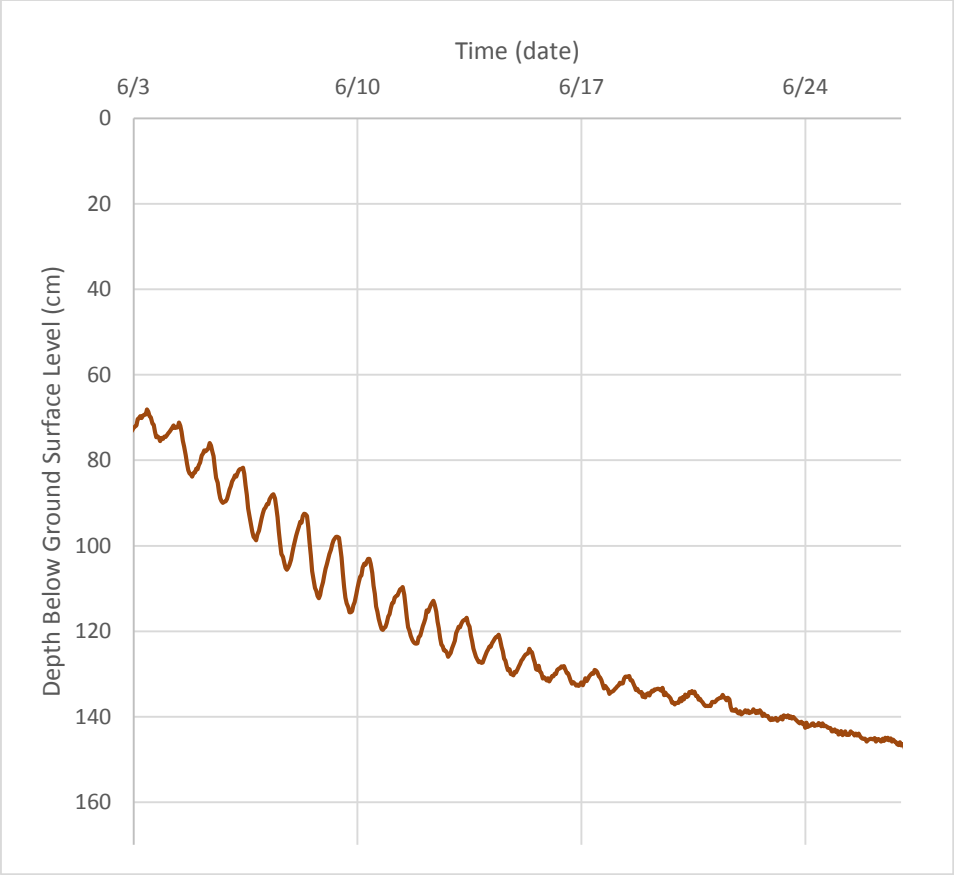

Figure 36. Water table observations at Granite Boulder Pasture.

Pore Drainage Expressed Through Pressure

Water flows from high to low mechanical potential (Dawson and Istok, 1991). The three components of this potential are elevation head, pressure head, and velocity head. In groundwater systems the water velocity is small, thus the velocity head is negligible. In the evaporation and upper transpiration affected zone the magnitude of the pressure head can be much larger than the magnitude of the elevation head. In a pump test the amount of water drained is from the zone where elevation head is relevant. Transpiration can exert 2 to 3 orders

of magnitude more negative pressure head than the change in elevation head communicated by a pump test (Appendix a.VII).

The relationship between pressure and volumetric moisture content for a small volume of soil is the water retention curve (Fig. 37). For a given pressure change, the amount of water either draining or filling the pore space can be determined using the water retention curve relationship. The water retention curve relationship arises from the behavior of water within a pore. In a pore the bond strength of water to a particle surface is roughly six times greater than the bond strength of water to itself (Selker et al., 1999). The surface area to volume ratio of a pore represents the amount of strong bond ion-dipole to weak hydrogen bond ratio a pore exhibits. Thus as the pore radius decreases the ion-dipole bond to hydrogen ratio increases resulting in water being held is smaller pores with more negative pressure. In soil they are many different pore sizes. The shape of the water retention curve for a soil is simply an expression of the pore size distribution of a given soil. The water retention curve represents the amount of volumetric moisture content change will occur for a give pressure.

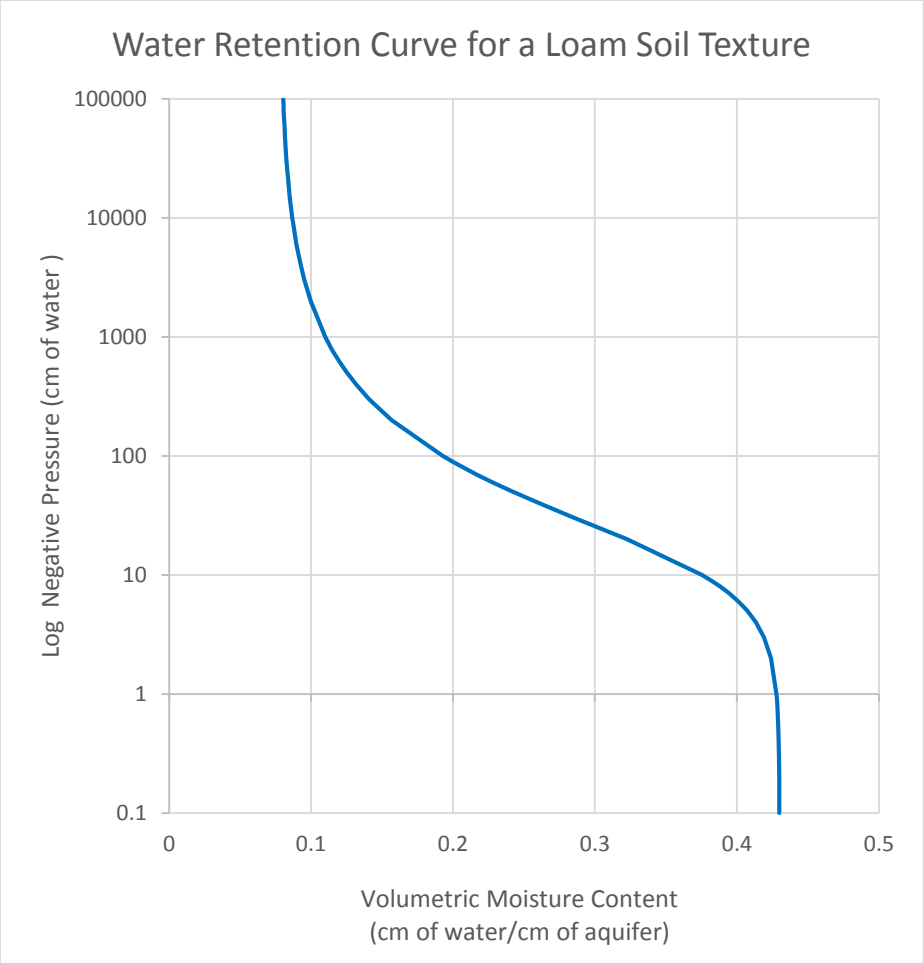

Figure 37. The water retention curve.

Soil Profiles Have Pressure Distributions

While a small volume of soil has a single pressure value, a soil profile may have a distribution of pressures. The one dimensional pressure distribution relates a given position below ground surface with a pressure. In the unconfined saturated zone the pressure distribution is such that the pressure head is compensated by the elevation head producing a hydrostatic pressure distribution. In the unsaturated zone the pressure distribution may be hydrostatic when gravity drainage is the only process removing water from the system,

however when evapotranspiration removes water the pressure distribution in the evaptranspirative affected zone becomes non-hydrostatic.

In Shallow Aquifers the Pressure Distribution is Not Hydrostatic

Evaporation and transpiration can drive the upper portion of a shallow aquifer into a highly negative head pressure condition. Evaporation can effectively exert a head pressure at the surface of the soil so negative that the water continuum is broken into isolated parcels of water that no longer communicate (Lehman, 2008). The evaporation extinction depth demarks the bottom of an evaporation affected zone. An observed evaporation extinction depth for fine sand was 9cm (Lehman, 2008). Transpiration effectively transfers the evaporative head pressure from the stomatal opening to the root surface. The head pressure gradient along the root-soil interface can drain pores, driving water into the plant. The physical limitation of the plant to transmit the evaporative head pressure is at the permanent wilting point, where the lack of turgor pressure within a plant allows separation of cell membranes from cell walls, or cavitation introduces air into the plant's xylem. Plants will exhibit stress before the permanent wilting point is reached and start to limit transpiration by regulating their stomata creating a deficiency in their ability to meet atmospheric water demand. Plant stress coupled with soil pressure distribution and root surface area distribution creates a behavior where roots preferentially take up water from soil that does not stress the plant. Once the stress free water has been accessed, which typically happens within a week into the dry season in the upper soil where the root surface area is typically large, the plant starts to limit the transpiration rate. During the plant stress period, when the transpiration rate is limited, the roots in the lower soil,

where the root surface area is typically small, is exerting a slightly negative head pressure to supply the majority of the limited transpiration rate. Although the exact behavior of plant water uptake is for more complex, it is often modeled using the Feddes Function (Feddes et al., 1978). My field data suggests that the head pressure at which the upper roots plateaus with access to water lower in the profile was near -5,000 cm of water. With the addition of evaporation and transpiration, the pressure distribution within a soil profile can be compartmentalized into three zones: the hydrostatic; the root affected zone; and the evaporation affected zone (Fig. 38)

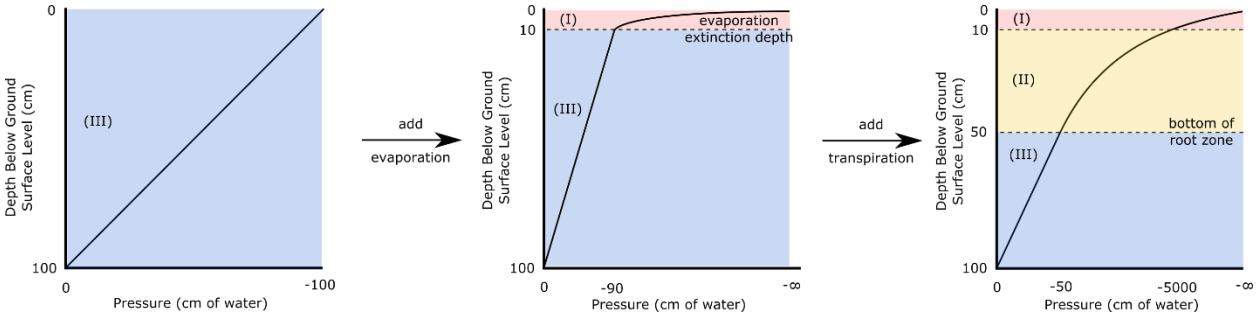

Figure 38. Pressure distribution of a shallow aquifer. **a)** Starting with a hydrostatic pressure distribution (III). **b)** The process of evaporation is added creating an evaporated affected zone (I). **c)** The process of transpiration is added creating a root affected zone (II).

Which Zones Yield Water Given a Small Pressure Change?

For the three pressure zones outlined in figure 34, each zone will yield an amount of water in accordance with the moisture retention curve relationship. When the water table rises it communicates a pressure change to the entire profile above the water table. After inducing a +10 cm of pressure change across the entire profile we can investigate which zones

yields appreciable amounts of water. Using the moisture retention curve we can see that in zone I and II yield very little when compared to zone III (Fig. 39)

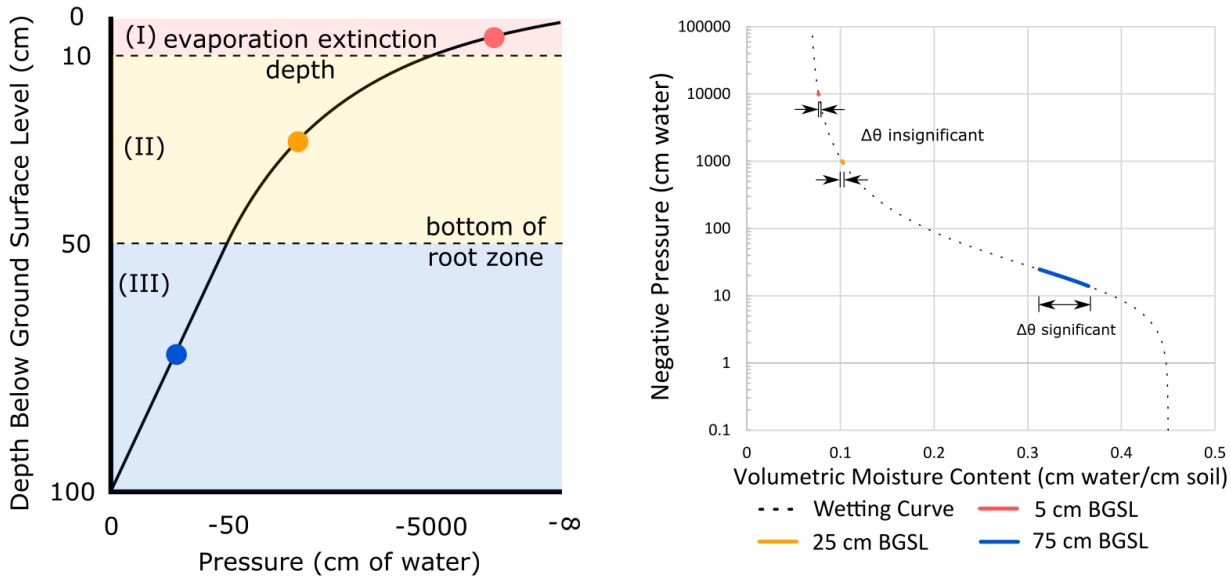

Figure 35. Change in volumetric moisture content. Three points, each in the middle of each pressure zones I, II, and III (left). At each point a pressure change of +10 cm of water was imposed to mimic a rise of a water table by 10cm.

For the same pressure change, zone III adsorbed 6% of the soils volume as water, which is considerably larger than the 0.5% and 0.1% of the soils volume as was in zone II and zone I respectively.

Specific Yield for a Shallow Unconfined Aquifer

Specific yield in the White Method is attributed to the pore draining and filling process of the entire aquifer material above the water table with fluctuations at a daily cycle. The pore draining and filling process can be related to pressure through the water retention curve (Fig.

39), where a given pore size distribution (λ) of an aquifer material produces a given water retention curve. In the shallow aquifer case the entire depth of the aquifer material above the water table is little. When evapotranspiration is considered two depths, the evaporation extinction depth and the bottom of the root zone, produce a pressure distribution of a soil profile (Fig. 34), where the hydrostatic zone (III) and the bottom of the root affected zone (II) contribute more volume of water for the same pressure change when compared to the evaporation affected zone (I) and the top of the root affected zone (II) (Fig. 39). The critical geometries that attribute to the specific yield are the depths of each of the pressure zones and the pore size distribution of the porous media (Fig. 40).

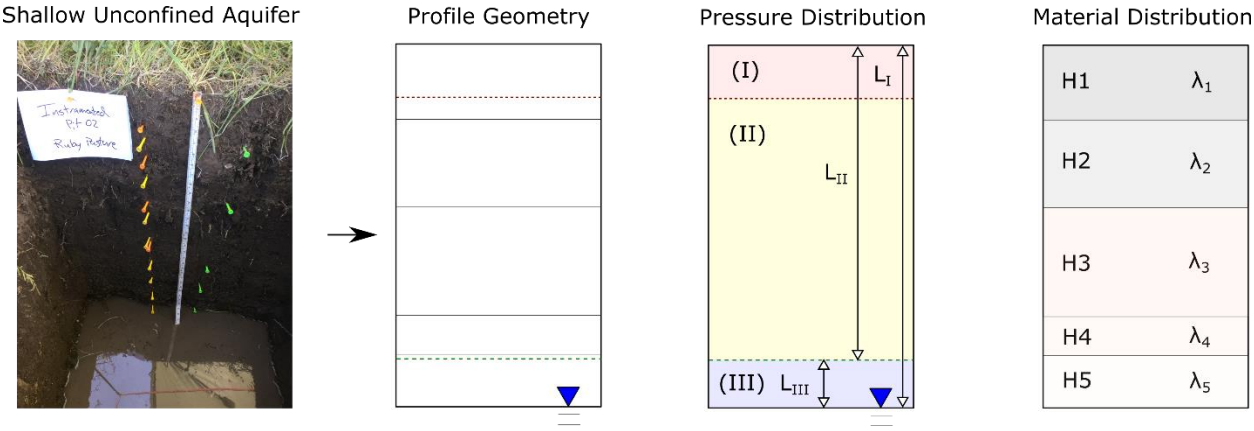

Figure 40. Visualizing critical geometry. For a given profile the two critical lengths that attribute the specific yield parameter is the depth of the water table (L), as well as the pore size distribution of the aquifer material (λ)

From the critical geometry (Fig. 40), which zone is the critical zone where significant amounts of water is being filled and drained well into the dry season? I propose that upper portion of the critical zone be demarcated where the head pressure is -100 cm of water and the lower portion of the critical zone be demarcated at the water table (Fig. 41). I chose -100 cm of

water as the upper because it is an order of magnitude greater than the elevation head imposed by fluctuating water tables and -100 cm of water is detectable by Decagon's MPS-1 dielectric water potential sensor. It would be convenient to thoroughly define the upper end of the critical zone to be soil specific or dependent upon the root distribution but by selecting the constant of -100 cm of water gives us a place to start.

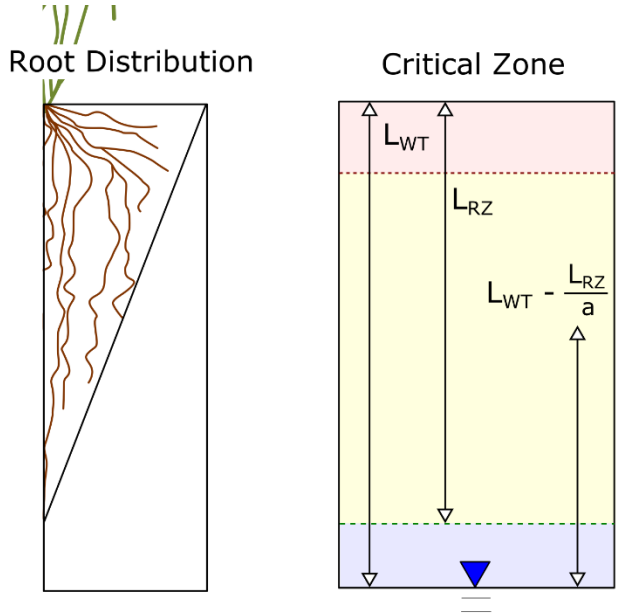

Figure 41. The critical zone. The critical zone for this problem is $L_{WT} - L_{RZ}/a$. Where **a** is 2.

The exercise of thinking through the critical geometry and critical zone of shallow aquifers is to give us the framework to develop specific yield function that is not a constant (Eq. 7).

$$S_y = f_x(L, \lambda, \dots) \qquad \text{Eq.7}$$

As the dry season progresses, water table decline over time (Fig. 32). As the water table elevation declines $L_{WT} - L_{RZ}/a$ increases thus the total depth of aquifer that can contribute to the pore draining and filling process increases. Moreover, as the water table elevation declines

below the bottom of the root zone L_{III} increases. As the water table drops on the seasonal time scale, the specific yield value should increase because $L_{WT} – L_{RZ}/a$ becomes larger producing a record of dampened water table fluctuations through time (Fig. 36). The caveat to this relationship between water table depth and specific yield, is that there is a chance that the water table will drop through a different soil horizon producing a different pore size distribution (λ) directly above the water table in zone III. This change in soil material can increase or decrease the specific yield value. To investigate the relationship between L and λ, I did some numerical modeling (appendix a.VIII)

Numerical Modeling Results

I was interested in addressing two questions. First, what is the relationship between specific yield and L (depth of the water table below ground surface level) (Fig. 42) ? Second, does that relationship break down when the water table drops past a soil texture changing the pore size distribution (Fig. 43)?

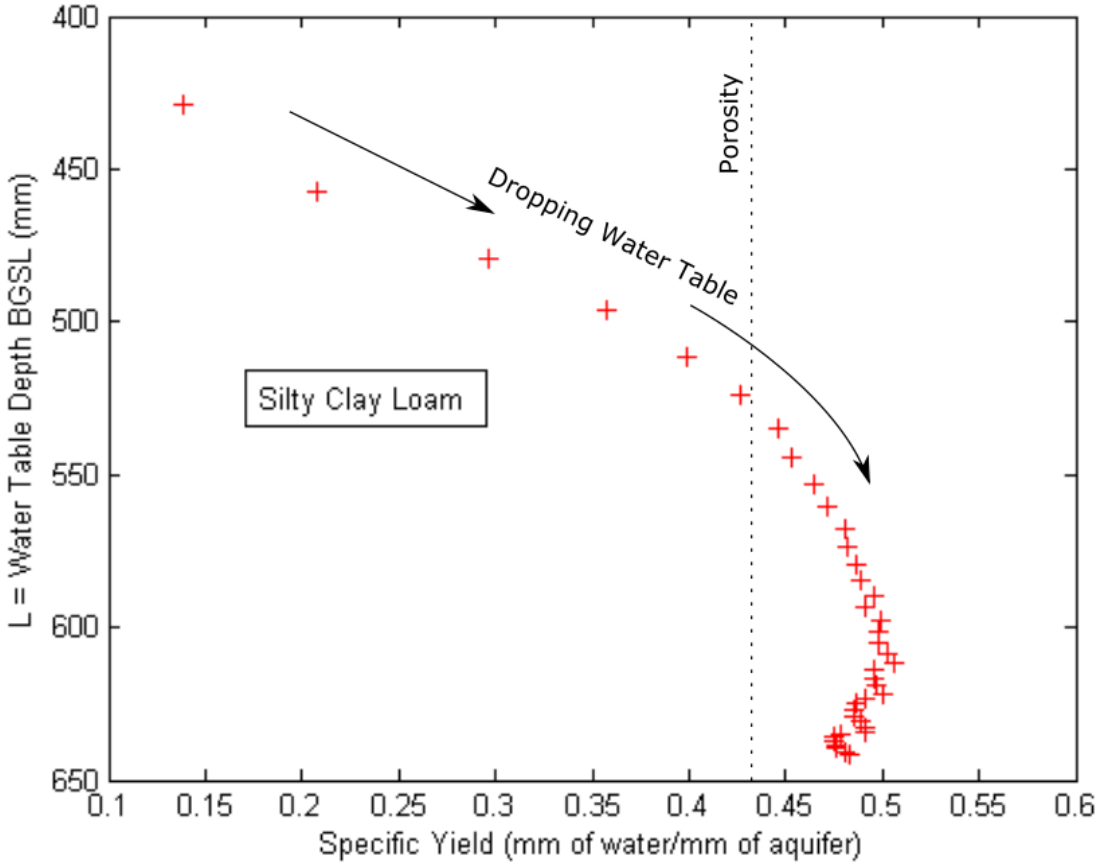

Figure 42. L vs S_y for a homogenous soil texture. Each point represents a daily estimate of specific yield.

The specific yield starts off low, approaches and passes porosity for the first 60 days of this model. Shah proposed that specific yield be modeled as an exponential as the water table drops (Shah et al., 2005) which this plot suggests. However the applicability of specific yield being a simple exponential is confounded if the water table drops past a textural change (Fig. 39).

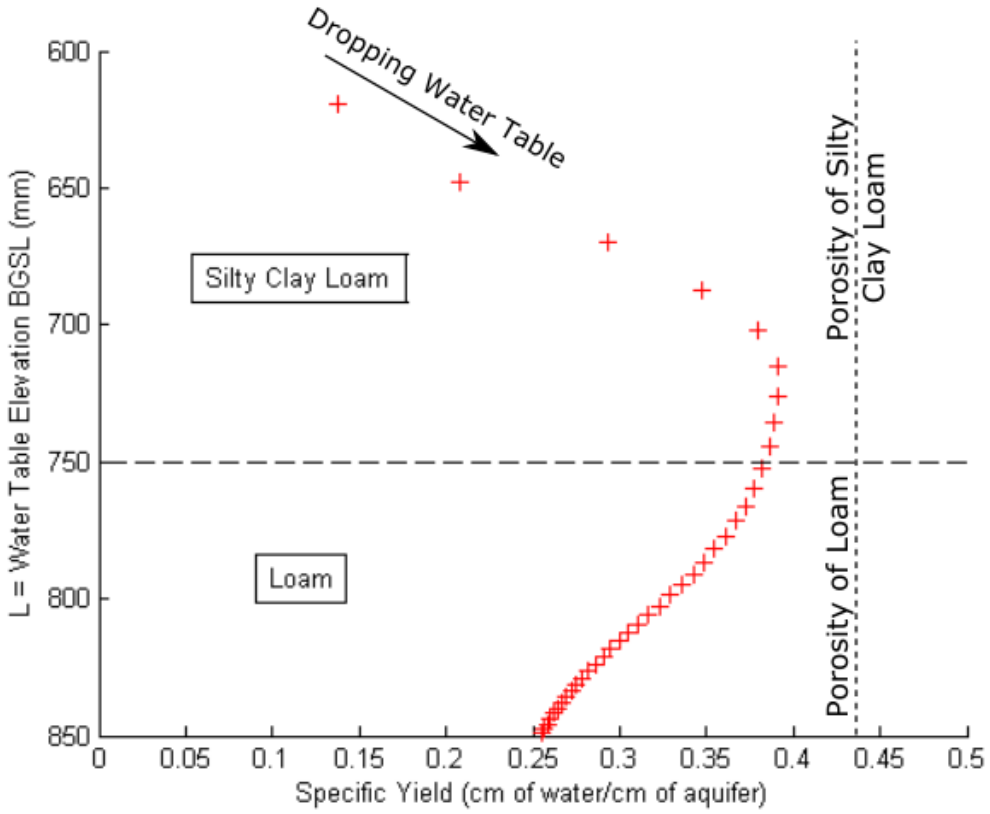

Figure 43. L vs S_y across a textural change.

Discussion and Conclusion

Even though most field methods of measuring specific yield calculate a constant value through time (Table 9), it appears that operationally specific yield is not a constant for a shallow aquifer through time. Nachabe proposed that a daily specific yield can be estimating by measuring total soil moisture (Nachabe et al., 2005). Shah proposed that specific yield be modeled by using an exponential decay relationship as the water table drops through dry season (Shah el al, 2005) but the applicability of this relationship is limited due the risk of the water table dropping past a textural change (Fig. 43). Specific yield could be a function of other parameters, such as drainage time, air entry pressure, Van Genuchten's n, porosity, volumetric moisture content, rooting depth, permanent wilting point, and evaporation potential. By

collecting a record of total soil moisture and water table elevation a daily specific yield could be calculated, however if you have a record of total soil moisture you can compute evapotranspiration directly. A more sound dimensional analysis, field data collection effort and numerical modeling is required to determine the true relationship of how specific yield is changing throughout the water year for a shallow aquifer.

The fundamental limitations that the specific yield concept imposes upon the White Method are three fold. First, the change in volumetric moisture content is the true storage term and the White Method utilizes $Sy*\Delta WT_{24h}$ as a storage term. For the White Method storage term to be representative of the change in volumetric moisture content the specific yield concept needs to be able to change through the season as plant accessible volumetric moisture content changes. Second, the magnitude of head pressure supplying water to the system at the bottom boundary condition is 2 to 3 orders of magnitude smaller than the head pressure removing water from the system at the upper boundary condition. The specific yield during the day is going to be smaller than the specific yield during the night as long as the plants are transpiring more than the daily groundwater upwelling rate. Third, the specific yield can change quite dramatically if the material properties right above the water table change which can easily happen as the water table drops past a soil textural change.

Appendix a.II: Hysteresis and Water Table Fluctuations

The Question

What is with that break in slope of the water table elevation during the night (Fig. 44, 45, and 46)? Walter White first described this break in slope.

> "At or soon after sunset the rate of transpiration and evaporation declines to a small fraction of the rate that prevails during the day but for a time the plants continue to draw some water to fill their circulatory systems which have become somewhat depleted. Nearly all plants become slightly wilted during the day particularly on hot days and tend to have a drooping appearance at night quite in contrast with their fresh turgid appearance in the morning. Moreover during the day the recharge of the capillary fringe from the zone of saturation lags somewhat behind the discharge by plant action. By midnight or slightly before the veins of the plants have become filled with water. Meanwhile capillary equilibrium has been nearly established in the capillary fringe and during the hours from midnight to morning there is little movement of water to the fringe from the zone of saturation." (White, 1932)

Hysteresis in the water retention curve is often acknowledged as important because it affects specific yield (Zhang et al., 2016; Acharya et al., 2014; Shah at al., 2007) however I have not found publications that attribute hysteresis to the break in slope.

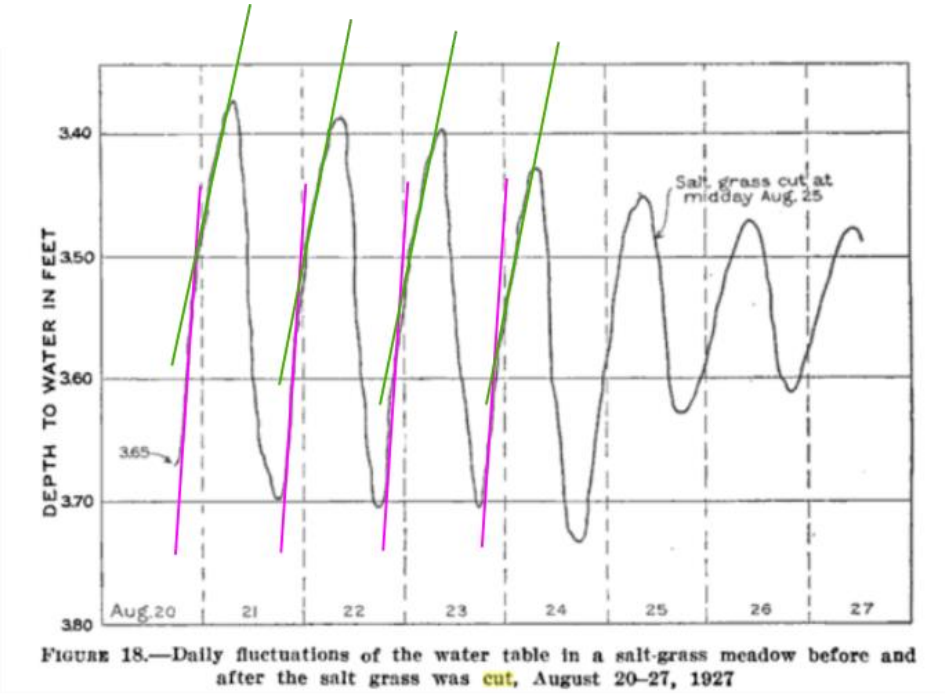

FIGURE 18.—Daily fluctuations of the water table in a salt-grass meadow before and after the salt grass was cut, August 20–27, 1927

Figure 44. Break in slope in White's dataset. This is figure 18 in White, 1932. The magenta line is fit to data during early night. The green line is fit to the data during late night.

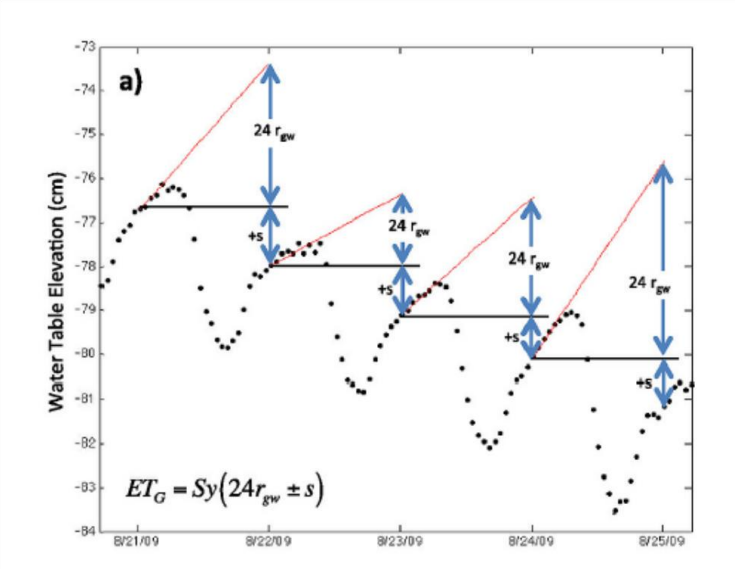

Figure 45. Break in slope in Soylu's dataset. This is figure 1 in Soylu et al., 2012.

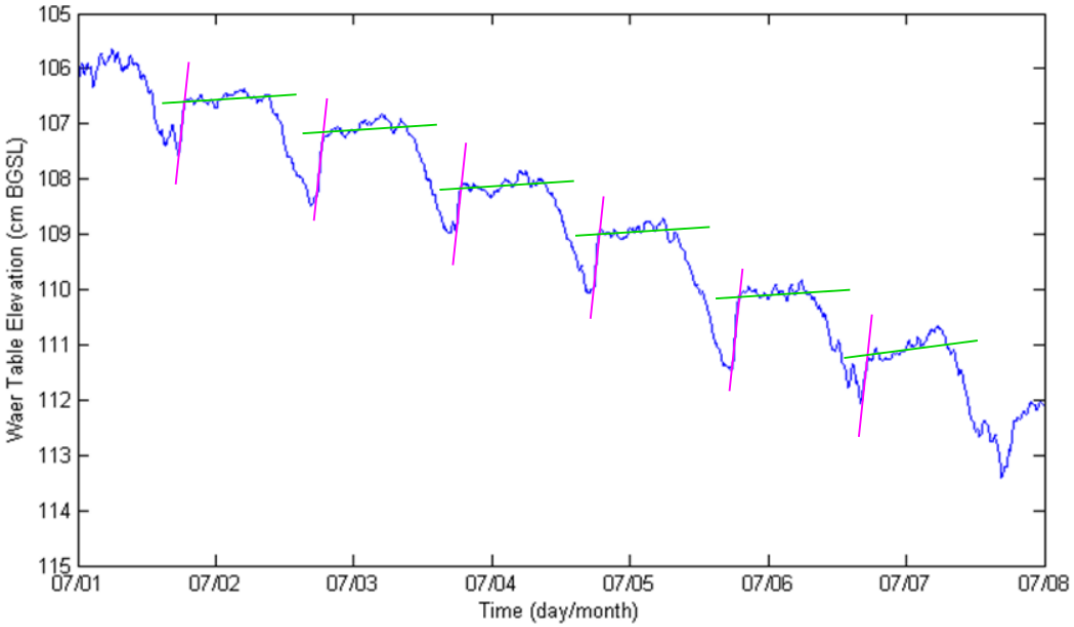

Figure 46. Break in slope at Ruby Pasture. The magenta line is fit to data during early night. The green line is fit to the data during late night.

Hypothesis

1. Hysteresis controls the break in slope.
2. Considering hysteresis, the difference between the air entry pressure of the wetting curve and drying curve controls the break in slope.
3. Without considering hysteresis, the curvature of the water retention curve near that of the of the air entry pressure controls the break in slope.

Since I cannot turn off and on physical processes in the real world, numerical modeling is well suited for this investigation. Before I jump to the numerical modeling I need to cover a hysteretic water retention curve.

The Hysteretic Moisture Retention Curve

The water retention curve is more complex than I originally put forth (Fig. 33). The water retention curve is actually hysteretic, meaning that for the same pore the pressure required to drain and fill are different values (Fig. 47). The hysteretic behavior is a result of many physical processes and is often modeled by setting the air entry pressure of the wetting curve to twice that of the drying curve (Simunek et al. 1998).

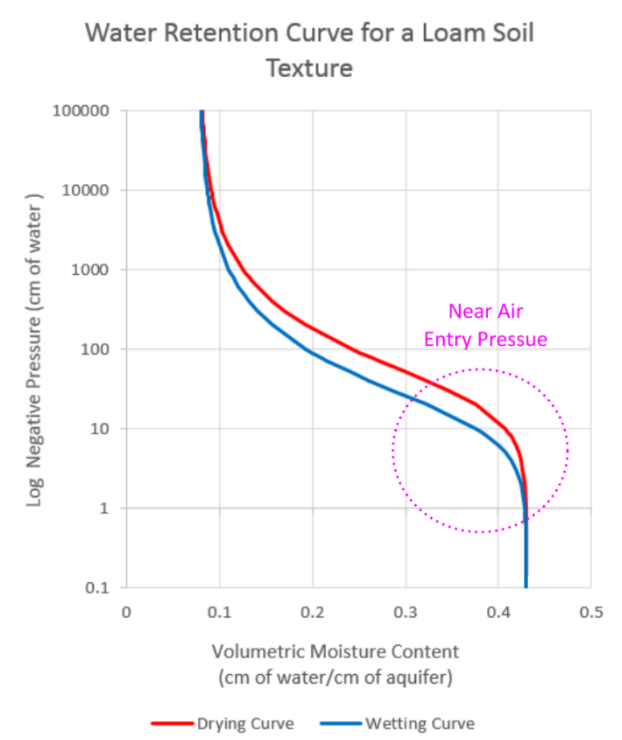

Figure 47. The hysteretic water retention curve. The portion of the water retention curve that is near air entry pressure is circled in bright purple.

Numerical Modeling

To test each hypothesis I developed two model runs, a control and a change that inputs the changes addressed in the hypothesis.

I. Hysteresis (Disabled vs Enabled)

II. Difference Between Air Entry Pressures (Small vs Large)

III. Texture Class (Silty Clay Loam vs Loam)

For each case I ran two HYDRUS 1-D models and produced graphs of the stable late time water table fluctuations. Using the modeled water table fluctuations I displayed the slopes fit to the early night and late night.

Case 1: Hysteresis (Disabled vs Enabled)

To investigate the effect of hysteresis on the break in slope I set up a HYDRUS 1-D model (Fig. 48) with hysteresis disabled and then ran the same model only turning on hysteresis (Fig. 49).

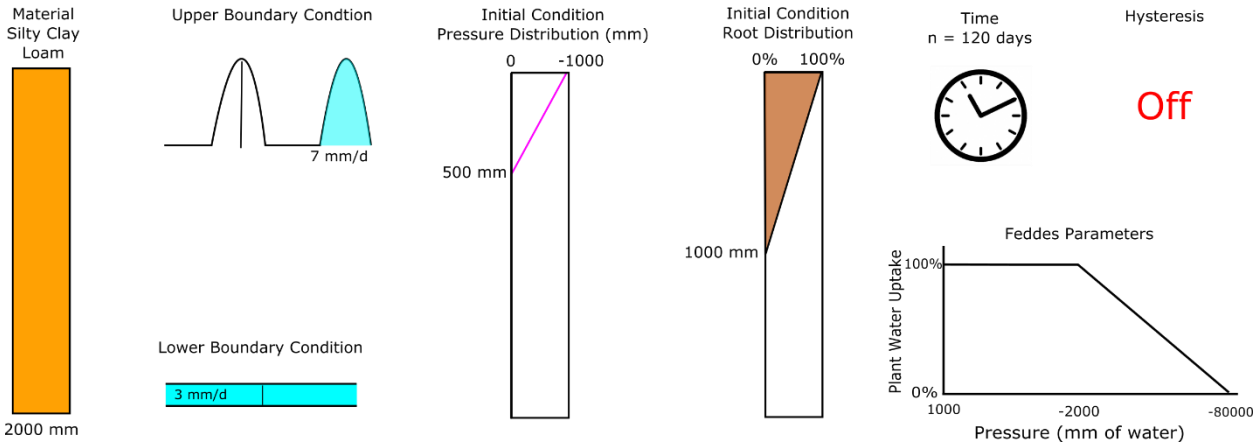

Figure 48. Model setup for the disabled hysteresis model run.

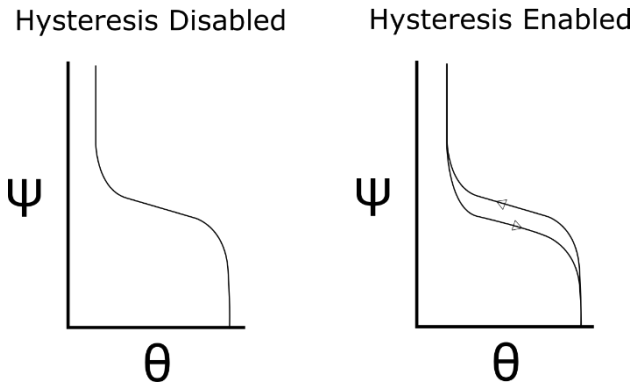

Figure 49. Visualizing the water retention curve with hysteresis disabled and enabled.

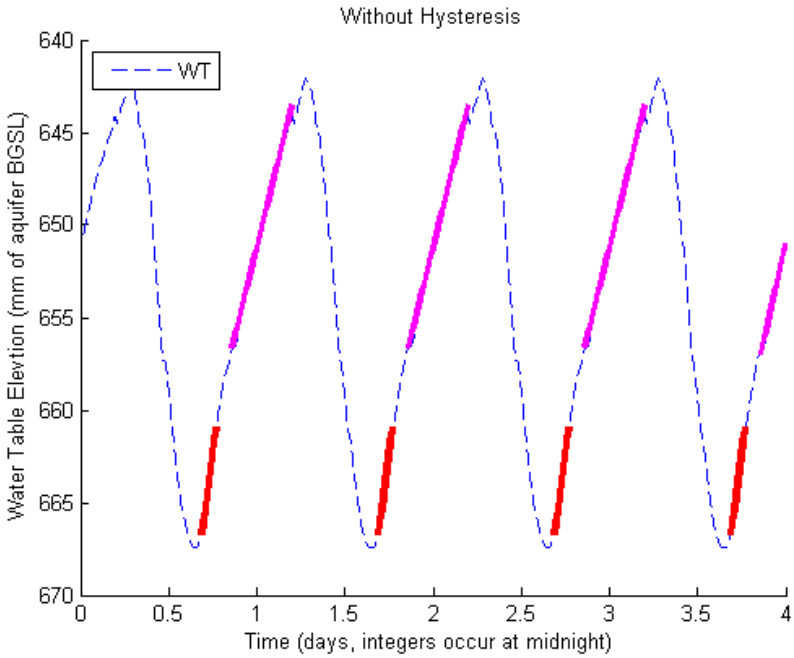

Figure 50. Stabilized fluctuations of the hysteresis disabled model run. The difference between the red slope (72 mm/day) and the purple slope (34mm/day) is 38 mm/day.

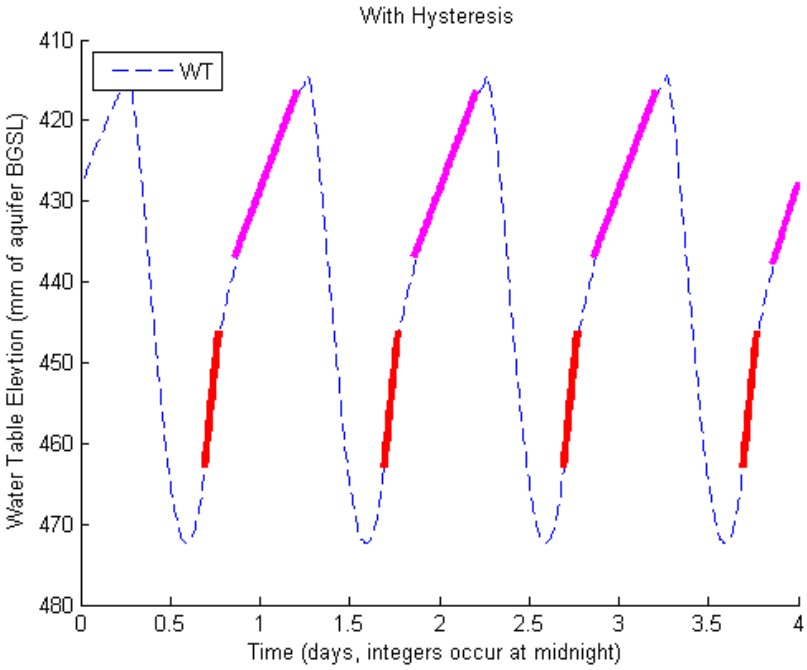

Figure 51. Stabilized fluctuations of the hysteresis enabled model run. The difference between the red slope (215 mm/day) and the purple slope (59 mm/day) is 156 mm/day.

The difference in slope between the Hysteresis Disabled and the Hysteresis Enabled run is a striking 122 mm/day, which suggests that hysteresis is a dominant factor contributing to the break in slope of the water table elevation record. With hysteresis enabled, a steeper pressure increase is required to reach a secondary behavior where the water is inputting into the system with a shallower pressure increase. One might attribute the steeper pressure increase as the early part of the water retention scanning curve of a hysteretic loop of the soil with a pressure slightly less than the air entry pressure. My second hypothesis is that the difference between the air entry pressure of the wetting curve and the drying curve would change the shape of the scanning curve of the soil near the air entry pressure.

Case 2: Difference Between the Air Entry Pressures (Small vs Large)

By changing the air entry pressure of the drying curve (α_d) and the air entry pressure of the wetting curve (α_w) I tested the second hypothesis. Two models were ran with the only difference being the parameters of α_w and α_d (Fig. 52). For the control I used the same model of that produced figure 51 where $\alpha_w = 0.001\ mm_{water}$ and $\alpha_d = 0.002\ mm_{water}$ representing a small difference in alphas (Fig. 53). The for test I just changed α_w to $0.0005\ mm_{water}$ and $\alpha_d = 0.004\ mm_{water}$ representing a large difference in alphas (Fig. 54).

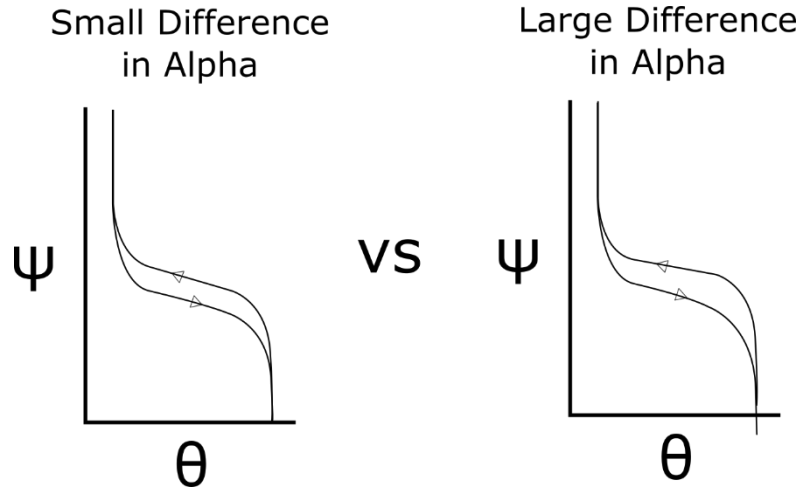

Figure 52. Visualizing a small and large difference in alphas on the water retention curve.

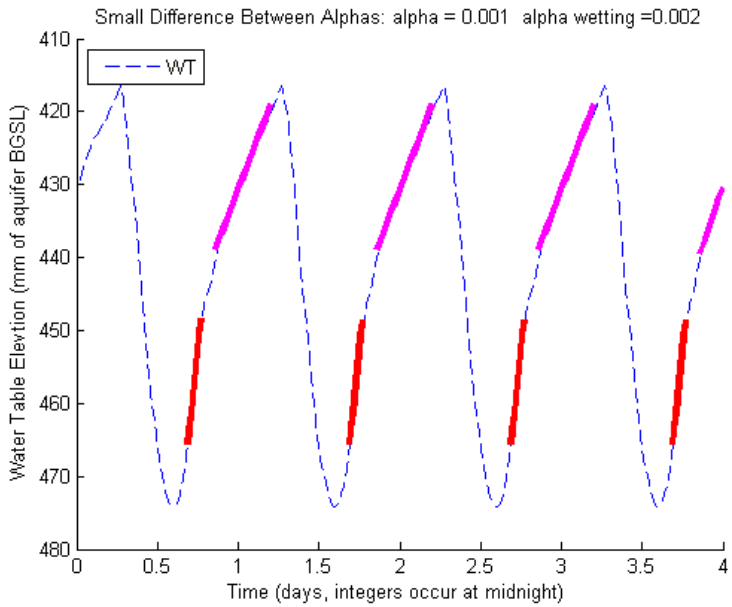

Figure 53. Stabilized fluctuations of the small difference in alphas run. The difference between the red slope (214 mm/day) and the purple slope (58 mm/day) is 158 mm/day.

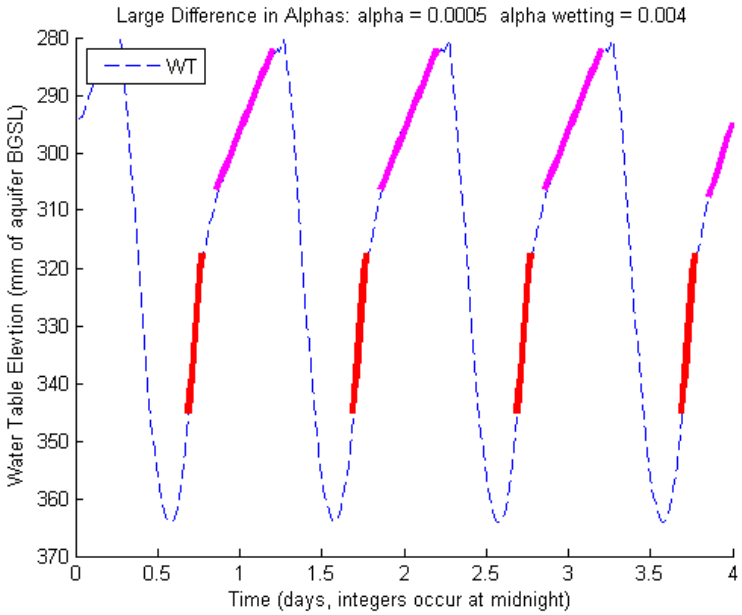

Figure 54. Stabilized fluctuations of the large difference in alphas run. The difference between the red slope (547 mm/day) and the purple slope (71 mm/day) is 475 mm/day.

The difference between the small and large difference in alpha runs is 319 mm/day, which suggests that the difference in air entry pressure from the wetting curve and the drying curve is a dominant factor contributing to the break in slope of the water table elevation record. The scanning curves of the soil in the pressure range near air entry pressures are provided (Fig. 55).

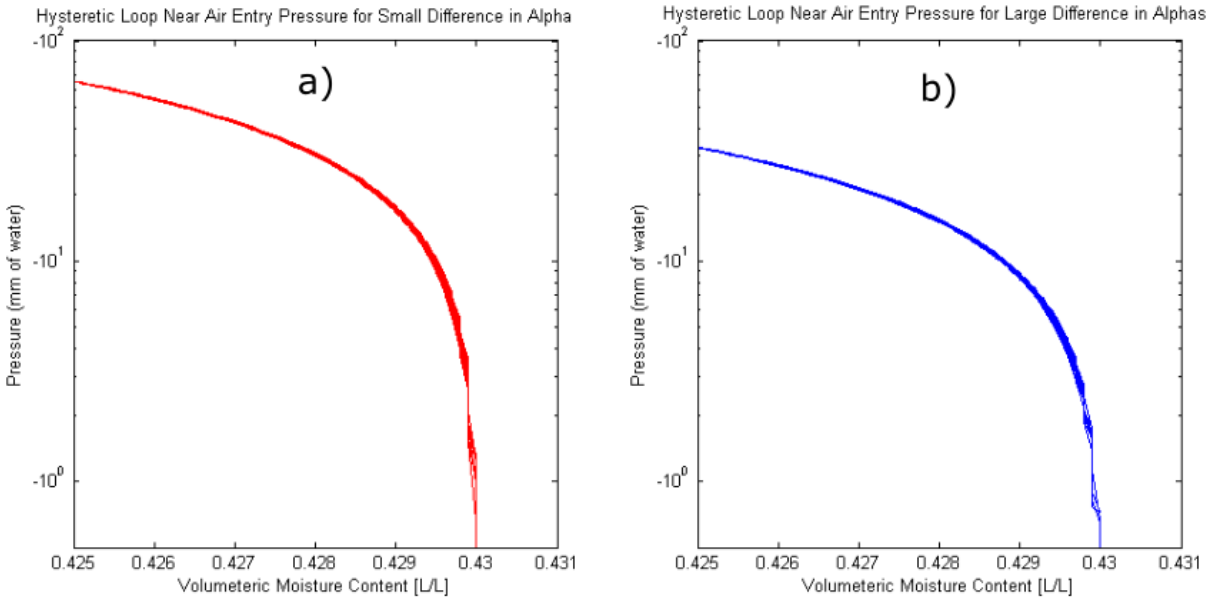

Figure 55. Comparing the scanning curves. Comparing scanning curves of soil near air entry pressure between the small **a)** and large **b)** difference in alphas. These curves were taken from an observation point in the capillary fringe during late time d50 to d120.

Case 3: Soil Texture Class

I looked at the effect of the soil texture class. For case one I ran a silty clay loam against a sandy loam with hysteresis disabled. The model parameters were similar to figure 48 however the length measurement were in cm and a slightly more sophisticated initial condition was employed (Fig. 56). For the second run the material type was set to a sandy loam. A cartoon of the shape of the water retention curves for the two runs is provided to help visualize the test (Fig. 57)

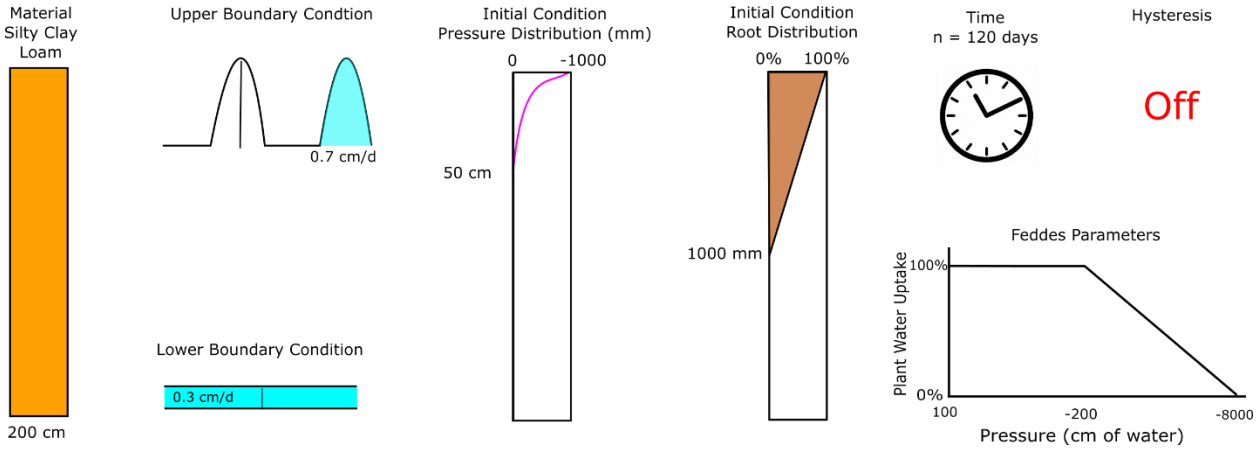

Figure 56. Model setup for the silty clay loam run.

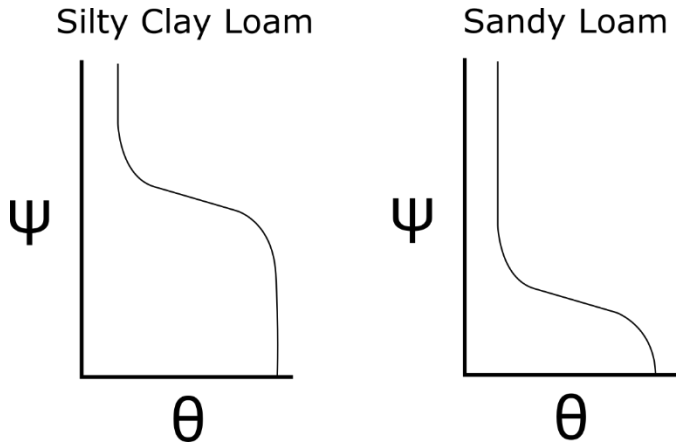

Figure 57. Visualizing a silty clay loam and a sandy loam on the water retention curve.

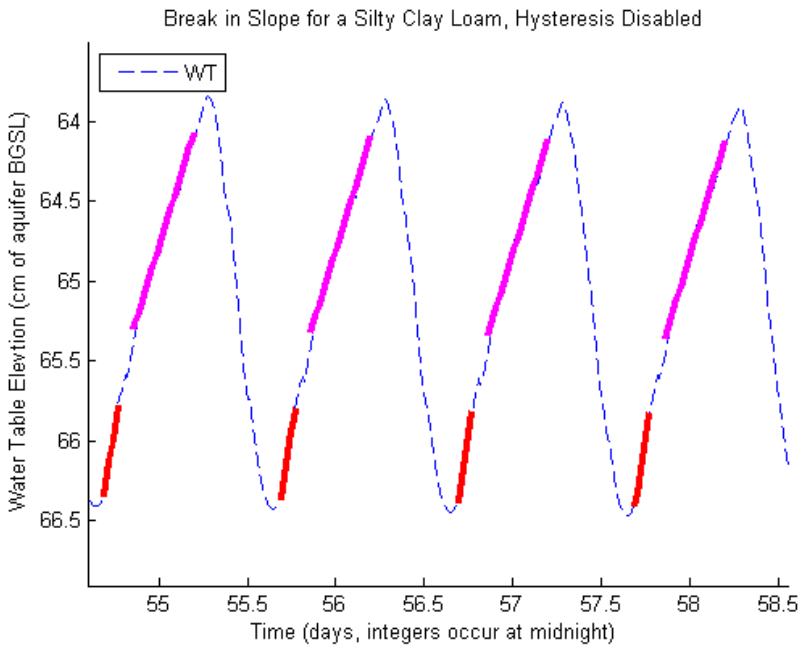

Figure 58. Stabilized fluctuations of the silty clay loam with hysteresis disabled run.

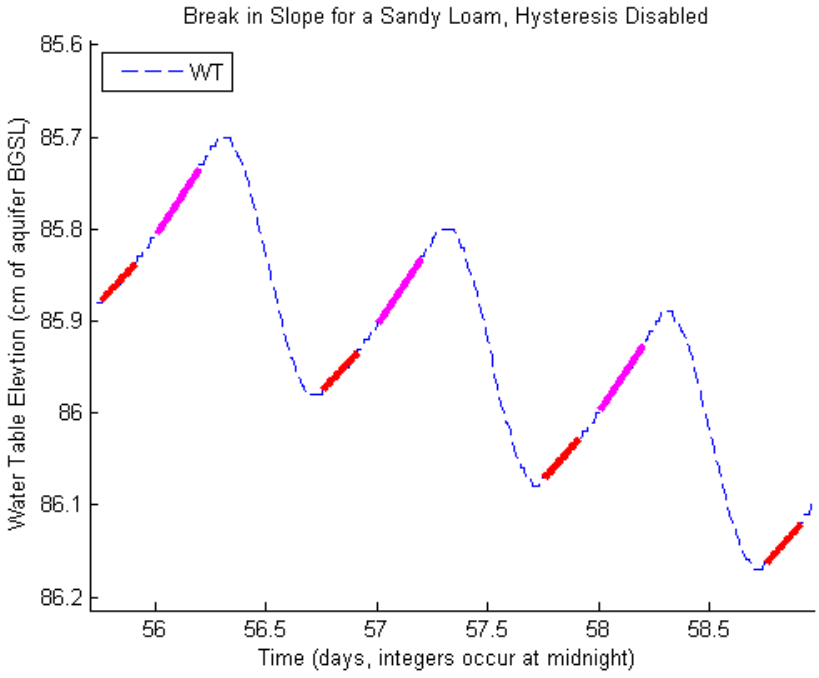

Figure 59. Fluctuations during days 56 to 59 of the sandy loam with hysteresis disabled run.

The most noticeable difference between the results from the Silty Clay Loam Texture Model Run (SiCL) (Fig. 58) and the Sandy Loam Texture Model Run (SL)(Fig. 59) is that the SiCL has reached a stabilized condition by 58d after the start of the model while the SL is still is a transitory condition by 58d after the start of the model. I have not provided the SL stabilized condition because in a stabilized state the water table was below the root zone and the signal was out of phase (data not shown). For the SiCL the difference between slopes is 34 mm/d while the SL is -1 mm of aquifer/day. The difference in slopes between texture classes without hysteresis enabled (35 mm/d) suggests that texture class is a factor in controlling the break in slope. Texture class does change other conditions within the model, to produce stabilized fluctuations within a rooting zone the boundary conditions would need to be altered making the comparison between models more uncertain.

Table 10. Summary table of the early and late night slopes.

Hypothesis (title)	Model (title)	Early Slope (mm/day)	Late Slope (mm/day)	Difference in Slopes (mm of aquifer/day)
Hysteresis?	Without Hysteresis	72	39	34
	With Hysteresis	215	59	156
Wetting Curve?	Small Difference Between Alphas	214	58	156
	Large Difference Between Alphas	547	71	475
Texture Class?	Silty Clay Loam	70	36	34
	Sandy Loam	3	4	-1

Conclusion

As White eluded they're many processes that can affect the break in slope occurring during the night of the water table record. Operationally White's method just uses the data during the night after the break in slope. However my curiosity for a physical understanding of

the break in slope drove me to test three hypothesis. From my modeling results hysteresis is dominant factor in controlling the break in slope. By exploring hysteresis in the modeling environment I did not explore the individual processes that give rise to the hysteretic behavior in the water retention curve, but simply enabled and disabled the equation that considers hysteresis. Looking deeper into the problem, my notion was that the curvature of the water retention curve of the soil right above the air entry pressure was controlling the break in slope. By changing the air entry pressure of the wetting and drying curve I could change the curvature of the soil near the air entry pressure which resulted in a change in the break in slope. This provides evidence that the difference between wetting and drying air entry pressures is a factor in controlling the break in slope. To test whether hysteresis was the real driver for the break in slope or was it just the shape of the water retention curve of the soil near air entry pressure I simplified the system by removing hysteresis, giving the soil one moisture retention curve to track, and compared the results from two soil textures. Even though texture affects many parts of the system the results were clear: by changing the texture from as Silty Clay Loam to a Sandy Loam the break in slope disappeared. All three hypothesis resulted a change in the break in slope (Table 10).

Appendix a.III: Estimating Groundwater Upwelling

Introduction

The White Method doesn't work well to estimate daily evapotranspiration (R^2 = 0.04) (Fig. 27). Can the white method estimate apparent groundwater upwelling (Fig. 60)? All we need is a reasonable estimate of specific yield and then back solve for apparent groundwater upwelling rate in lengths of water per time.

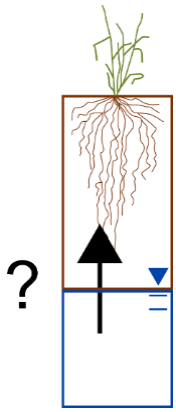

Figure 60. What is the apparent groundwater upwelling?

Estimating Specific Yield

One interest thing about shallow aquifers is that we can say something about the aquifer properties by looking at evapotranspiration rate. By using an observation well and a nearby well I estimated a constant specific yield by using the Fitting $ET_{(weather\ station)}$ to $ET_{(White)}$

method. The correlation is poor (Fig. 61) (SSE = 190.9) but the estimate of specific yield is better than using an educated guess (Fig. 62) (SSE = 94.2).

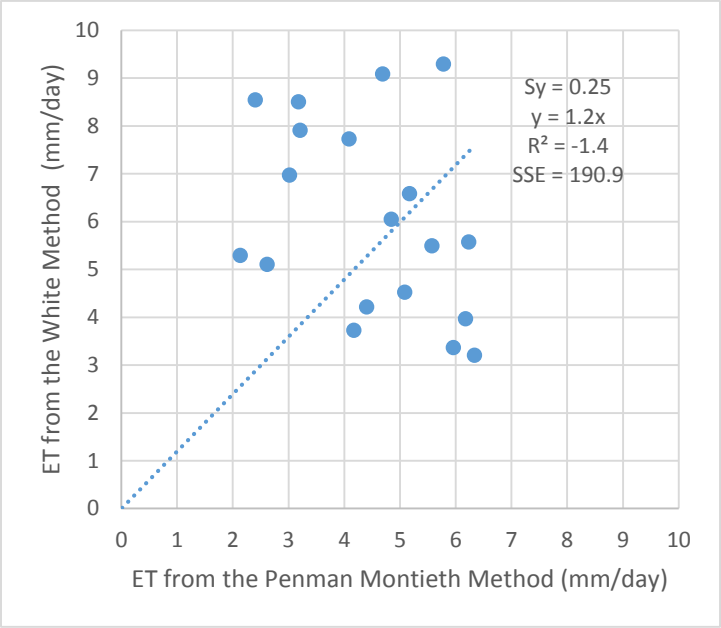

Figure 61. Linear regression without minimizing SSE.

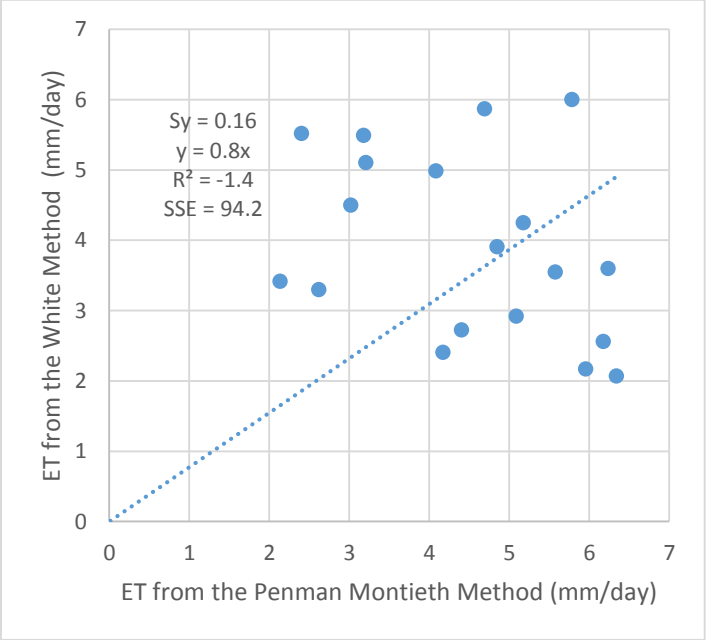

Figure 62. Linear regression after minimizing SSE.

By deriving specific yield this way I am assuming that the daily evapotranspiration rate is the daily groundwater upwelling rate (Fig. 63).

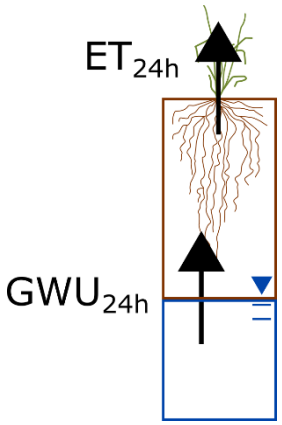

Figure 63. The big assumption.

Back Solving

Now that I have an estimate of specific yield (Sy = 0.16) I rearranged the white equation (Eq. 3) and solved for apparent groundwater upwelling in cm_{water}/day (Fig. 64).

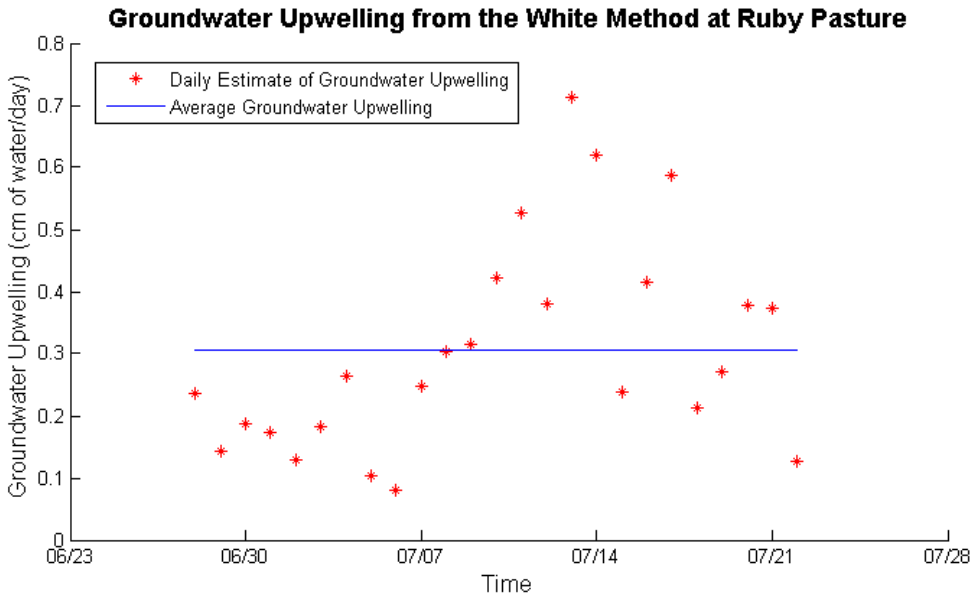

Figure 64. Apparent groundwater upwelling rate at Ruby Pasture.

Notice that before the precipitation events on 7/12 and 7/13 the groundwater upwelling rate was relatively constant and below the mean. On 7/13 and 7/14 the upwelling rate spiked followed by a decay until the end of the record on 7/22.

Conclusion

Groundwater upwelling rate is intrinsically a slowly changing variable. Although I would expect the apparent groundwater upwelling rate to increase after a precipitation event at this point in the landscape, the day to day variation ranging from less than 0.1 cm_{water}/d to greater than 0.7 cm_{water}/d is indicative that the estimate of groundwater upwelling is useless. This day to day variation can be explained by error associated with sensing pressure below the water table and correcting that signal with a noisy barometric pressure signal (Fig. 65)

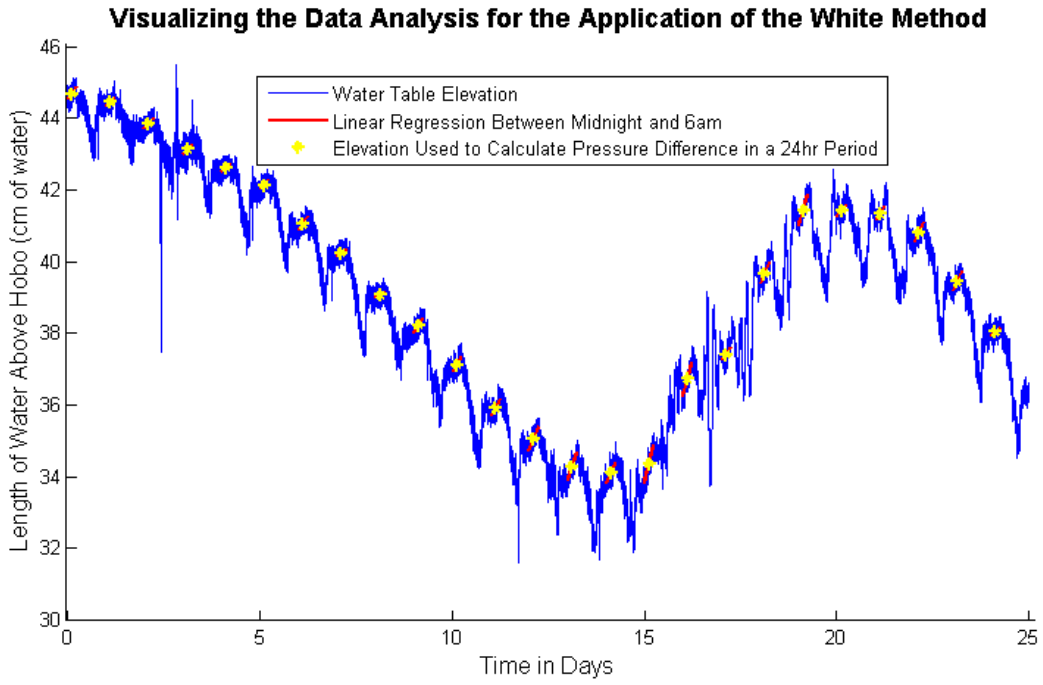

Figure 65. The water table elevation record after only being corrected for barometric pressure.

Appendix a.IV:

Vegetation Clues into Spatiotemporal Water Availability

The Question

What vegetation variable could provide insight into the spatiotemporal availability of stored soil water and groundwater accessibility?

The Answer

The physiology of a plant is partially tailored to the water availability in its habitat. Hydrophilic plants have developed a physiology that allows them to deal with anoxia due to saturated soils (Tiner, 1991). Xerophytic plants have developed mechanisms that allow them to transpire during the night when conditions allow for minimal water loss. To develop easily interpretable maps of water availability across a site using vegetation data we developed a hydrologic index that assigned a number to each species related to its ecophysiology classification where 1 for xerophyte, 2 for xeromesophyte, 3 for mesophyte, 4 for mesohydrophyte, and 5 for hydrophyte. The weighted mean at each observation point was taken to provide a single number at each observation point so that an experimental variogram (Fig. 66) could be developed and an ordinary kriging model could be applied (Bossong et al.,

1999). The hydrology index map can be associated with the spatial extent of inter-seasonal water availability (Fig. 67) (Williams, 2006).

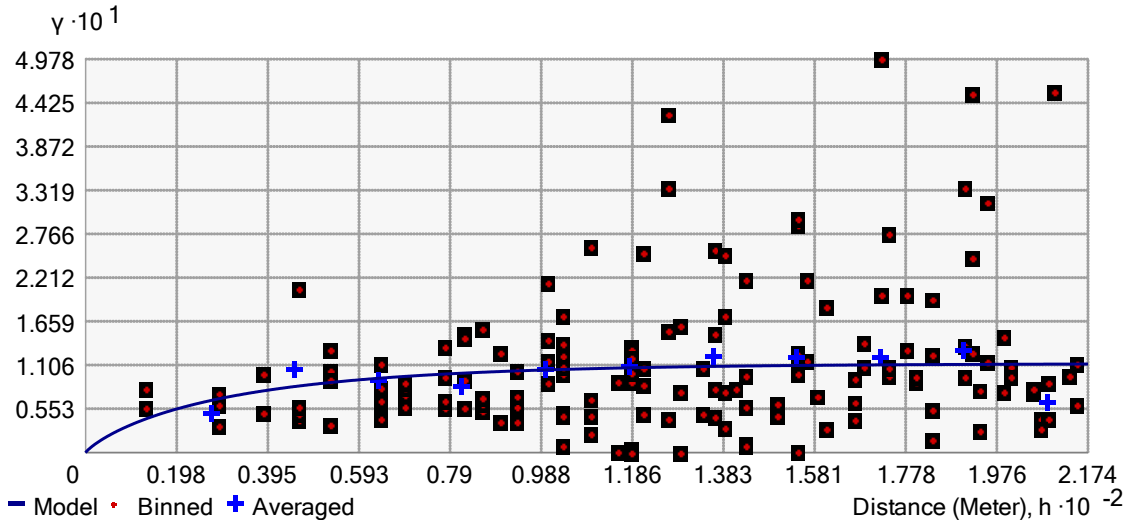

Figure 66. Theoretical variogram for the vegetation hydrologic index at Granite Boulder Pasture. This sill is at 11.1 and the range is at 120m.

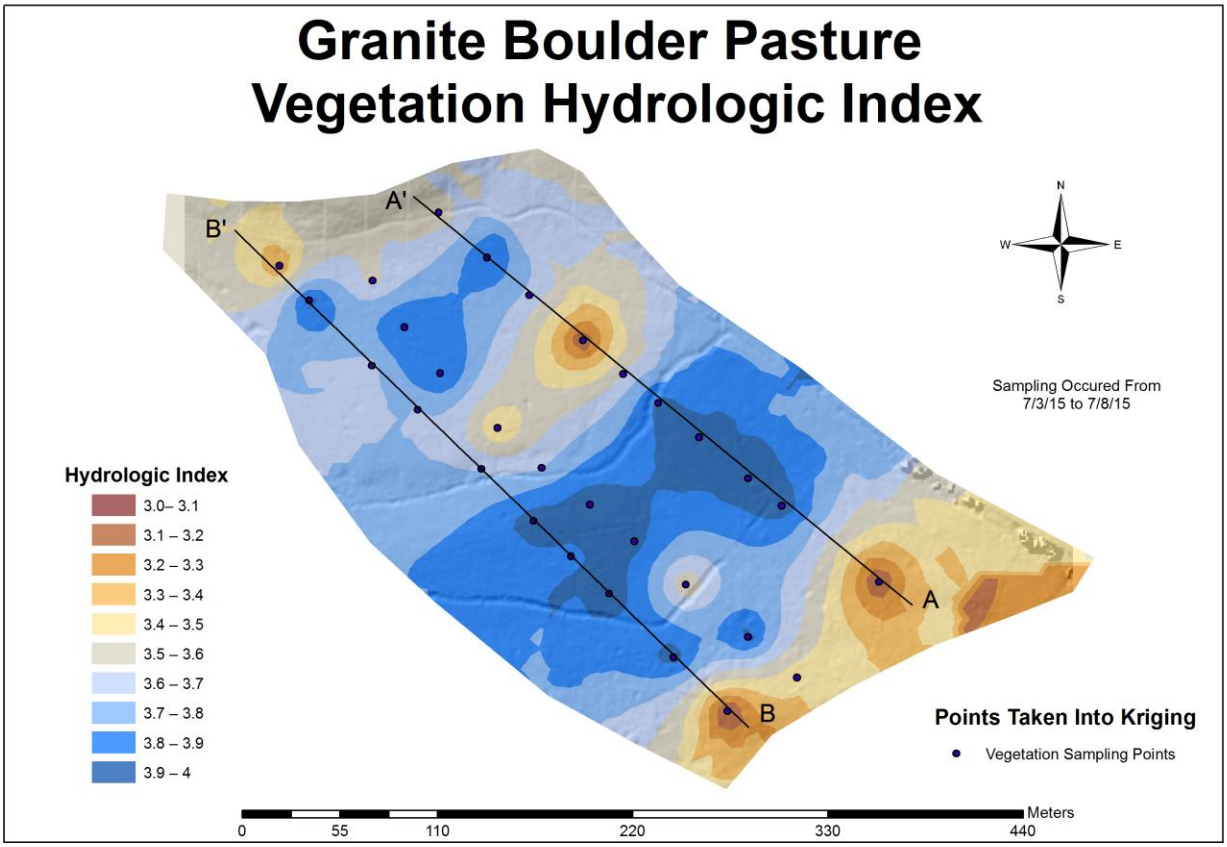

Figure 67. Vegetation hydraulic index across Granite Boulder Pasture.

Notice the linear trends across the site going from Northeast to Southwest. Along the Southeast there is a dry trend. At the center of the site between the two surface drainages there is a wet trend. It appears that the raised elevation on either side of the two surface drainages have a lower vegetation hydrologic index than between the two surface drainages. There also appears to be an increase in vegetation hydrologic index on the downslope side of the break in slope of the hillslope bounding the site along the Northwestern edge of the map (Brinson, 1993). Elevation of cross sections A to A' and B to B' are provided (Fig. 68)

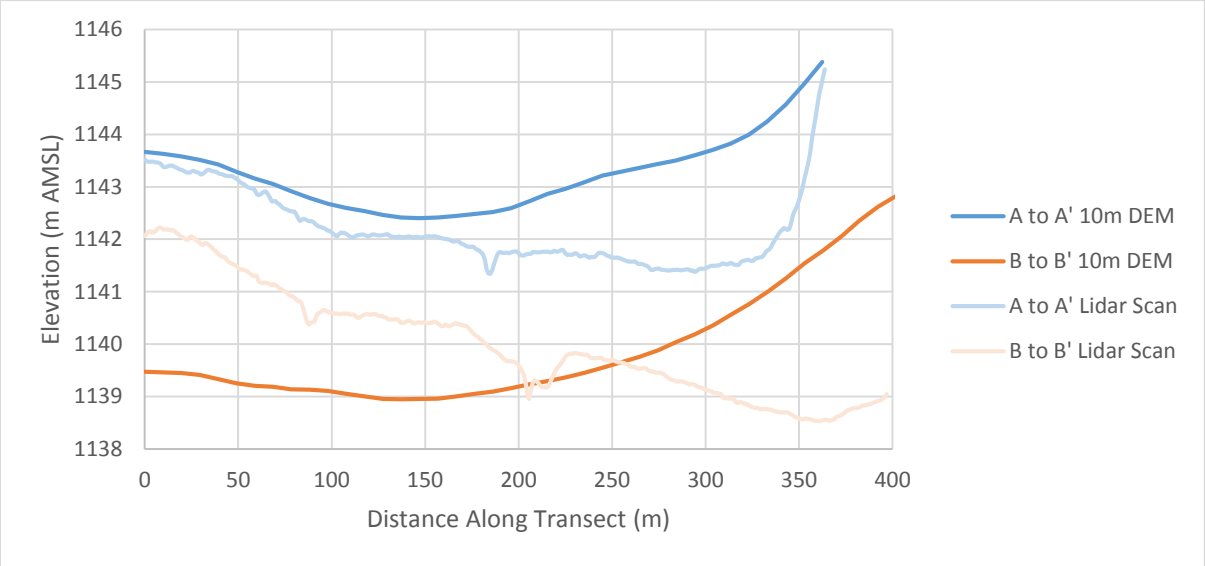

Figure 68. Elevation cross sections across Granite Boulder Pasture. The high resolution Lidar captures surface drainages but the absolution position skewed across the site. The 10m DEM captures the surface but the resolution is too coarse to capture the surface drainages.

Geomorphic position is key to a predicted depth to water table (Brinson, 1993). At Granite Boulder Pasture the higher vegetation hydrologic indices were located in low positions across the site (distances 100m to 200m along both transects) as well as break in slopes where the hillslope transitioned into alluvial fan deposits (distances 300 to 350 along the transects). The higher vegetation hydrologic index indicates that the vegetation's physiology is better tailored to deal with anoxia, which implies locations that have shallow water tables (Tiner, 1991). For the vegetation hydrologic index to change, the community composition has to change, a process that changes at a decade timescale (Williams, 2006). Water table elevation can drop out of the root zone through the course of the dry season (Fig. 36) and I would not expect the vegetation hydrologic index to capture this change in intra seasonal water

availability. The percent standing dead vegetation is better suited to capture the changes in intra-seasonal water availability.

The percent standing dead is an estimate of the percentage of ground cover that appears to be recently deceased vegetation. Large values of percent standing dead can be thought of as having had water availability during the early part of the dry season and then loosing access to water by the time the sampling date occurred. A small value of percent standing dead suggests consistent water availability through the time of sampling. Since each observation point was assigned a single value for percent standing dead, an experimental variogram was developed (Fig. 69) and an ordinary kriging model was applied to produce a map of the percent standing dead across the site (Fig. 70). The percent standing dead map can be associated with the spatial extent of the intra-seasonal water availability.

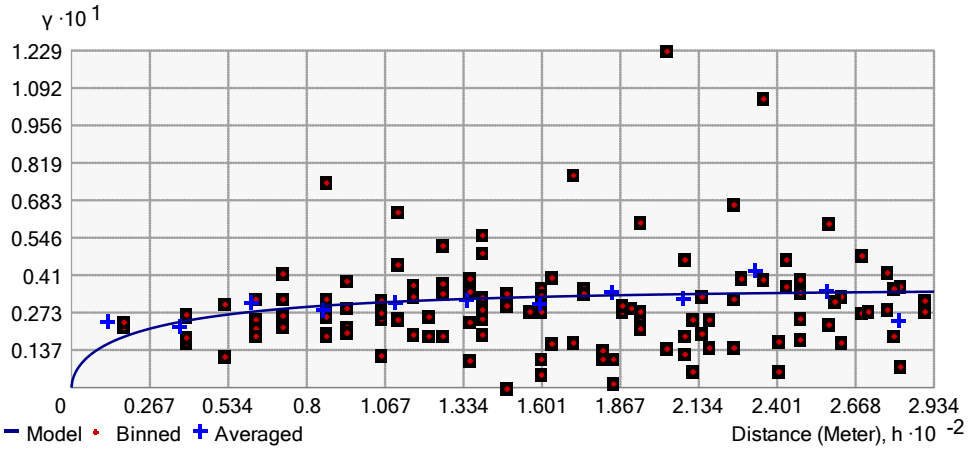

Figure 69. Variogram for the percent standing dead at Granite Boulder Pasture. The sill is at 3.3 and the range is at 140m.

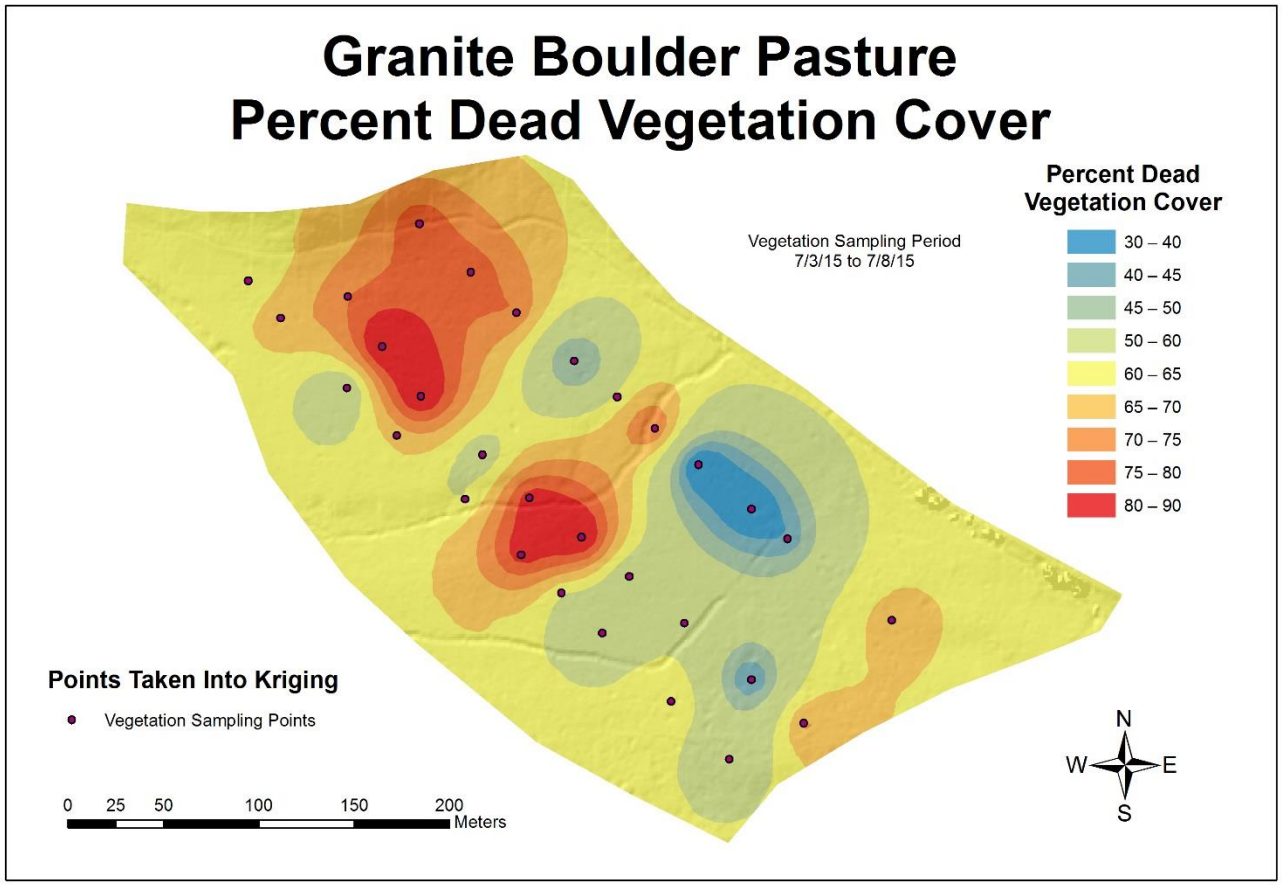

Figure 70. Percent standing dead across Granite Boulder Pasture.

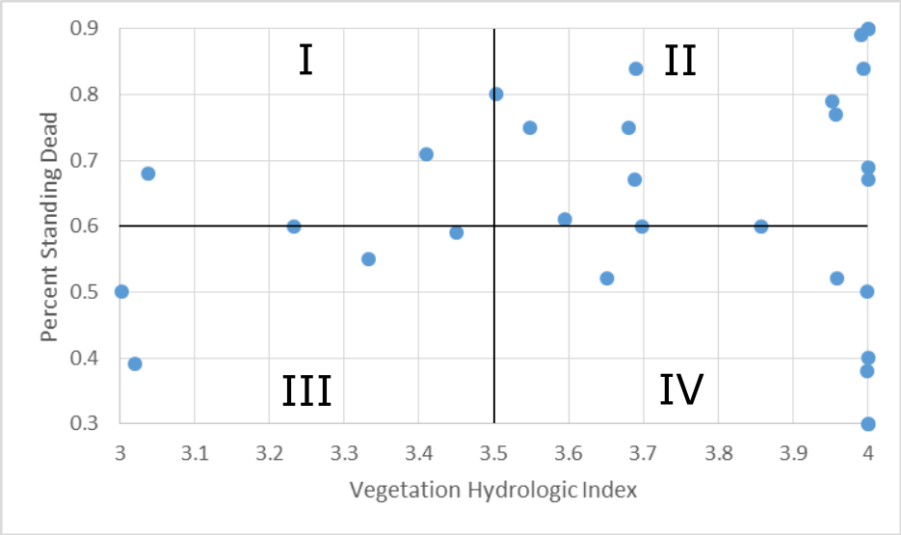

Figure 70. Vegetation hydrologic index vs percent standing dead at Granite Boulder Pasture. **I)** Low VHI and High PSD. **II)** High VHI and High PSD. **III)** Low VHI and Low PSD. **IV)** High VHI and Low PSD.

Discussion and Conclusion

During the dry season of a semi-arid watershed, the variables of a vegetation hydrologic index and percent standing dead can provide insight into the depth water table between water years as well as the relative water table depth to the root zone between the start of the dry season and the time of sampling. With the reasonable assumption that at the time of sampling (~50d since the start of the dry season) the accessible stored soil water had been depleted, the percent standing dead variable implies the connectedness of the root zone to the water table. A large percent standing dead value (>~0.6) represents a disconnected root distribution from the water table, while a small percent standing dead value (<~0.6) represents a strong connection between the root distribution and the water table at the time of sampling. Since a vegetative community composition response to water availability occurs on the order of years the vegetation hydrologic index closer to 5 represents an inter-seasonal shallow water table,

while a vegetation hydrologic index closer to 3 represents an inter-seasonally deep water table. An inter-seasonally shallow water table is shallow enough to inhibit mesophytes by generating anoxic conditions in the root zone. An inter-seasonally deep water table is deep enough to provide a deep enough vadose zone that mesophytic root systems have enough access to oxygen which allows the mesophytic plants to outcompete the hydrophytic plants.

The relationship between vegetation hydrologic index and percent standing dead could provide insight into the placement of an observation well to produce a useable record for the White Method. For the White Method it would be preferable if the water table is inter-seasonally shallow and drops to a depth that is moderately connected to the root zone, thus areas that have a high vegetation hydrologic index (3.75 to 4) and a moderate percent standing dead (~0.5) would be favorable for sensing a water table record that could be used in the White Method. Coincidentally, I placed the center of my experiment at a point where the vegetative hydrologic index was 4 and the percent standing dead was 50 percent. I made the decision to place the center of my experiment based on an abundance of water table records at Granite Boulder Pasture, there will be many time future White Method users will need to install an observation well or focus an experiment without water table records.

Appendix a.V: Pump Test Analysis

Introduction

A pump test is a classical groundwater hydrologists approach to characterizing an aquifer's specific yield (Ramsahoye et al., 1961). The four components of a pump test are selecting and installing the wells, performing the pump test, selecting a conceptual model, and analyzing the data for specific yield.

Selecting and Installing the Wells

The spatial limitations, such as a maximum observation well depth of <~2m due to equipment and site characteristics, as well as unknown spatial heterogeneity in material distribution, limited the placement of the observation wells to be within ~3m of the pumping well. Temporal limitations, due to the background change in water table elevation on the diurnal cycle, limited the duration of pumping to ~3h. The objective was to place the top of the screened interval at 1m BGSL and to place the observation wells in a cross in map view such that the pumping well is placed at the center and the lengths of the arms of the cross such that in radial coordinates an observation well would land at ~0.5m, ~1m, ~1.5m, and ~2m. The geometry of the final installation are provided for Granite Boulder Pasture (Fig. 72) and Ruby Pasture (Fig. 73).

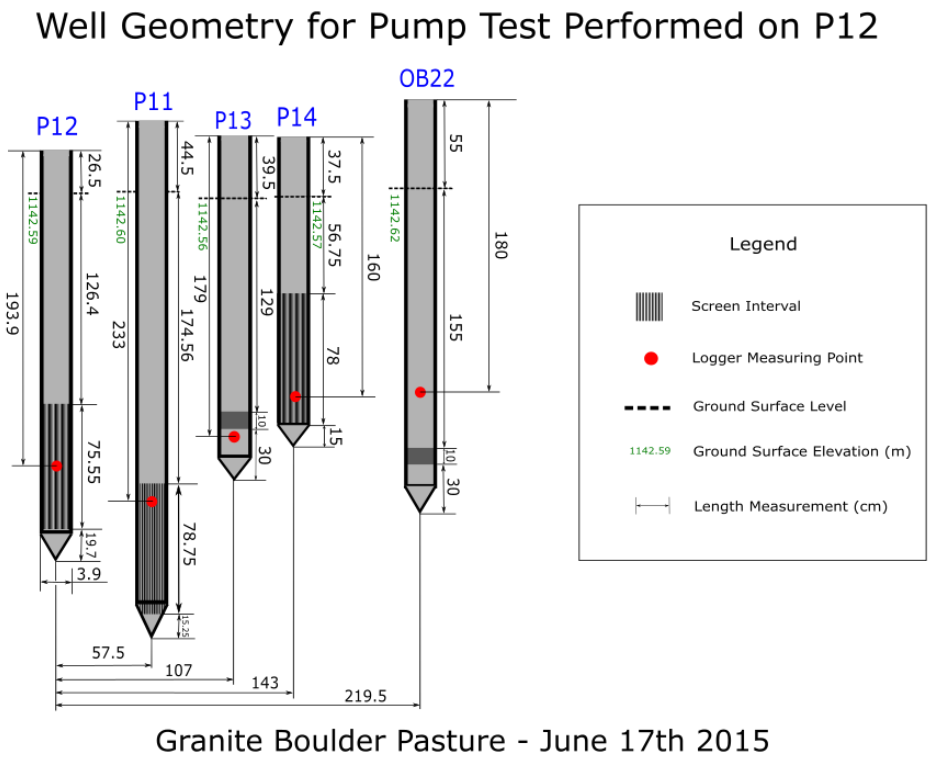

Figure 72. The well geometry at Granite Boulder Pasture in radial coordinates.

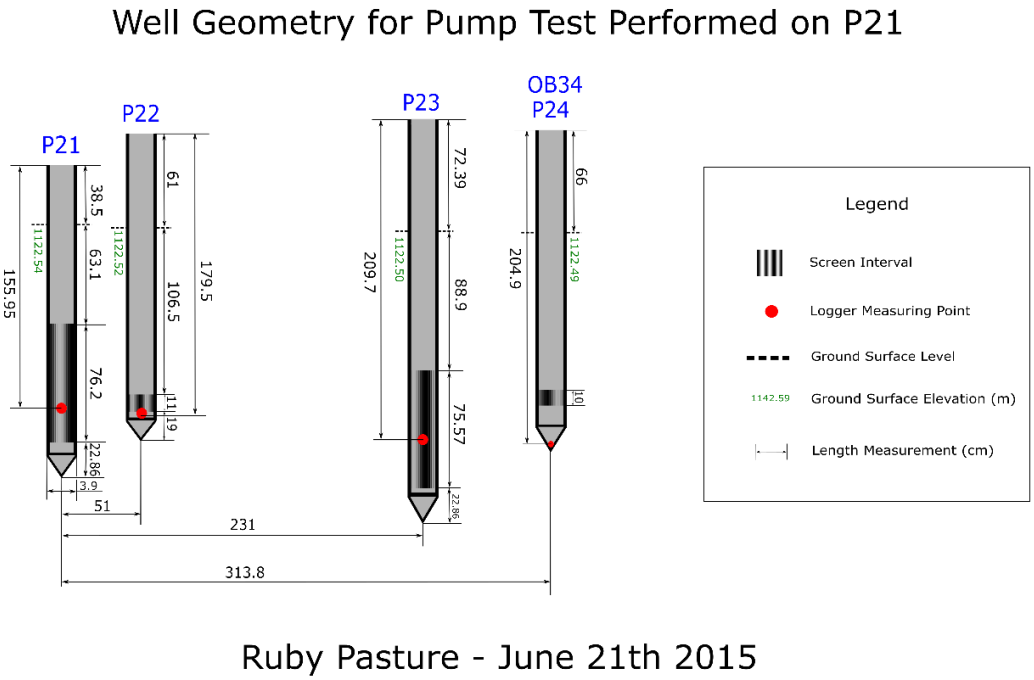

Figure 73. The well geometry at Ruby Pasture in radial coordinates.

Performing the Pump Test

To select a pumping rate a stepped drawdown (Jacob, 1947) test was performed (electronic appendix filenames: Losses_model-P12 and Losses_model-P21). Due a shallow maximum allowable drawdown, well losses, and pumping time constraints, pumping rates of 1.68 m^3/d and 3.10 m^3/d were selected for Granite Boulder Pasture and Ruby Pasture respectively. The long time pump test occurred at Granite Boulder Pasture starting at 4pm 6/17/2015 (electronic appendix filenames: Pump Test_GBP_P12_Pump Well; Pump Test_GBP_P11_Obs Well; Pump Test_GBP_P13_Obs Well; Pump Test_GBP_P14_Obs Well; Pump Test_GBP_OB22_Obs Well; Pump Test_GBP_Manual Measurements). The long time pump test occurred at Ruby Pasture starting at 11am 6/19/2015 (electronic appendix filenames: Pump Test_RP_P21_Pump Well; Pump Test_RP_P22_Obs Well; Pump Test_RP_P23_Obs Well; Pump Test_RP_P24_Obs Well; Pump Test_RP_Manaual Measurements).

Selecting a Conceptual Model

In addition to stratigraphy (electronic appendix filename: Hydraulic Characterization Summary) a derivative drawdown test was performed to diagnose the aquifer type (Renard et al., 2009). Granite Boulder Pasture was diagnosed to be a double porosity or unconfined aquifer (Fig. 74). The Ruby Pasture derivative drawdown test was inconclusive but the stratigraphy suggests an unconfined aquifer (Fig. 75).

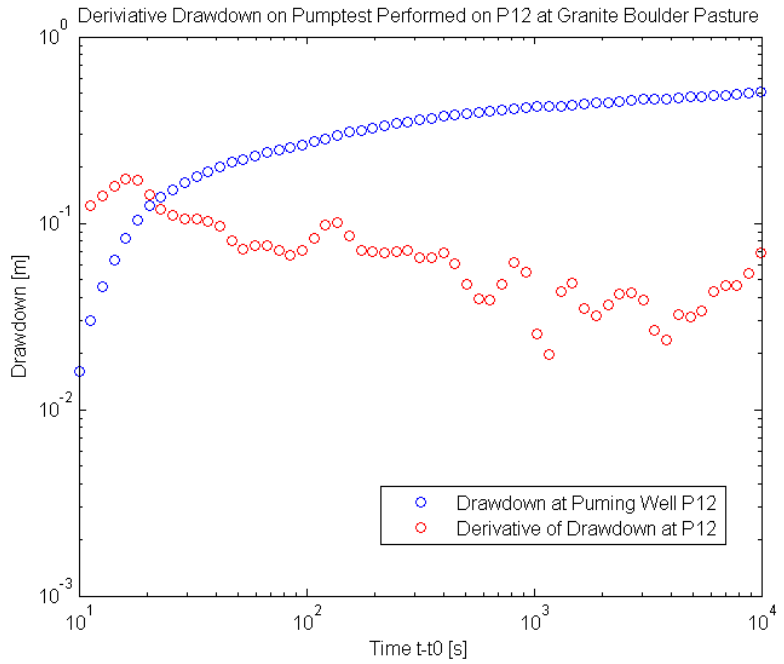

Figure 74. Derivative drawdown test at Granite Boulder Pasture.

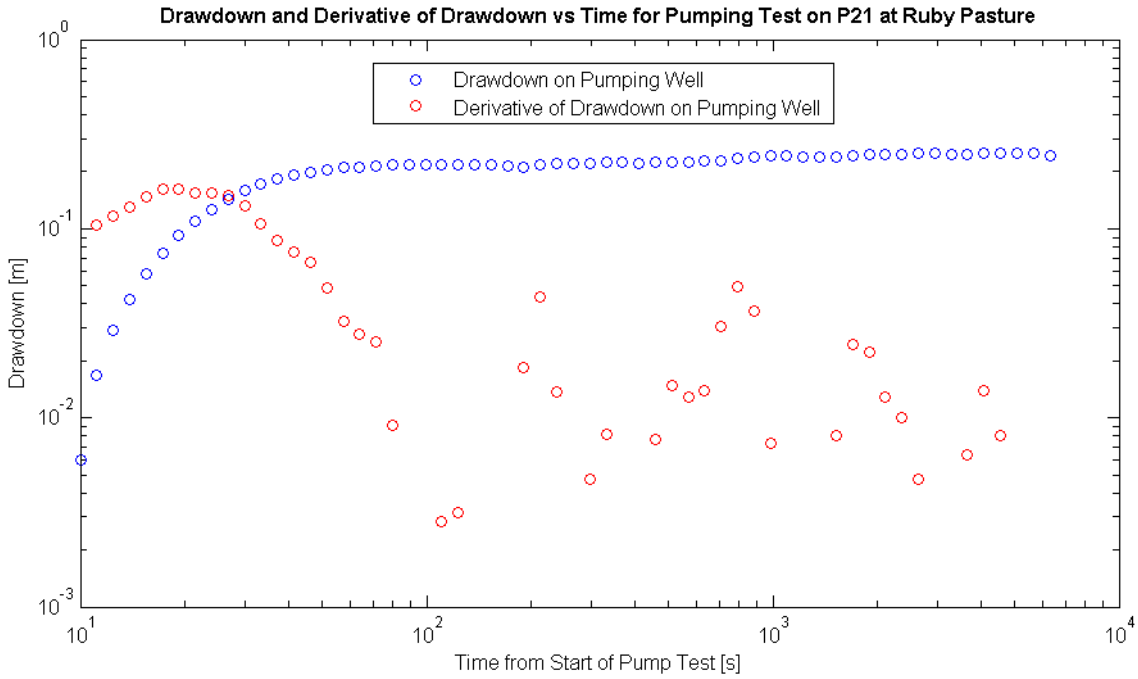

Figure 75. Derivative drawdown test at Ruby Pasture.

Two conceptual models were selected to perform the pump test analysis. The Theis Model for a transient confined aquifer was selected due to its ease of applicability with an excel solver (Theis, 1935) (Fig. 76). The key assumption to use the Theis Model is that the storage coefficient consists of specific storage and specific yield, for an unconfined case the specific yield much greater than the specific storage thus the storage coefficient is specific yield. Other key assumptions were: since the drawdown is small the effect of partial penetration is small, in late time the effects of elastic storage are negligible, and the depth to bedrock is 15 m (electronic appendix filename: Well Log_GRAN 38; Well Log_GRAN 51085)

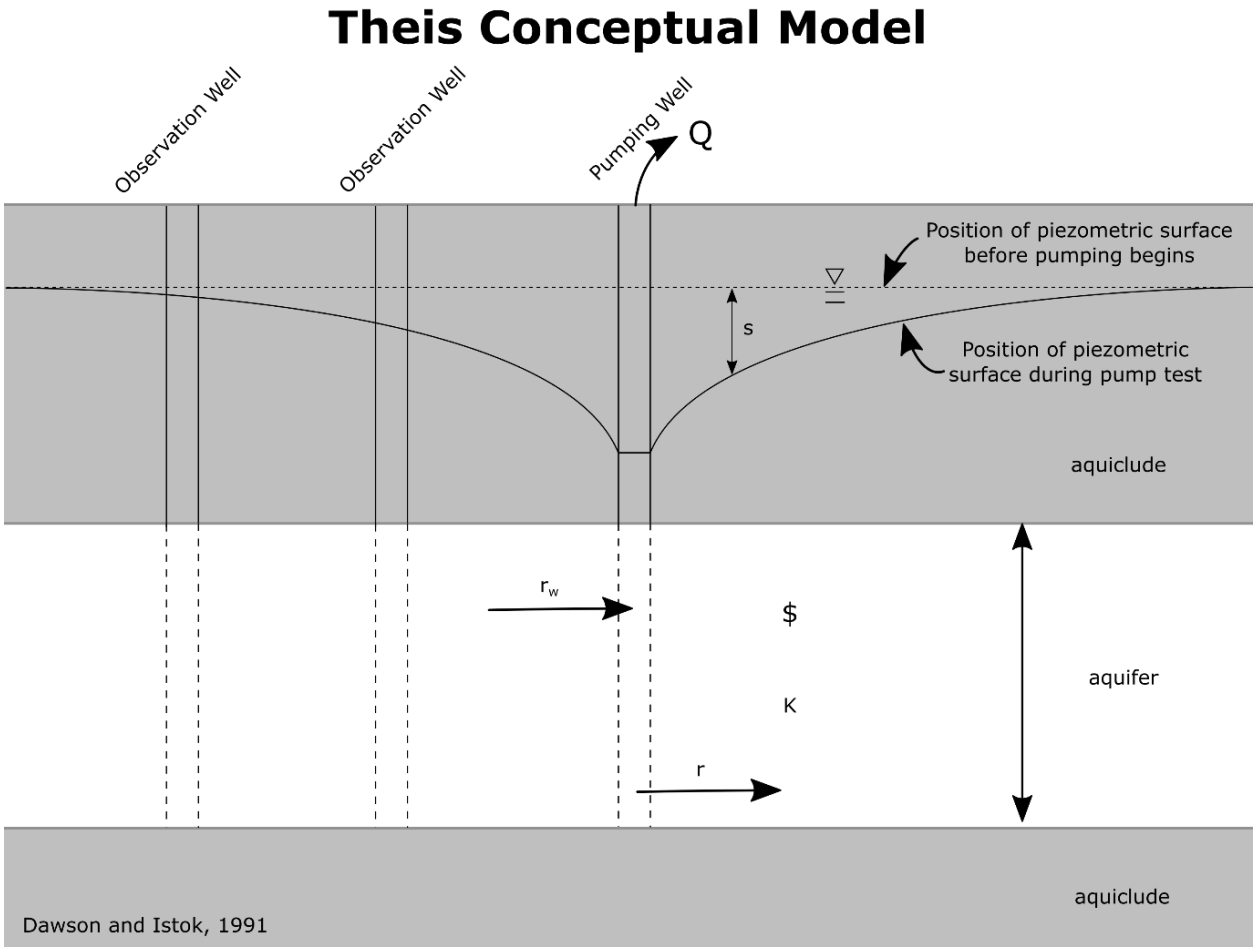

Figure 76. The Theis Model for a transient confined aquifer.

The second conceptual model selected was the Neuman Model for a transient, unconfined and anisotropic aquifer (Neuman, 1972) (Fig. 77). The advantage for selecting this model is that is designed to for an unconfined aquifer and solves directly for specific yield. The disadvantage of this model is its applicability is limited to a curve fitting exercise with an assumed beta number. The other key assumptions made using the Theis Model were also made using the Neuman Model.

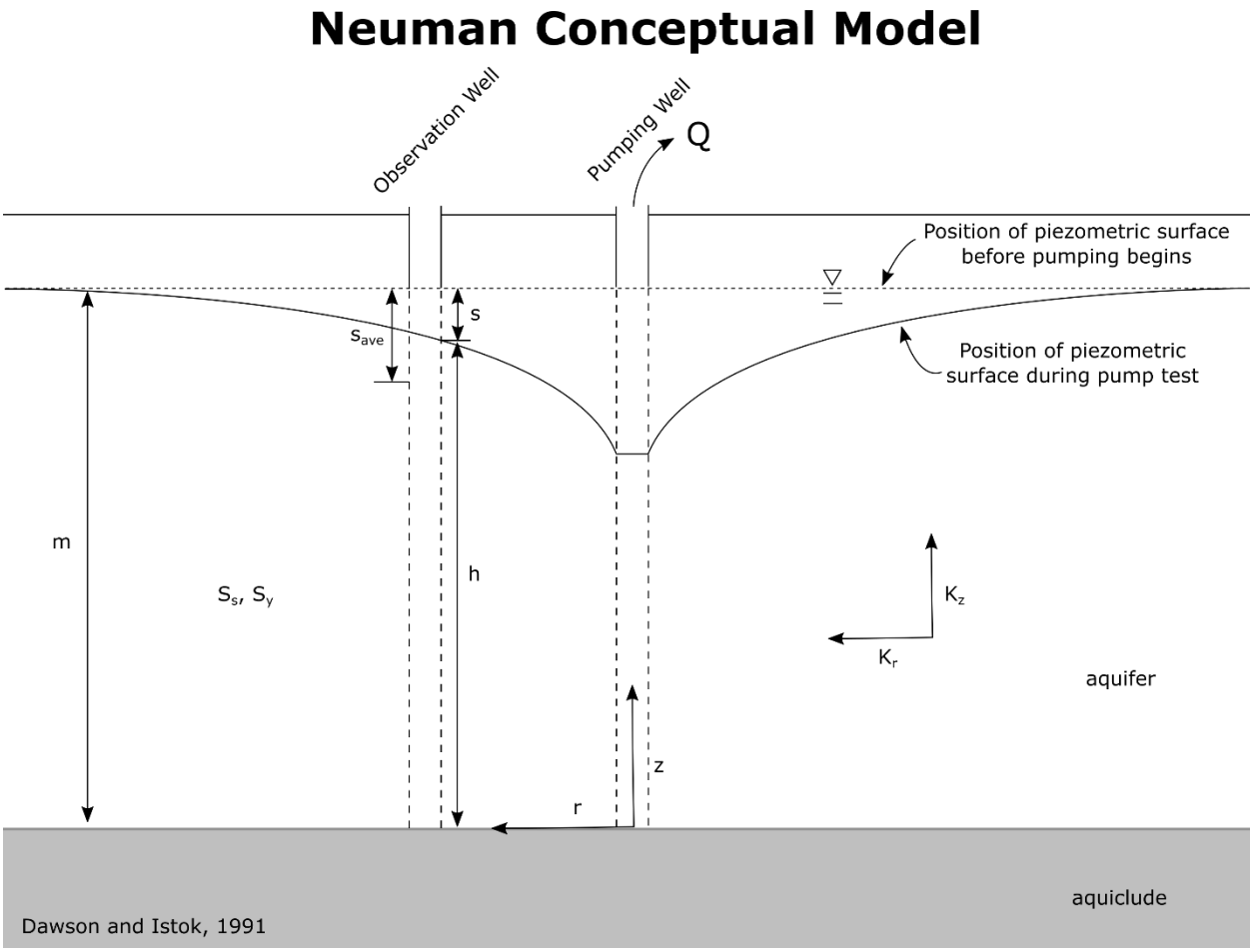

Figure 77. The Neuman Model for a transient, unconfined and anisotropic aquifer.

Analyzing the Data for Specific Yield

The drawdown versus log time plots were developed for well participating the pump test at Granite Boulder Pasture (Fig. 78) and Ruby Pasture (Fig. 79). Observation wells that had a dampened signal, signifying large losses through the well screen were not included into the evaluation for specific yield. For the set of solver solutions to the Theis Model, the transmissivity was determined at the pumping well (Halford et al., 2006) and the specific yield determined at the observation wells by optimizing the model to late time (Fig. 80 and 81) (electronic appendix filename: Solver_OB22; Solver_P12; Solver_P13; Solver_P14; Solver_P21; Solver_P22; Solver_P23; Solver_P24). Manual curve fitting using the Theis and Neuman Models produced specific yields and transmissivities at each observation well (Table 11 and 12).

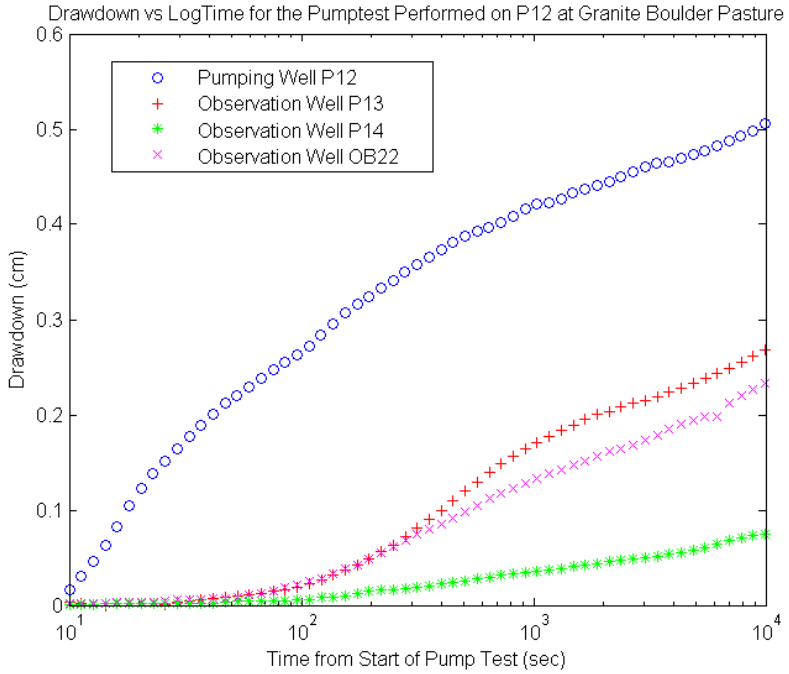

Figure 78. Drawdown vs log time during Granite Boulder Pasture pump test

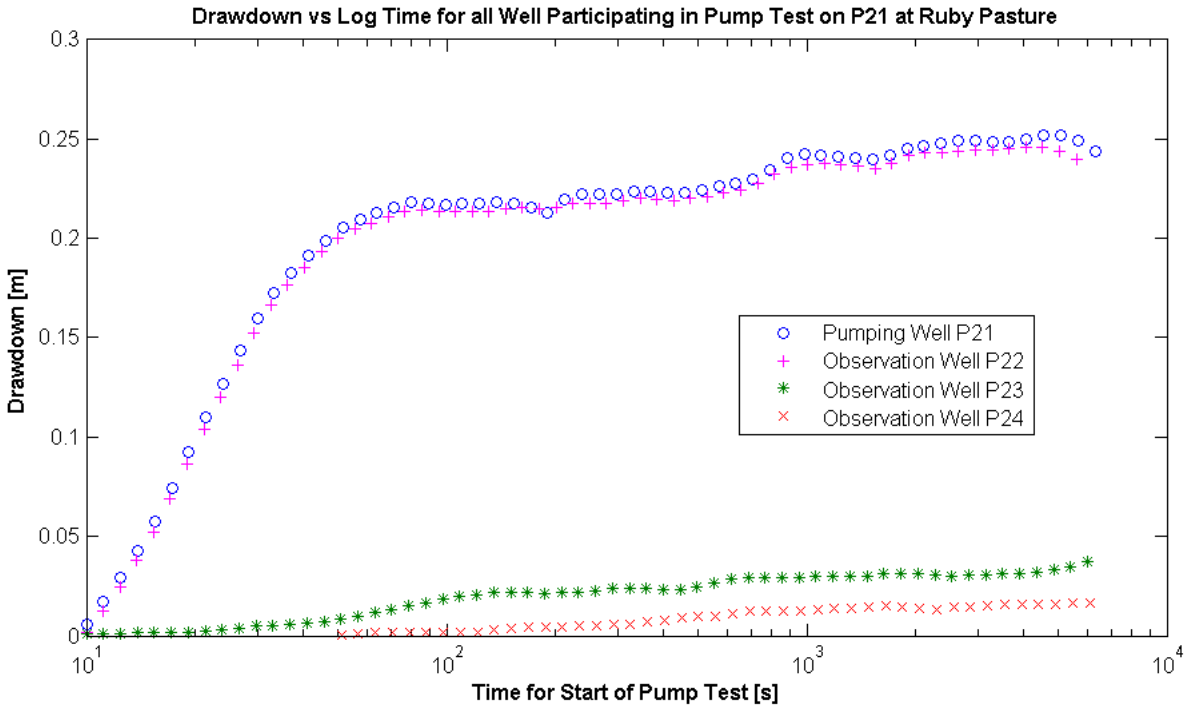

Figure 79. Drawdown vs log time during Ruby Pasture pump test.

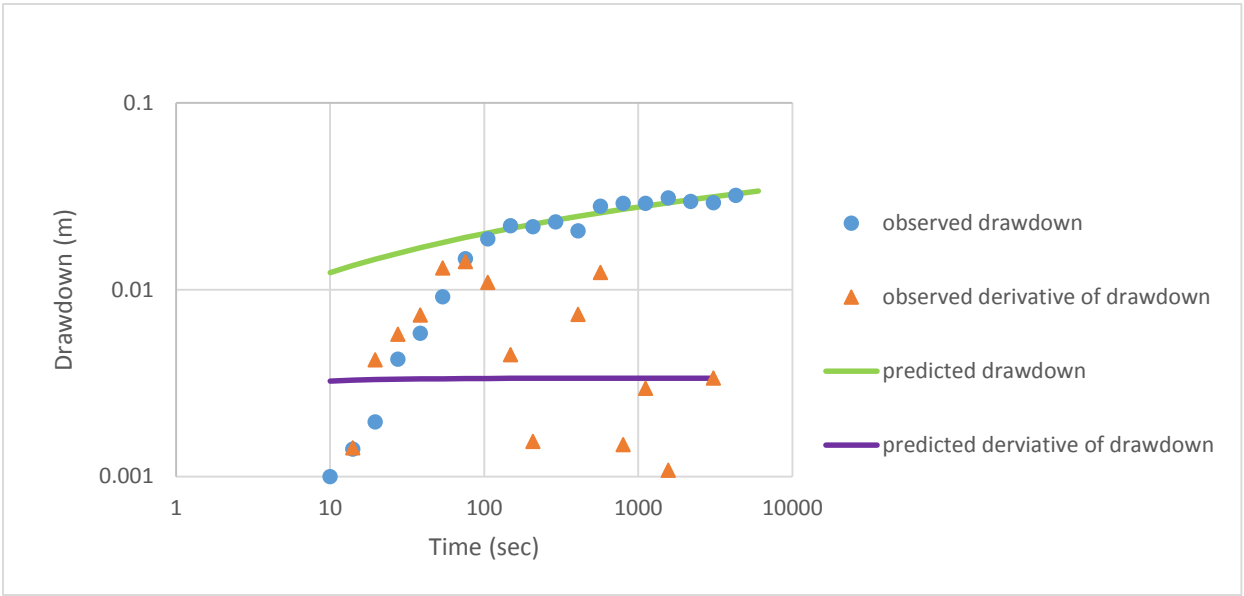

Figure 80. Theis solution using solver at observation well P23 at Ruby Pasture.

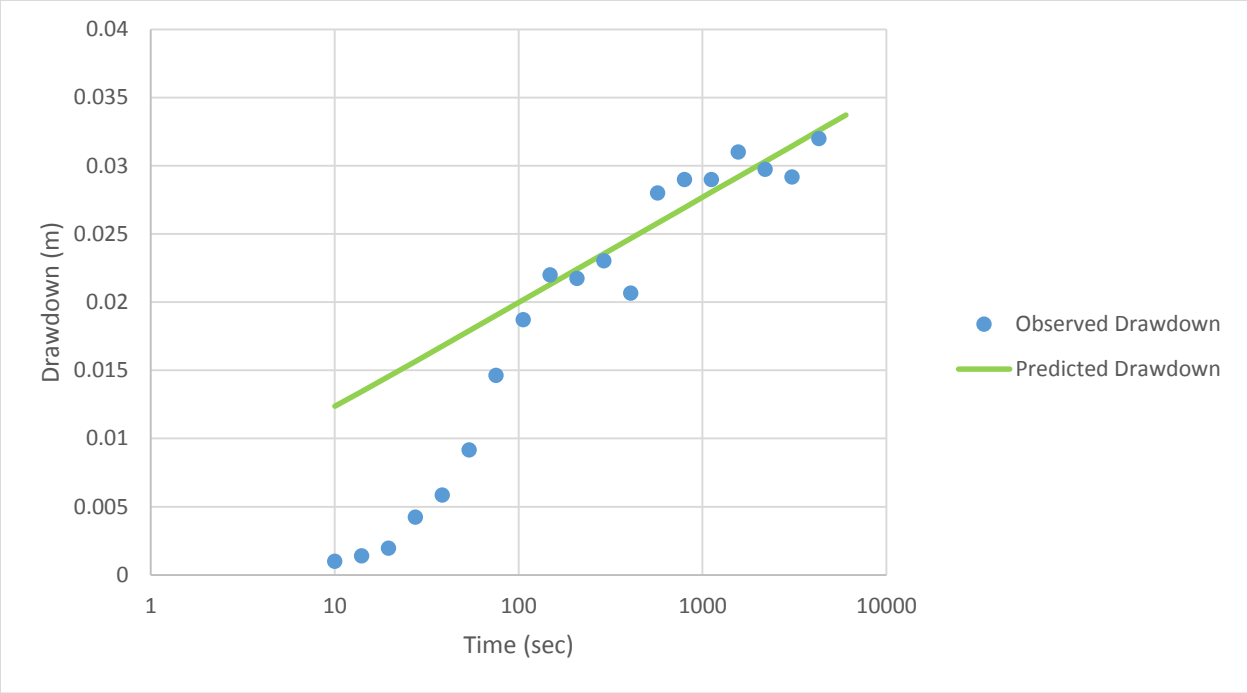

Figure 81. Theis solution using solver at observation well P23 at Ruby Pasture late time.

Table 11. Specific yield summary table from pump test at Granite Boulder Pasture.

Granite Boulder Pasture			
Specific Yield Summary Table [$L_{water}/L_{aquifer}$]			
Method	**P13**	**P14**	**OB22**
Theis Solver Curve Matching	2.0E-02	2.2E-01	5.2E-03
Neuman Curve Matching	2.9E-03	1.0E-02	1.2E-03
Mean of All Values		4.3E-02	

Table 12. Specific yield summary table from pump test at Ruby Pasture.

Ruby Pasture		
Specific Yield Summary Table [$L_{water}/L_{aquifer}$]		
Method	**P23**	**P24**
Theis Manual Curve Matching	4.0E-03	1.5E-02
Theis Solver Curve Matching	2.6E-02	1.8E-02
Neuman Curve Matching	3.6E-03	1.2E-02
Mean of All Values	1.3E-02	

Discussion and Conclusion

The most striking result from the pumping test analysis is that the mean of all the specific yield values for both sites (Table 11 and 12) were an order of magnitude smaller than the results from the other methods (Table 9). The error likely lies in our conceptual understanding. Keep in mind that water table elevation is diurnally fluctuating with an amplitude of ~1cm at Ruby Pasture (Fig. 35). Both conceptual models assume a constant known discharge rate, however in a shallow aquifer there is evapotranspiration, an additional unknown variable discharge rate is imposed upon the system (Fig. 82). At the observation well, a drawdown of ~3cm is attributed to a pump running for ~3h. Over the course of three hours the background diurnal fluctuating water table signal can drop the water table at the observation well by ~1cm. We could attempt to be more strategic as to when to apply a three hour long pump test however they're 3 time periods within a day that might where I suspect that a pump test in a shallow aquifer would produce unexpected results: during the day when evapotranspiration affects the water table elevation, during the night when groundwater upwelling affects the water table elevation, during the transition from day to night when the soil is shifting from drying to wetting. Perhaps a pump test during the transition from night to day, just after the soil shifts from wetting to drying and before the ET rate is large, could produce favorable results.

The groundwater hydrology definition of specific yield is the volumetric fraction of the bulk aquifer volume that a given aquifer will yield when all the water is allowed to drain out if under the forces gravity (Johnson, 1967). The evapotranspiration process can impose negative pressures with 3 to 4 orders of magnitude greater than pressure imposed by gravity drainage.

White's specific yield used to estimate evapotranspiration is going to be a different than the groundwater hydrologist's specific yield based solely on the pressures imposed by the processes considered.

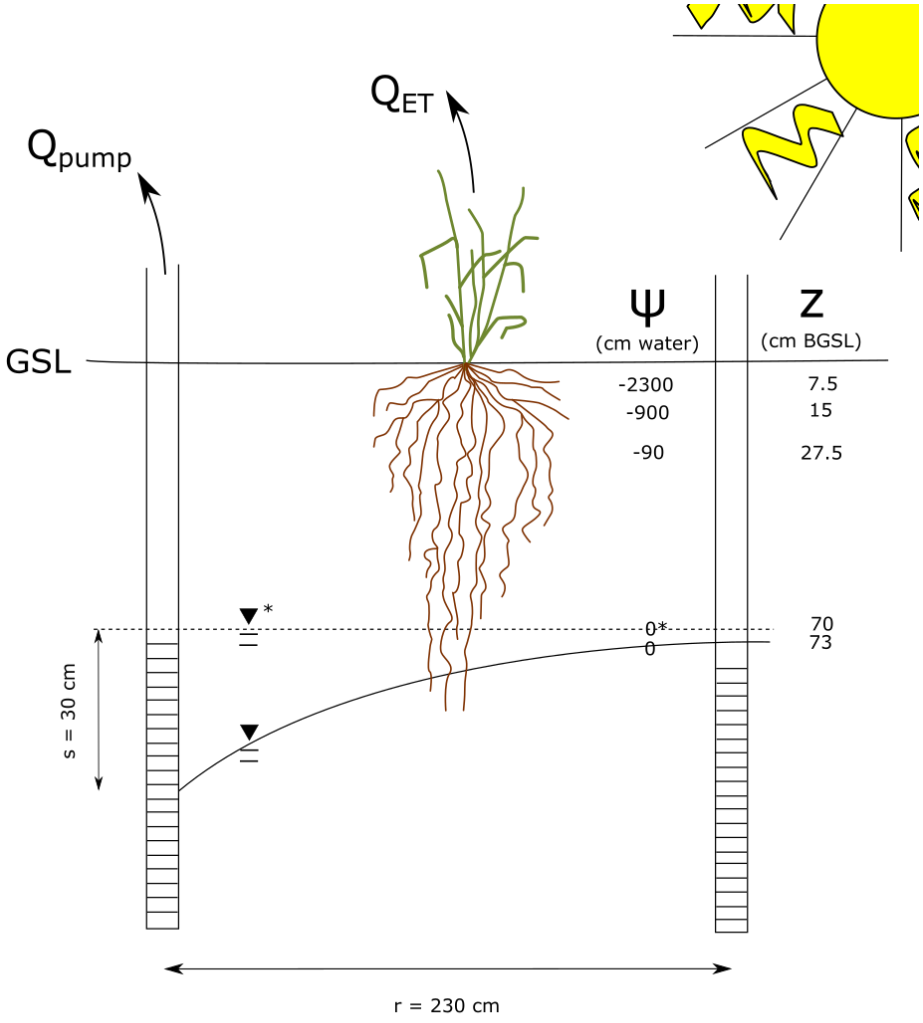

Figure 82. Shallow aquifer pump test at Ruby Pasture.

Appendix a.VI: HYDRUS 1-D Modeling Parameters

Introduction

In the appendix section cartoon representations of model parameter selections for select HYDRUS 1-D model runs are provided. All HYDRUS 1-D files for the numerical models used in this paper are provided in the electronic appendix.

Full Soil Hydraulic Characterization

Lab characterization of soil cores provided the material hydrologic parameters. The resulting parameters (Fig.83) were informed from field data and were adjusted produce a water table elevation record representative of a nearby observation well.

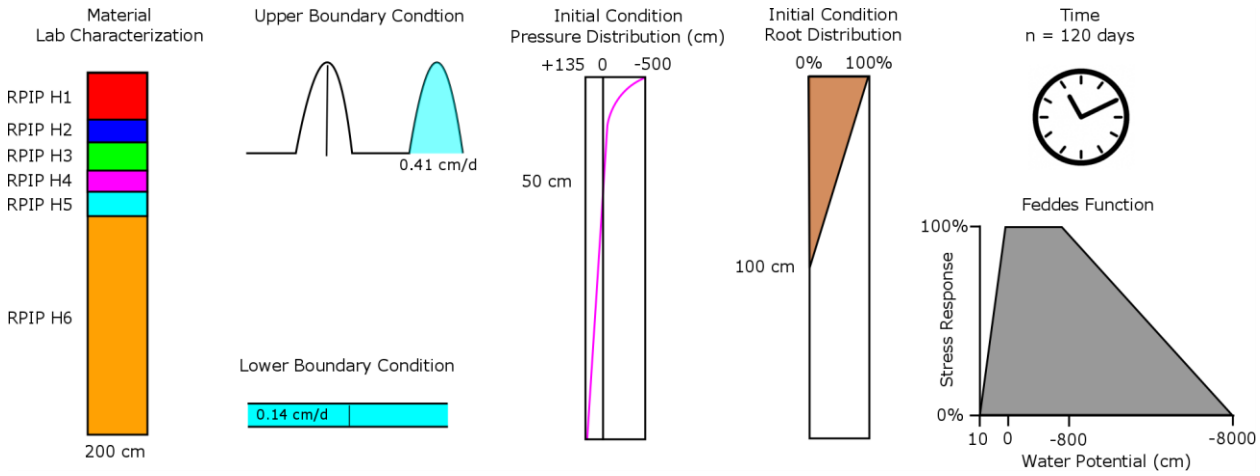

Figure 83. Parameters for full soil hydraulic classification at Ruby Pasture model.

Variable vs Constant Specific Yield

Diurnal water table fluctuations through a homogeneous loam (Fig. 84) were model to evaluate the output for the accuracy of a constant and variable specific yield (Fig. 85).

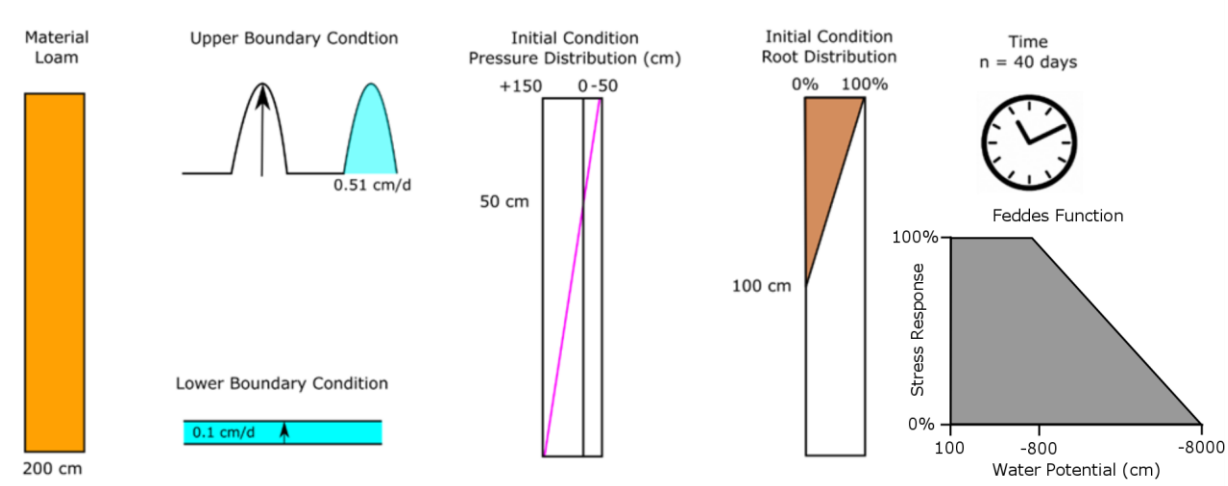

Figure 84. Parameters for the variable vs constant specific yield model.

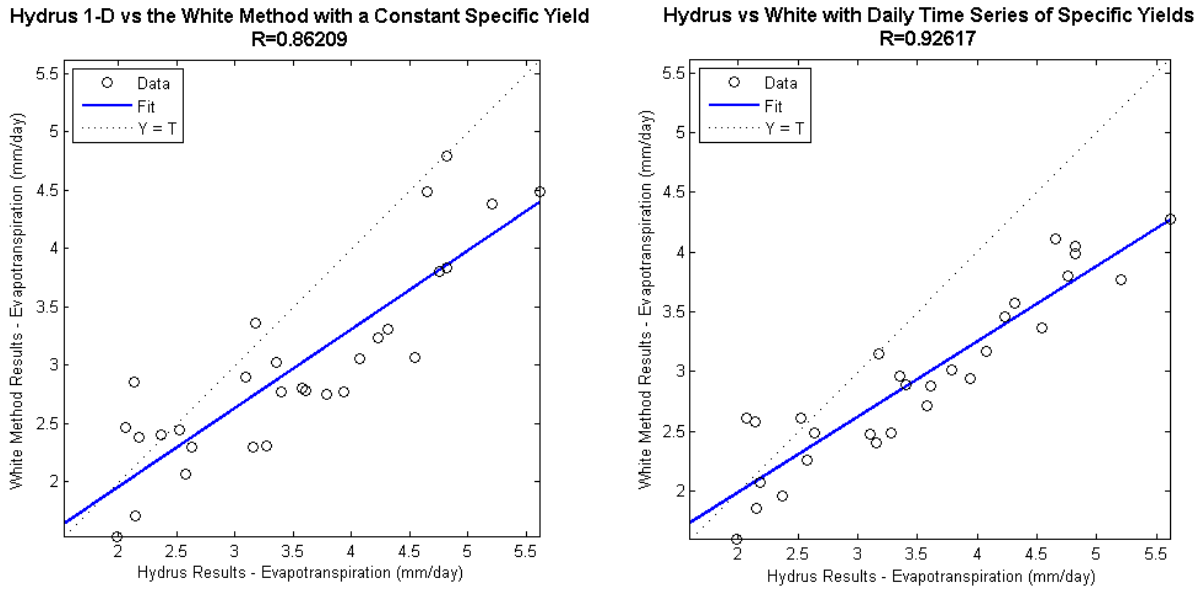

Figure 85. Regressions comparing the White Method against the HYDRUS 1-D output

White vs Nachabe Method with Triangular Roots

Diurnal water table fluctuations through a homogeneous loam with a saturated initial condition (Fig. 86) were modeled to evaluate the output for the applicability of the White and Nachabe Method.

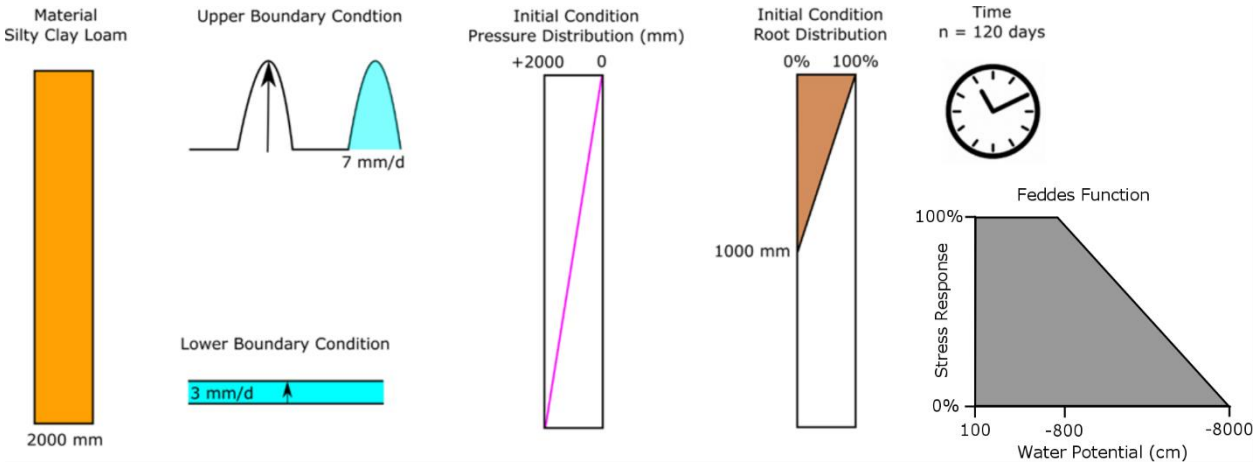

Figure 86. Parameters for the White vs Nachabe with triangular roots model.

Water Table Depth versus Specific Yield with Material Transition

An exponentially decaying water table was modeled through a material transition to be evaluated for the water table depth versus specific yield relationship (Fig. 87).

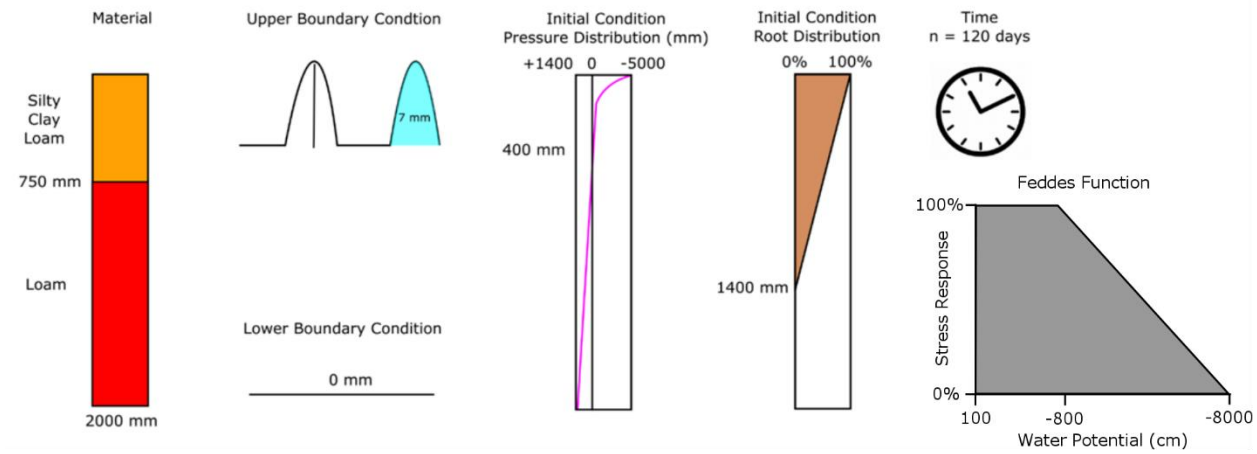

Figure 87. Parameters for the water table depth vs specific yield with material transition model.

Hysteresis and the Break in Slope with a Large Difference in Alphas

Diurnal water table fluctuations through a homogeneous silty clay loam with the large difference in air entry pressures (Fig. 88) used to investigate the difference in slope between the early night and late night.

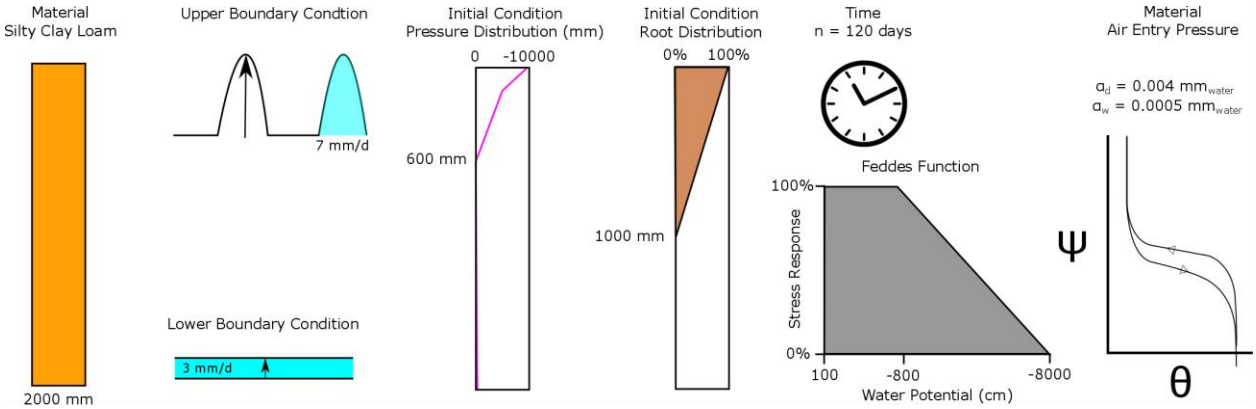

Figure 88. Parameters for the hysteresis and the break in slope with a large difference in alphas model run.

Appendix a.VII: Soil Material Description

Introduction

In this appendix section provide the soil hydrologic parameters measured in the lab. The raw data that yielded the hydrologic parameters is provided (electronic appendix filename: Hydraulic Conductivity Calculations.xlsx, Hydrometer Results and Particle Size Distribution.xlsx, Water Retention Results.xlsx, Water Retention Analysis.xlsx). In addition to laboratory soil description, field soil descriptions are provided (electronic appendix filenames: Field Soil Descriptions_GBP.xlsx, Field Soil Descriptions_RP.xlsx)

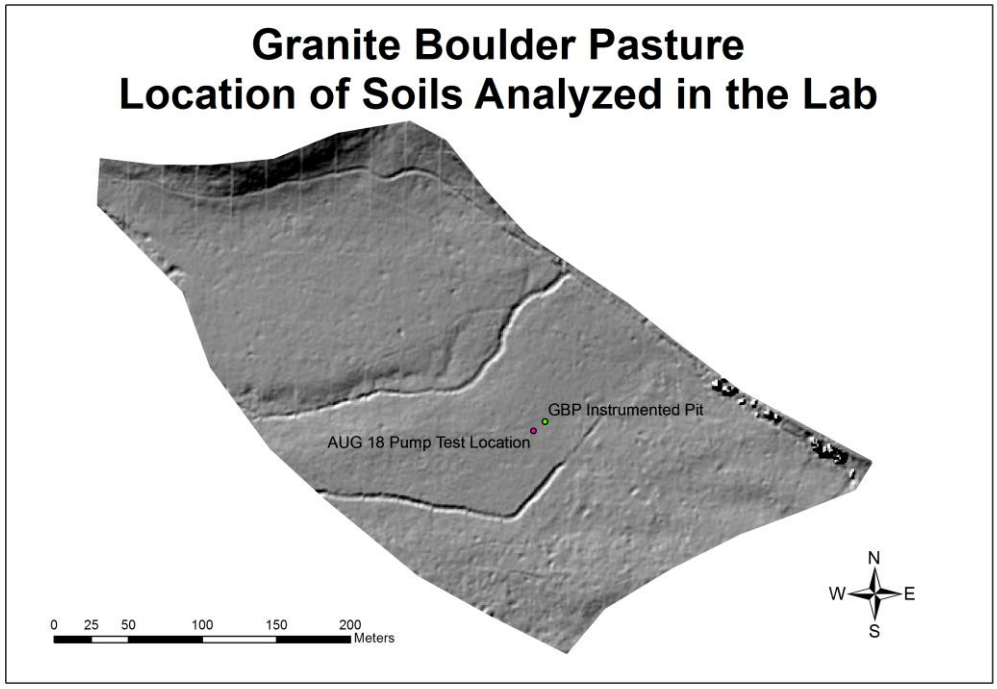

Figure 89. Location of soil profiles sampled for cores at Granite Boulder Pasture.

Table 13. Soil hydraulic parameters at Granite Boulder Pasture.

Granite Boulder Pasture Instrumented Pit						
Horizon Number (#)	Depth Range (cm)	Horizon Designation (Classification)	Texture Class (Classification)	Sand (%)	Silt (%)	Clay (%)
1	0-15.5	Oi	Fiberous			
2	15.5-29.5	A	Silt Loam	40.6	47.9	11.5
3	29.5-50	Btg	Silty Clay Loam	22	49.5	28.5
4	50-63	A/Cgt	Silt Loam	27.8	54.1	18.1
5	63-84+	2Btg	Loam	47.4	34.8	17.8

Horizon Number (#)	Ksat (cm/day)	n (-)	α (cm^{-1})	θ_{sat} (Vol/Vol)	$\theta_{residual}$ (Vol/Vol)	Bulk Density (g/cm^3)
1	3.7E+03	1.15	1.1E-02	0.57	0.05	0.51
2	4.8E+02	1.11	5.6E-03	0.56	0.05	0.95
3	4.2E+01	1.11	6.4E-03	0.47	0.05	1.33
4	1.3E-02	1.06	1.0E-02	0.48	0.05	1.32
5	1.9E+03	1.15	6.1E-03	0.32	0.05	1.18

Auger Hole 18 Pump Test Location						
Horizon Number (#)	Depth Range (cm)	Horizon Designation (Classification)	Texture Class (Classification)	Sand (%)	Silt (%)	Clay (%)
1	0-14	Oi	Fiberous			
2	14-28	2Atg	Silt Loam	33	49.2	17.8
3	28-38	2Btg1	Silt Loam	22.5	52.9	24.6
4	38-74	2Btg2	Loam	44.5	36.7	18.8
5	74-90.5	3C1	Sandy Loam	62.1	26.2	11.7
6	90.5-102+	3C2	Sandy Loam	72.6	18.5	8.8

Horizon Number (#)	Ksat (cm/day)	n (-)	α (cm^{-1})	θ_{sat} (Vol/Vol)	$\theta_{residual}$ (Vol/Vol)	Bulk Density (g/cm^3)
1	3.7E+03	1.15	1.1E-02	0.57	0.05	0.51
2	4.3E+02	1.16	2.2E-03	0.41	0.05	1.43
3	8.1E+01	1.12	3.4E-03	0.48	0.05	1.12
4	7.8E-02	1.09	1.1E-02	0.34	0.05	1.74
5	3.0E+04	1.20	1.5E-02	0.23	0.05	1.30
6	5.0E+02	1.22	2.6E-02	0.31	0.05	1.48

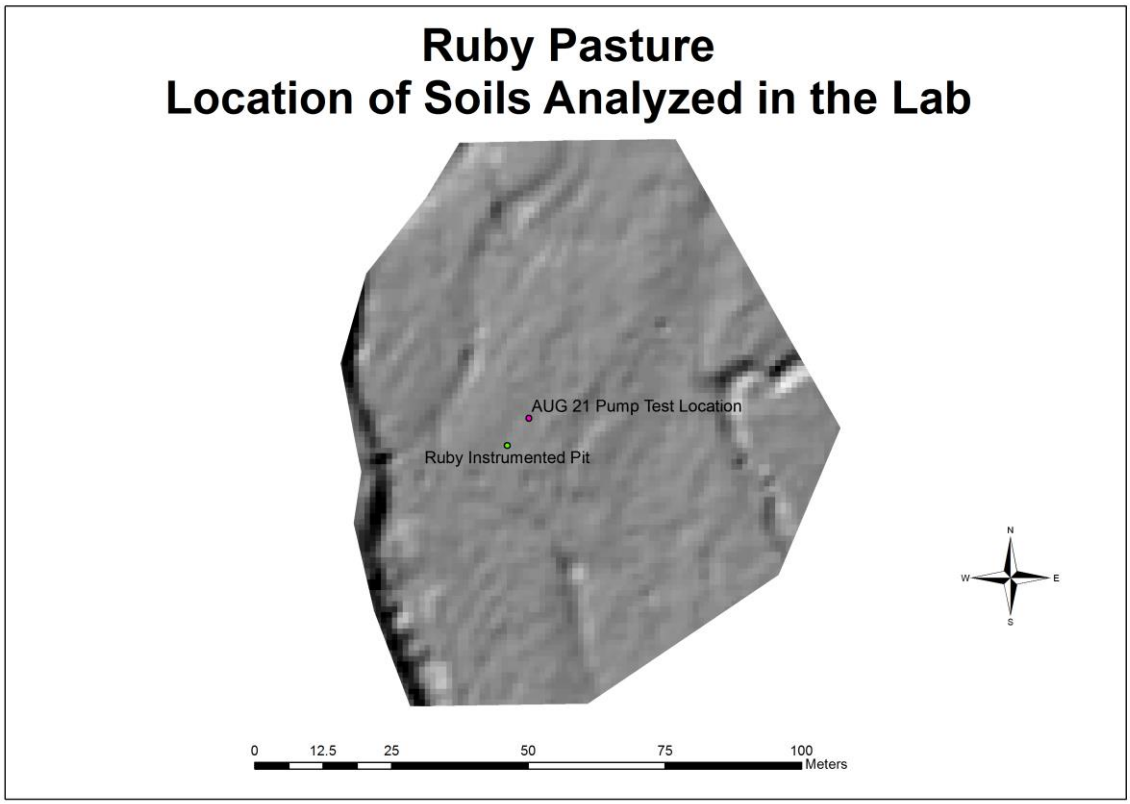

Figure 90. Location of soil profiles sampled for cores at Ruby Pasture.

Table 14. Soil hydraulic parameters at Ruby Pasture.

Ruby Pasture Instrumented Pit						
Horizon Number (#)	Depth Range (cm)	Horizon Designation (Classification)	Texture Class (Classification)	Sand (%)	Silt (%)	Clay (%)
1	0-11	A	Sandy Loam	60.4	37.8	1.8
2	11-26.5	B	Loam	47	46	7
3	26.5-51	2Bw	Silt Loam	43.9	44.3	11.8
4	51-62	3C	Fine Gravelly Loamy Sand	84.7	13.8	1.5
5	62-79	4C	Med Gravelly Sandy Loam	70.8	26.3	2.9
6	79-85+	5C	Cobbly Loamy Sand	-	-	-
Horizon Number (#)	Ksat (cm/day)	n (-)	α (cm^{-1})	θ_{sat} (Vol/Vol)	$\theta_{residual}$ (Vol/Vol)	Bulk Density (g/cm^3)
1	1.4E+03	1.14	3.8E-01	0.64	0.05	0.81
2	5.6E+03	1.13	2.0E-01	0.53	0.05	1.15
3	1.1E+02	1.24	1.9E-03	0.40	0.05	1.32
4	3.2E+04	1.35	4.2E-02	0.28	0.05	1.49
5	4.8E+03	1.29	5.5E-02	0.45	0.05	1.54
6	-	-	-	-	-	-
Ruby Auger Hole 21						
Horizon Number (#)	Depth Range (cm)	Horizon Designation (Classification)	Texture Class (Classification)	Sand (%)	Silt (%)	Clay (%)
1	0-27	AB	Sandy Loam	54.3	43.2	2.5
2	27-39	B	Silt Loam	39.1	49	11.9
3	39-54.5	Bw	Silt Loam	45.3	42.8	11.8
4	54.5-67	2C1	Fine Gravelly Silt Loam	38.7	57	4.3
5	67-79	2C2	Medium Gravelly Silt Loam	45.4	53.4	1.2
6	79-84+	3C	Course Gravelly Silt Loam	44.3	52.4	3.3
Horizon Number (#)	Ksat (cm/day)	n (-)	α (cm^{-1})	θ_{sat} (Vol/Vol)	$\theta_{residual}$ (Vol/Vol)	Bulk Density (g/cm^3)
1	1.2E+03	1.15	7.4E-03	0.44	0.05	0.87
2	7.1E+02	1.18	1.7E-02	0.37	0.05	1.04
3	2.7E+02	1.18	1.1E-02	0.39	0.05	1.35
4	3.5E+03	1.26	5.2E-03	0.26	0.05	1.70
5	1.1E+03	1.33	3.7E-02	0.25	0.05	1.76
6	2.0E+02	1.38	2.9E-03	0.28	0.05	1.77

Appendix a.VIII: Next Steps

Introduction

There were many ideas in this manuscript. Each idea either had a chapter or an appendix section. This Next Steps appendix section is an effort to distill the big learning points from each idea and communicate my understanding of a point a future researcher could start from.

Instrumentation Challenge for Estimating ET Using GW Signals

Measuring groundwater signals in shallow aquifers with the aim to estimate a daily rate of evapotranspiration possess some unique challenges. To be able to fully understand the dynamics of water movement in shallow aquifers and it's relation to evapotranspiration, it would be informative to sense is the water table elevation, total soil moisture and the soil water pressure profile as the water table evolves from a shallow position to a deep position through the dry season.

The variables that need to be sensed are:

1. Volumetric moisture content by depth to determine total soil moisture
2. Negative pressure by depth to determine the unsaturated pressure profile
3. Positive pressure in an observation to determine water table elevation

A volumetric moisture content sensor that has a high resolution (<1cm resolution) with the ability to sense at depth (~1m) and the ability to be deployed below the water table should do the trick. The volumetric sensors I employed either had low spatial resolution (Decagon 5TE)

or could not be installed below the water table (Sentek Diviner 2000). Programmable automatic measurements logged on a data logger is another requirement for a modern instrument design. Most volumetric moisture content sensors require a temperature calibration and thus when and where volumetric moisture content is being sensed temperature should be sensed as well.

Negative pressure with depth is an essential to predict water movement in soil. The soil water pressure probes I employed either could not sense above -100 cm of water (Decagon M1) or were not automatic measurements (tensiometer). It would be useful to develop a soil water pressure sensor that can measure the range of +10 cm to -150 cm of gauge pressure at depth (~1m) the can be automated to measure and log the reading.

Site Selection

The Granite Boulder and Ruby Pastures were highly heterogeneous sites reflected in soils, vegetation, and elevation distribution due to its landscape position. I selected these sites due to historic water table records that proved the presence of diurnal water table fluctuations. If you were to select a site to describe the limitations of the White Method would you chose a heterogeneous site or a homogeneous site? If you were to install one observation well to produce a record of diurnal water table fluctuations, what data would you use to inform your decision?

Both heterogeneous and homogeneous sites have their advantages and disadvantages. To test the limitations of a method a heterogeneous site provides challenges. If a method is developed with reasonable assumptions at a heterogeneous site it is most likely applicable at a

more homogeneous site. To more clearly isolate signals that can be attributed to specific processes, a homogenous site would provide a form of blocking against processes that could affect the signal you would be deriving your conclusions from. However, some assumptions that can be made at a homogeneous site could limit a methods applicability to a heterogeneous site.

Vegetation information across a watershed and a site can inform the decision to place an observation well in the effort of sensing diurnal water table fluctuations. To identify a site, select areas within a watershed that remain vibrant green during mid to late dry season. At a site the vegetation hydrologic index can provide evidence as to the shallowness of the water table and the percent standing dead can give clues as to the connectivity of the roots to the water table. I recommend placing an observation well where the vegetation hydrologic index is near 4 and the percent standing dead is near 50% during mid dry season to measure a water table that is shallow in the wet season and transitions too deep during the dry season but does not become disconnected from the root zone.

Modeling Specific Yield for a Shallow Aquifer

The big difference between the typical groundwater hydrologist definition of specific yield and the specific yield that the White Method employs is the magnitude of pressures applied to drain the water filled pore space. A typical definition of specific yield refers to the amount of water the will drain under the force of gravity, while the White Method refers amount of water that will drain under pressures induced by the root during the day and the amount of water that will fill under pressures induced by groundwater upwelling. One of the

largest issues that a constant specific yield introduces into the White Method is that the change in volumetric moisture content is only accurately inferred during the time the specific yield has been optimized for. The White Method is well suited to the time period when the plant accessible volumetric moisture content has been depleted and the transpiration rate is equal to the upwelling rate, the specific yield should be optimized for this time period. To further extend the applicability of the White Method earlier in the dry season it would be useful to develop an analytical expression to infer the change in volumetric moisture content before the plant accessibly volumetric moisture content has been depleted. The expression should be a redefinition of the specific yield. The depth of critical zone (Fig. 37) between approximately half of the total rooting depth and the water table depth provides an easily measureable variable with the units of length that changes the specific yield. After performing a dimension analysis, the groomed list of variables that I think affect specific yield include the soils characteristic length, the porosity, Van Genuchten's n, the difference between the water table depth and half of the total rooting depth, the difference between the pressure at volumetric moisture content and the pressure at wilting point, the day length, and the evapotranspiration potential. The starting point is at the end of my dimensional analysis where further relationships between specific yield and combinations of variables should be explored in a numerical modeling environment.

Hysteresis and the Break in Slope

The break in slope during the night in diurnal water table fluctuations can be attributed to the curvature of the water retention curve slightly below air entry pressure. When wetting and drying hysteresis is considered a soils path along the water retention curve is a scanning curve. When considering hysteresis the curvature of the scanning curve near air entry pressure is greater than the curvature of the water retention curve used when hysteresis is not considered. The curvature of a soils scanning curve can be altered by changing the air entry pressures of the soils wetting and drying curves.

The break in slope during the night doesn't clearly occur in all records of diurnal water table fluctuations. This is most likely attributed to the air entry pressure of the porous media directly above the water table being near zero. Another explanation for the inconsistent presence of the break in slope is that the systems the water table elevation records are taken from are only slightly hysteretic. A curios dataset to support this idea is White's salt grass meadow (Fig. 44) where the break in slope disappeared when the salt grass was cut.

An Application to Capture Field Scale Variability in ET

In the experimental design, the procedure to validate the White Method was to compare evapotranspiration derived from the White Method against evapotranspiration derived from a nearby weather station. The weather station methods computes an averaged evapotranspiration rate of the area within the weather station's fetch. The White Method produces small area estimate of evapotranspiration (Fig. 91). To make a direct comparison between the White Method results and weather station results requires an assumption that

the observation well is 'representative' of the area within the fetch. Spatial distribution of soil materials, vegetation type, and water table behaviors at both field sites suggest that evapotranspiration rate is heterogeneous in the x-y plane at both sites (electronic appendix filenames: Distant Wells of GBP.xlsx, Distant Wells of Ruby Pasture.xlsx). In heterogeneous sites the direct comparison of an evaporation estimate that represents a small area to an estimate representing a large area is invalid.

Figure 91. Comparing the results from a 1-D system to a 3-D system.

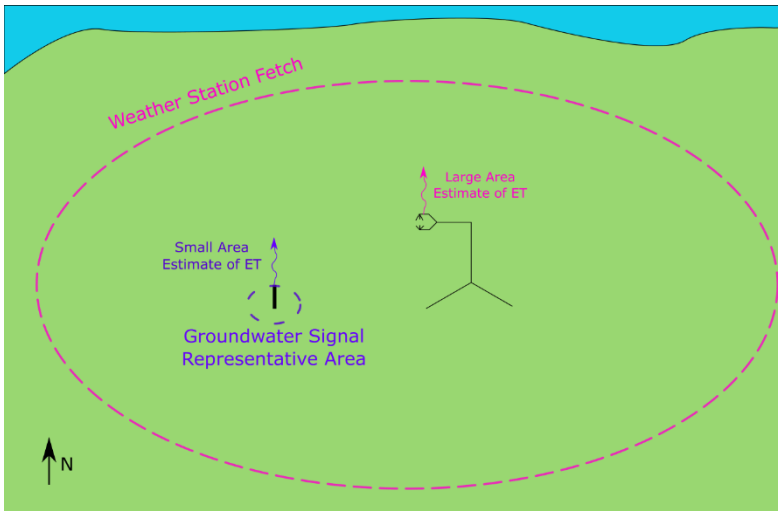

Use caution when making a direct comparison between the evapotranspiration rates derived from the slow moving groundwater zone and the rate derived from the fast moving atmospheric zone. While this late observation shines light on the uncertainty in making direction comparisons between methods, it does provide a unique opportunity to test the assumption of horizontal homogeneity. Weather station methods often assume that the evapotranspiration rate is homogeneous across the area within the fetch of the weather station. Since the White Method generates small area estimates of evapotranspiration, small area estimates of evapotranspiration could be weighted by a larger area that each observation

could represent. A weighting function could be generated to weight each well by a representative area and produce a continuous mosaic of evapotranspiration rates across a larger area. The average evapotranspiration rate across the mosaic can be compared the weather station with a fetch across the same area for verification. The proposed method of taking a number of observation wells and weighting them in space would produce an area averaged estimate of evapotranspiration while preserving information regarding difference in evapotranspiration rate across the site. The difficult aspect of this proposition is how to properly weight each observation point. A potential solution is to utilizing hyper spectral imagery to infer vegetation stage and stress at specified to generate a weighting function. The weighting function should be generated multiple times through the dry season as vegetation stage and stress changes differently across Ruby and Granite Boulder Pasture.

Field Tips: Timing of Sensing

My suggestions to the next person who strives to implement a field experiment in the efforts of applying the White Method are:

1. Select two methods to measure volumetric moisture content by depth, a method to measure negative pressure distribution to the depth of the water table is a plus.
2. Select two trusted methods of measuring local (think square meter scale) evapotranspiration rate.
3. At the end of the water year when the water table is the furthest below ground surface level, install automated instrumentation, describe soils and take samples

4. Select multiple White like methods of data analysis (Soylu et al, 2014) (Wang at al, 2012)
5. Run HYRDUS 1-D simulating your expected signals
6. Apply the methods of data analysis to the simulated groundwater signals (WTE and TSM) selected at step 4
7. Select your White like method of data analysis to be applied to the WTE and TSM
8. Perform lab work on soil cores if needed
9. Before the beginning of the recession double check that your instrumentation is working properly
10. Observe the recession
11. Process the data for daily evapotranspiration rate you should have for estimates of evapotranspiration rate
    a. Trusted Method 1
    b. Trusted Method 2
    c. White Method
    d. Nachabe Method
12. Compare ET estimates from methods a-d

Conclusion

We covered many facets of the White Method: notably were the limitations of the White Method, the conceptualization of White's specific yield, understanding the break in slope, and vegetation clues to help place an observation well. While the method has certain potential, it is striking because it has many limitation.